SIEMENS

# MAGNETOM Flash

The Magazine of MRI

Issue Number 1/2015 | SCMR/EuroCMR Edition

Not for distribution in the US



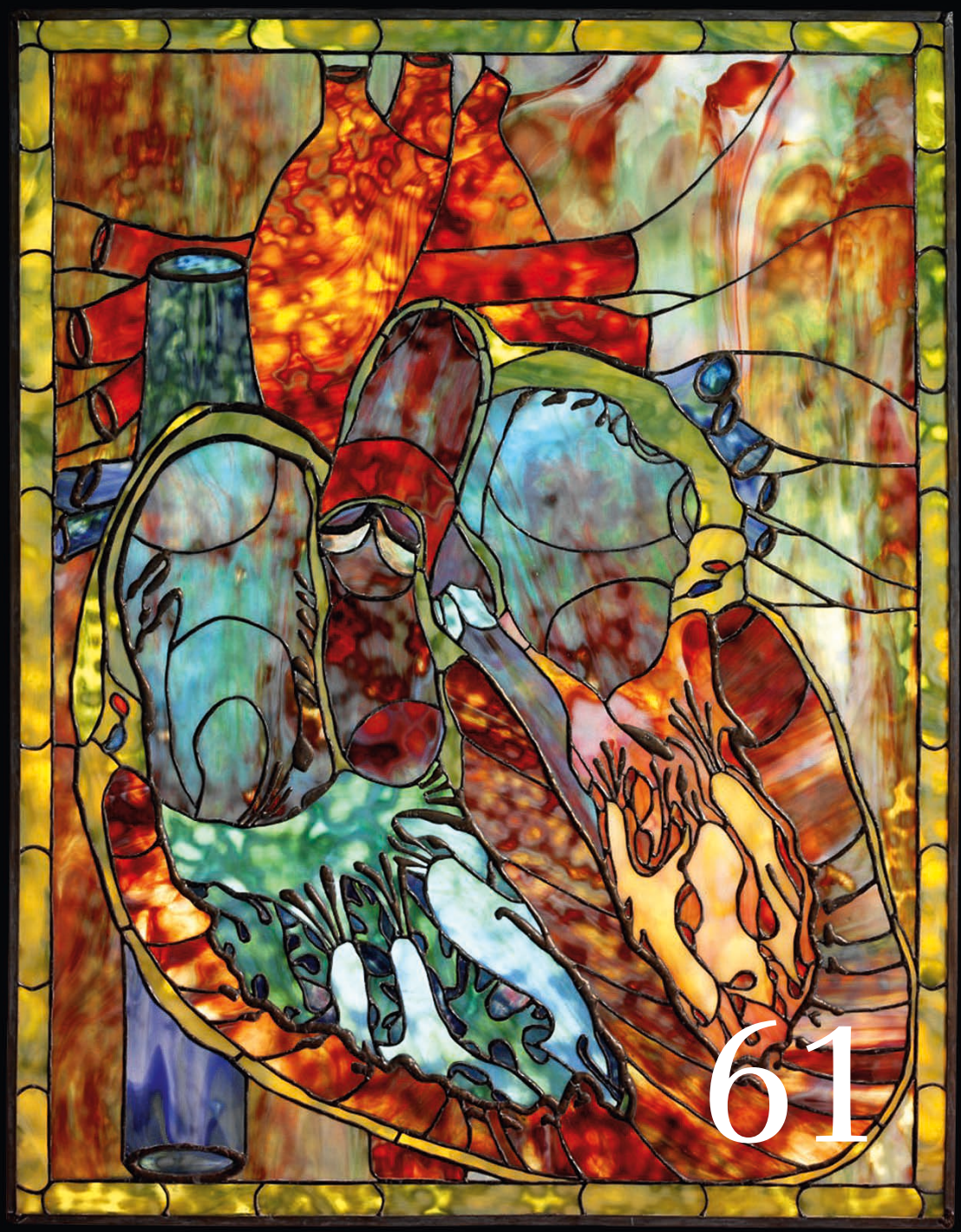

61

# SCMR recommended protocols now available for Cardiac Dot Engine

To aid standardization of CMR, the Society for Cardiovascular Magnetic Resonance (SCMR) released CMR exam protocol recommendations for the most frequent CMR procedures.
In a collaborational effort Siemens Healthcare and the SCMR prepared clinically optimized exam protocols in accordance to the SCMR recommendations for 3T MAGNETOM Skyra and 1.5T MAGNETOM Aera, since software version *syngo* MR D11.

The following SCMR Cardiac Dot protocols are available:

- Acute Infarct Dot
- Adenosine Stress Dot
- Aorta Dot
- Arrhythmic RV Myopathy Dot
- Chronic Ischemia Dot
- Coronaries Dot
- Mass & Thrombus Dot
- Nonischemic Myopathy Dot
- Pericardium Dot
- Peripheral MRA Dot
- Pulmonary Vein Dot
- Valves Dot
- Pediatric Teen* Dot
- Pediatric Child* Dot
- Pediatric Infant* Dot
- Library Cardiac Shim
- Library TuneUp Shim

## Please contact your Siemens Application Specialist for the .edx files of these protocols.

**Acknowledgement:** We would like to thank all SCMR members who were on the guidelines committee
Christopher M. Kramer *(University of Virginia, Charlottesville, VA, USA);*
Jörg Barkhausen *(University Hospital, Lübeck, Germany);*
Scott D. Flamm *(Cleveland Clinic, Cleveland,OH, USA);*
Raymond J. Kim *(Duke University Medical Center, Durham, NC, USA);*
Eike Nagel *(King's College, London, UK)* as well as
Gary R. McNeal *(Senior CMR Application Specialist; Siemens Healthcare, USA)*
for their tremendous efforts and support.

* MR scanning has not been established as safe for imaging fetuses and infants less than two years of age. The responsible physician must evaluate the benefits of the MR examination compared to those of other imaging procedures.

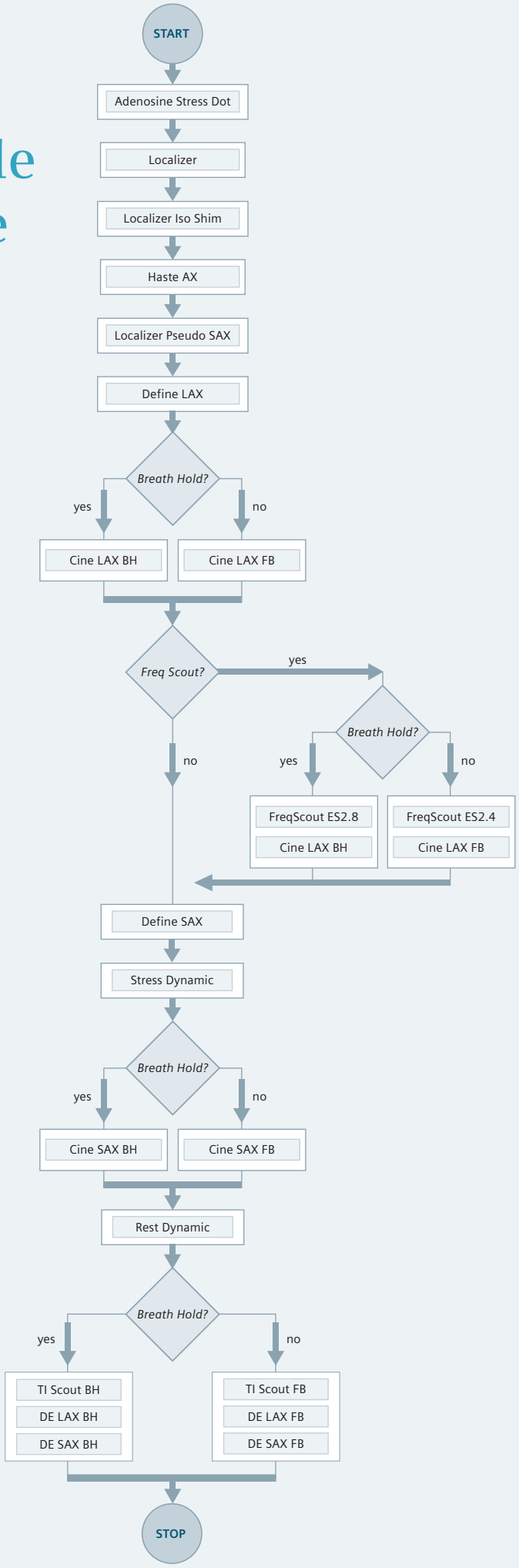

**Dr. Chiara Bucciarelli-Ducci,** MD, PhD, FESC, FRCP is Consultant Senior Lecturer in Cardiology / Non-Invasive Imaging at the Bristol Heart Institute, University of Bristol, UK. Since 2010, she is the imaging lead of the Bristol National Institute of Health Research (NIHR) Biomedical Research Unit (BRU) and the co-Director of the Clinical Research and Imaging Centre (CRIC Bristol).

Her previous CMR experience includes a research fellowship at the Feinberg Cardiovascular Research Institute, Northwestern University, Chicago, USA (2004-2005), and a PhD degree on CMR from Imperial College London/Royal Brompton Hospital (2006-2010), London, UK, as well as having provided senior clinical supervision to the weekend CMR service of the Heart Hospital, UCL (2008-2010).

She has been recently elected the vice-chair of the CMR section of the European Association of Cardiovascular Imaging (EACVI) within the European Society of Cardiology (ESC).

# Dear MAGNETOM Flash reader,

It is a real honor for me to introduce the first 2015 edition of MAGNETOM Flash published in conjunction with the joint SCMR/EuroCMR 2015 meeting.

Imaging is increasingly at the core of personalized cardiovascular medicine and over the last few years we have all witnessed tremendous improvements in CMR technology and in its clinical applications. CMR is becoming an integral part of the international guidelines for managing patients with cardiovascular disease. For example, in the recent 2014 ESC/EACTS guidelines on myocardial revascularization, CMR stress perfusion received a class I indication as a diagnostic test for patients with intermediate risk of CAD. The cardiology community is therefore embracing CMR as a test to offer to their patients in various clinical settings, reflecting modern cardiology practice.

The centrality of imaging, particularly CMR, in the day-to-day delivery of cardiac care is well demonstrated by the new advanced imaging department at Barts Heart Centre, London, UK. Strategically located between inpatient and outpatient cardiology services, the unit is equipped with three CMR dedicated scanners and networked to five other scanners located in allied hospitals. Its anticipated volume of 9,000 CMR scans per year shows the extent to which CMR is used in clinical practice, but also provides an excellent platform for research and educational opportunities.

## Myocardial parameter mapping

A significant part of this issue is dedicated to myocardial parameter mapping, namely native T1 and extracellular volume fraction (ECV), new methods that have brought a new dimension to non-invasive myocardial tissue characterization.

Both native T1 and ECV now offer the unprecedented opportunity to non-invasively quantify changes in the myocardial structure and interstial compartment facilitating diagnosis and prognosis in a variety of cardiovascular disease. Schelbert et al. illustrate how native T1 is generally increased in a range of acute and chronic conditions such as myocardial infarction, myocarditis or stress cardiomyopathy, and amyloidosis or other cardiomyopathic processes, respectively. Conversely, native T1 is reduced in conditions such as iron overload and Anderson-Fabry's disease. However, it is important to note that myocardial edema, fibrosis and amyloidosis can all increase native T1 values suggesting an overlap across disease categories, and the need to interpret abnormal values within the clinical context.

Whilst alteration in native T1 may result from processes affecting the myocardium, the interstitium, or both, ECV mapping specifically quantifies expansion of the interstitial space. Whilst both can represent early markers of disease, recent evidence suggests that ECV may improve risk stratification, representing a therapeutic target for therapy and predicting outcome better than traditional markers.

Lundin and Ugander from Sweden complement these concepts by presenting a series of clinical cases demonstrating the clinical utility of myocardial parameter mapping in a variety of clinical conditions. This is a great example of how this latest technology is being successfully translated into clinical practice.

However, the ability to quickly and reliably detect diffuse myocardial

*"This issue addresses a variety of clinical topics that demonstrate the successful translation of technological developments into clinical practice aimed at improving patients' management but also increase work efficiency."*

**Dr. Chiara Bucciarelli-Ducci**

fibrosis continues to be the drive for further technical developments. Currently there are various techniques available to quantify T1 and ECV, each with advantages and limitations. After reviewing some of the most commonly used methods, Chow and Thompson from Canada illustrate the rationale and promising performance of a new sequence called SASHA[1] (SAturation-recovery single SHot Acquisition). The robustness of the SASHA sequence appears to significantly reduce systematic confounders that affect other sequences increasing their variability.

Colleagues from Brazil take us through the journey of parametric mapping applied to the spectrum of iron overload disease. Lara Fernandes et al. then present the interesting results of the All Iron Detected (AID) Project that saw the implementation of a prototype MyoMaps package[1] to increase productivity, decrease training needs and increase clinical throughput in patients with iron overload. The results of their study show the feasibility of the protocol, with a median scan time of 5.2 minutes (IQR 4 to 7 minutes) in patients with a wide age range (2 to 91 years of age). This has the potential to allow the evaluation of 70 patients in a 12-hour shift, boosting productivity to 200%. Most importantly, this does not come at the expense of compromising image quality or robust T2* quantification.

## How-I-do-it

This issue has a strong focus on How-I-do-it with colleagues around the world sharing their vast practical experience on various different CMR applications that have improved their clinical practice.

CMR is not immune from the pressures of cost-reduction and cost-effectiveness dictated by the current financial climate. But challenges also represent opportunities and Pleyo et al. from Spain describe how the Cardiac Dot Engine has improved CMR efficiency with the introduction of shorter MR sequences and automated scanning techniques, which translate into reproducible and efficient studies, reduced scan time, ultimately improving patients' experience, without compromising image quality.

Similarly, Avery et al. show how the *syngo*.via MR Cardiac Analysis provides a solution to the time-consuming CMR image post-processing offering a semi-automated workflow. This system is based on a computer-aided ventricle contour detection and valve planes delineation, recognition of defined anatomical references such as the apex, anterior RV insertion point, and others, and depiction of the designated end-diastolic and end-systolic frame. This method aims at improving significantly the post-processing time, therefore reducing costs without compromising the accuracy of the analysis. This article presents a rich iconography that easily guides the readership though the use of the software with useful tips and tricks.

The article by Gottlieb and Camargo describes how CMR can be performed reliably with a standard 1.5T magnet such as the MAGNETOM ESSENZA. Whilst the system presents some limitations for cardiac imaging, these can be overcome by some adjustments and good routine cardiac image quality can be obtained. This is quite an important concept because it emphasizes that in contexts where the access to a more sophisticated CMR scanners might be limited or perhaps even prohibitive, the delivery of a CMR service is not compromised. This article is indeed an encouragement that CMR has increasingly less barriers with ease of

[1] WIP, the product is currently under development and is not for sale in the US and in other countries. Its future availability cannot be ensured.

cardiac potential even in less sophisticated systems, which represents in fact an invite to perform it more globally.

## Non-contrast MR angiography

The article by Edelman et al. describes a new non-contrast MR angiography called QISS (Quiescent Interval Single Shot), a very promising alternative to standard contrast-enhanced MR angiography or CTA, particularly in those patients with renal dysfunction and contraindication to contrast media. The sequence, unique to Siemens, has been recently launched in the market.

A series of clinical cases is then presented by Carr et al. where the image quality obtained with QISS speaks for itself, particularly in comparison with a standard contrast-enhanced MRA and CTA.

QISS helps improving patients' safety and compliance with higher accuracy and better disease management, while maintaining the diagnostic certainty you need in peripheral MRA exams.

Finally, Viallon et al. illustrate the interesting MUST project that involved CMR technology in detecting structural and functional changes in both myocardial and skeletal muscles induced by ultra-endurance running. This study contributes to the understanding of adaptive response to extreme physical exercise both during exercise and in the recovery phase. The CMR protocol used for this study spanned from the standard cine and LGE technique to myocardial tagging, T1 and T2 mapping and feature tracking analysis, and the preliminary data is described in the article.

In conclusion, this issue addresses a variety of clinical topics that demonstrate the successful translation of technological developments into clinical practice aimed at improving patients' management but also increase work efficiency. The outstanding contributions from colleagues throughout the world is evidence of CMR becoming an increasingly mature technique used worldwide.

This wouldn't have been possible without the passion of the researchers around the world and certainly not without the joint dedication of the industry, like Siemens, in continuing to invest in innovation and the development of new products to address clinical needs.

Happy reading, and see you at the joint SCMR/EuroCMR 2015 meeting

Chiara Bucciarelli-Ducci

# Content

8 The New Barts Heart Center

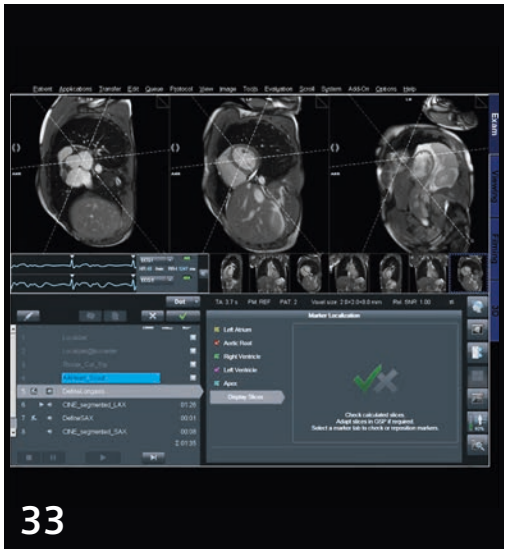

33 Significant Time Reduction Using the Cardiac Dot Engine


## Learn from the experience of other MAGNETOM users

The MAGNETOM World is the community of Siemens MR users worldwide, providing you with relevant clinical information. Here you will find application tips and protocols to optimize your daily work. Lectures and presentations from experts in the field will allow you to be exposed to new ideas and alternative clinical approaches.

Put the advantages of the MAGNETOM World to work for you!

**www.siemens.com/magnetom-world**

## Editorial



## Business


CMR at MAGNETOM ESSENZA

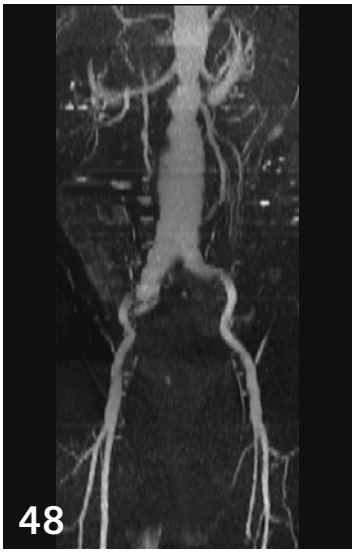


QISS Non-Contrast MRA


MUST Project

## Cardiology



## How-I-do-it



## Vascular Imaging



## CMR Spotlight

# CMR at the Center of Cardiac Care: Case Example Service Delivery at Barts Heart Centre – Advanced Imaging Department

James C. Moon; Charlotte Manisty; Anna S. Herrey; Steffen Petersen; Mark Westwood

Institute of Cardiovascular Science, University College London;
The Inherited Cardiovascular Diseases Unit and Cardiac Imaging Department, The Barts Heart Centre, London, UK

## Introduction: The Barts Heart Centre

Cardiac services for a catchment area approaching 1/3 of greater London, specifically, North Central London, North East London and West Essex, are being reconfigured with a new state-of-the-art cardiovascular hospital – the Barts Heart Centre (BHC). Work will begin with the merger of cardiac services from St Bartholomew's Hospital, The London Chest Hospital and The Heart Hospital to be centralised at Barts site from Spring 2015, whilst construction work to complete BHC is carried out.

The Barts Heart Centre will be fully open from Autumn 2016 with a large scale operation – 232 cardiac inpatient beds, 10 catheter labs (incl. 1x hybrid), 8 cardiac theatres, 40 outpatient rooms with three additional hospitals within Barts Health NHS Trust and other secondary care hospitals outside the Trust all feeding into BHC, serving a catchment area of around 5 million. In addition the service will provide supraregional services including congenital heart disease and national services for cardiomyopathy.

We believe that imaging has an important role to play in the cardiac pathways putting imaging at the heart of this exciting initiative. Here we describe the UK position of CMR, the proposed structure and format of the new imaging department and the role of cardiovascular magnetic resonance (CMR) within it.

## CMR in the UK

CMR in the UK is growing fast. There are more than 60 centres performing CMR. Growth has over the last 5-10 years been consistent at 10-15% a year. Some of this has been new imaging, but much has been disinvestment in other modalities (e.g. nuclear imaging for ischemia). CMR is seen as essential for many well known areas – congenital heart disease, cardiomyopathies, many systemic rarer disease, and acute situations (e.g. troponin elevation with non-obstructive coronary arteries or post cardiac arrest); but it is also a preferred field for many practitioners. In the UK National Health Service CMR is not reimbursed according to a 'fee per procedure' structure, which enables national services to be managed and coordinated to maximize care quality. This means that the traditional 'turf war' between radiology and cardiology is generally more benign than in other environments. There are some training issues however – too many cardiology trainees want to learn CMR, whereas too few radiologists do.

## The imaging context at the Barts Heart Centre

The scale of the new unit is large. Anticipated activity per annum on site is 20,000 echocardiograms (plus 8,000 in satellite hospitals), 9,000 CMR scans, 3,500 cardiac CT scans and 500 nuclear scans (plus 500 in satellite hospitals). Advanced cardiac imaging will operate a network of 8 dedicated cardiac MRI scanners with 3 dedicated cardiac MRI scanners on site, and a further 5 operational in allied hospitals/services within a year (one additional research/private scanner planned, 2 dedicated cardiac scanners at Great Ormond Street, one new cardiac scanner at Royal Free Hospital and the existing scanner at The Heart Hospital continuing until 2018. Strategically the aim is that cardiac MRI functions within a multi-modality framework where the individual modalities work hand in hand – not just to share the clinical burden, but to ensure that patients are

investigated using the optimal technique to answer the clinical question cost-effectively, and to facilitate training and research opportunities. There will be a coherent operational model where the governance system is common across imaging, there will be common reporting rooms (echo, MRI and CT) – with distinctions being made between 'quiet' and 'teaching' reporting areas rather than modalities.

## CMR subspecialisation: New workflows

The main CMR department will have two 1.5T MAGNETOM Aera scanners and a 3T MAGNETOM Prisma. We chose Siemens because of the proven technical quality of their equipment, strong existing research relationships and their trajectory of investment and innovation in CMR. The first Aera and Prisma are currently operational. With 9,000 patients a year anticipated, we are aiming for CMR subspecialization: The 3T Prisma is anticipated to become almost exclusively a dedicated adenosine perfusion CMR platform, capitalizing on the high homogeneity and very high performance gradients. We aspire that perfusion scanning will be sufficiently robust on this magnet that the rest scan can be dropped, improving patient tolerability and workflow (we aim for two patients an hour instead of the standard 45 minute slots).

However, the narrow bore is not for all – the two MAGNETOM Aera scanners with 70 cm bores will take the larger or claustrophobic patients. Here there will also be further specialization – one of these magnets is going to be technician led as is standard, but the other will be mainly doctor run – our research fellows (currently >10) are all trained to run the CMR scanners and, at the Heart Hospital pass through 4 grades (observer, junior fellow, senior fellow, and level 3 supervisor – who are capable of running clinical lists at weekends without on-site consultant cover). This training is invaluable and generates a cohort of medics with PhDs capable of really leading and innovating in CMR – even if they never press the buttons themselves again. For reporting we have switched to a 3rd party server based viewing and reporting solution with

1 The new hospital sits behind the existing façade of the Barts square top (this is computer generated imagery from the architects) – a blend of the old and new.


2 The first 2 magnets – a Siemens 1.5T MAGNETOM Aera (**2A** – after a hard days work) and 3T MAGNETOM Prisma **(2B)** are up and running with the third arriving in around 6 months.

3 The atrium – which is hard to capture on just one view – serves as a focal point for the hospital.

25 floating licences. We will also be increasing the number of patients with implantable cardiac devices *in situ* that we scan – many local hospitals are unwilling to scan patients with even MR conditional devices and we have therefore found ourselves providing a regional service for this area.

## CMR research

Although there is a major service provision aspect, the BHC will have CMR clinical and research activity integrated. To this end, the Barts Cardiovascular Registry was set up to approach all our patients to consent for clinical and image data use and sharing for research, audit and service improvement purposes with consent for the acquisition of additional sequences that may not yet be part of clinical service provision. Major research interests span the entire translational pathway: From rapid imaging and new sequence design to establish new imaging biomarkers to using imaging surrogate endpoints in clinical trials to better diagnosing, prognosticating and monitoring treatment in cardiomyopathy, heart failure and coronary artery disease to cost-effectiveness analyses of imaging strategies.

One particular focus is in the use of T1 mapping to identify abnormal myocardium. Major new insights have been gained in rare diseases – amyloid, Fabrys and myocardial iron overload, and rapid progress is being made in diffuse fibrosis in the more common diseases such as aortic stenosis and hypertrophic cardiomyopathy. These developments and a community approach (in part coordinated by the 'T1 mapping development group' led to an international consensus statement on T1 mapping and very rapid technical improvements leading to a commercial sequence 'MyoMaps' containing a suite of mapping sequences.

The magnets are available for use for researchers out of hours at cost – to maximize flexibility and value-for-money from precious research funds. We also work closely with academic physics and engineering groups to maximize the potential of the scanners, and are acting as a Corelab facility for multicenter trials. Our research has been successful over the last few years – more than 15 young investigator awards or shortlists at international meetings have been achieved by the fellows over the last five years in the now merging units. The 2015 SCMR meeting in Nice emphasises this synergy – three fellows are shortlisted for investigator awards, each with a different supervisor, all now coming together under one roof in one institution – a great platform to grow from.

## CMR teaching

Course fellows are an integral part of the unit. We limit the numbers to ~two per MR scanner and typically for three months so there is involvement – helping with 'first reads' and providing a fresh perspective. Any fees paid are cycled into the research program – particularly for funding fellow travel, education, small equipment items and bridging costs. Several more didactic courses exist e.g. a biannual stress perfusion course, and the course portfolio is expected to expand to multimodality. We also host the London CMR meeting, a quarterly meeting of approximately 80 CMR specialists who meet to share clinical and research ideas and information. We have been

leading the European CMR certification and exam boards for the last few years.

## First impressions

The Cardiac Imaging unit has been open since 15 September 2014 with the other units due to decrease activity in Spring 2015, which means the service is currently working across multiple sites, increasing the capacity to remove waiting lists. Weekly staffing meetings are helping to define the culture and operating procedures, a process approached with the good will that is needed when the methods and cultures of three sites have to merge. We have not even started to touch the potential of the scanners – certainly much of our basics are being rewritten with new standards e.g. two cine slices per breath-hold typical, motion correction (MOCO) for perfusion always, PSIR for LGE always with T1 mapping on the majority and a future of new approaches such as potentially ceasing to breath-hold for the majority, dropping rest perfusion.

A visitor to the unit, Peter Kellman, MR physicist from NIH sums it up: "To see a new facility, a brand new hospital with CMR at the centre of cardiac care is very exciting. There is nothing niche about this high throughput environment. As a researcher in CMR, I feel proud of the efforts of the CMR community – their commitment, talent and resources is putting CMR to the forefront for decision making."

We endorse Peter's views. The future potential of the unit is hard to scope in detail – we look forward to delivering excellent care and the research aspects that go hand-in-hand – exploiting the gradient performance of the Prisma, a closer relationship with Industry to transition academic ideas and innovations into clinical practice and commercial products; and the use of new CMR endpoints for drug development and the at-scale use of CMR in biobanking studies, such as UK Biobank. Certainly, the future potential of the unit as a trail-blazing unit is massive.

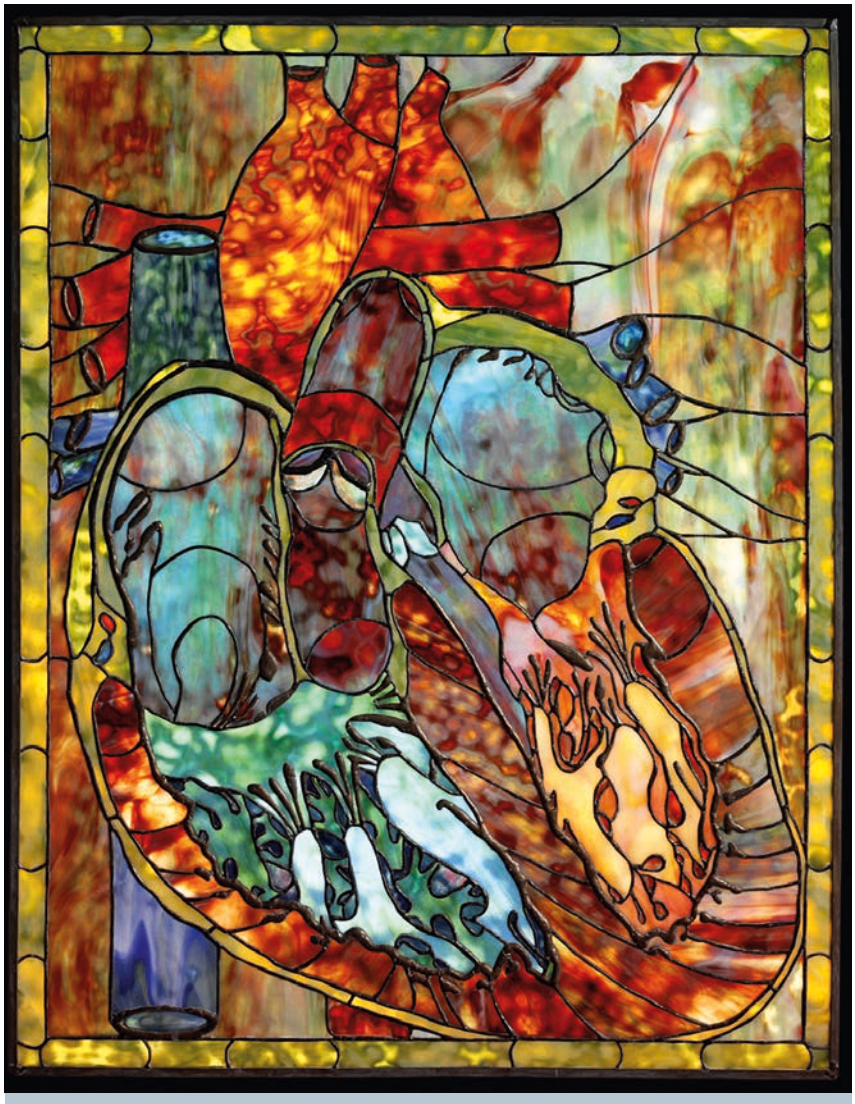

4 The reception of the unit will benefit from a new stained glass window being created and gifted by the artist Erica Rollings and her husband Robert Rollings, a CMR practionner from Savannah, GA, USA. This is a coronal view example of her work.

## Contact

James C. Moon
Institute of Cardiovascular Science
University College London
The Barts Heart Centre
16-18 Westmoreland Street
London W1G 8PH
UK
Phone: +44 (20) 34563081
james.moon@uclh.nhs.uk

# Clinical Benefits of T1 and ECV Mapping

Erik B. Schelbert, M.D., MS; Timothy C. Wong, M.D., MS

UPMC CMR Center, University of Pittsburgh Department of Medicine, Division of Cardiology, Pittsburgh, PA, USA

## Introduction

Clinicians and researchers can now quantify important changes in human myocardium using native T1 and extracellular volume fraction (ECV) measures. These novel parameters can facilitate diagnosis and prognosis and may enable the clinician to identify vulnerable patients and individualize therapy. These advances introduce new tools to detect focal and diffuse derangements in myocardial structure occurring in cardiac disease that can be otherwise difficult to detect. Increased ECV generally reflects expansion of the interstitial compartment (which includes the myocardial vasculature) whereas native T1 alterations may occur with processes affecting the myocyte or interstitium or both. These advances complement the traditional functional and geometric surrogates of vulnerability such as left ventricular ejection fraction and volumes [1], and may facilitate new paradigms of cardiac vulnerability [2]. Various aspects of T1 mapping and ECV have been reviewed in several publications [2-15].

## Increased native T1

Native T1 mapping images (without the use of gadolinium (Gd) contrast) are expressed in units of time, typically milliseconds, whereby each pixel encodes the non-contrast T1 value of the corresponding tissue region. These values can be depicted either with gray scale images or in color images with a scale bar typically on the T1 map image (Fig. 1). Clinical T1 mapping images are usually derived from a pixelwise parametric fit of a series of images acquired after one or more radiofrequency pulses. Image quality depends on image co-registration and many other factors that have been reviewed previously [5]. If reference values are carefully established for the particular protocol by which T1 is measured, the 'parametric' nature of T1 mapping then allows one to detect focal and diffuse disease processes, whether intracellular or interstitial, acute or chronic. The ability to detect diffuse disease is an important advantage of T1 mapping, because T1 weighted or T2 weighted images depend on focality (i.e., spatial heterogeneity) to detect changes, and they are inherently insensitive for the detection of diffuse disease processes [16].

If the clinical context is known, native T1 mapping can provide useful information. Native T1 generally increases in conditions that increase total myocardial water. These may include focal myocardial insults such as acute myocardial infarction [17, 18], myocarditis [16, 19], or stress cardiomyopathy [20]. Diffuse and acute myocardial insults also can increase native T1 including global myocarditis [16] and even hyperemia associated with vasodilator stress [21]. Chronic diffuse disease also increases native T1 including diffuse fibrosis [22] in cardiomyopathy [23, 24], amyloidosis [25, 27], and even systemic capillary leak syndrome [3]. In systemic light-chain amyloidosis, the extent of myocardial native T1 elevations relate to prognosis [27].

Similar to a multitude of other cardiac parameters, abnormalities in native T1 need to be interpreted within the clinical context. Edema, fibrosis, and amyloidosis can all increase native T1 values. Because the clinical context is usually known, (e.g., a chest pain syndrome or a new cardiomyopathy), T1 mapping remains promising. Investigations into the diagnostic and prognostic performance of native T1 remain an active area of research.

## Decreased native T1

Recent work suggests that low T1 appears sensitive and specific for detecting: a) iron overload [28] in hemochromatosis (Fig. 1), thalassemia, or other disease associated with excess iron, or b) myocardial glycosphyngolipid accumulation in Anderson-Fabry disease [29-30].

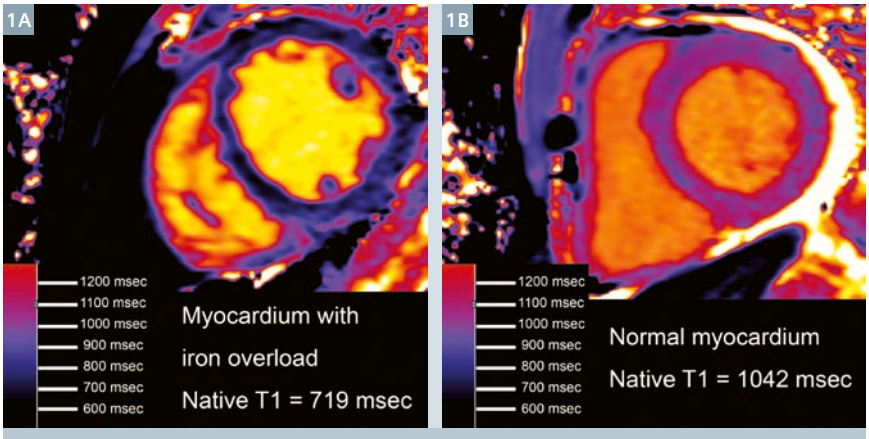


1 Native T1 in myocardium decreases with iron overload [28]. Native T1 maps are shown from a patient with hemochromatosis and iron overload **(1A)** and a remarkably low myocardial T1. The native T1 maps contrast with those from a patient with normal myocardial T1 who also happened to have a small pericardial effusion **(1B)**.

T1 mapping therefore introduces an important CMR tool to detect these important but uncommon conditions that may have immediate diagnostic implications. Native T1 mapping may also allow one to track response to therapy in these conditions given their ability to quantify disease burden, but such data have not yet been published. Still, T1 mapping could follow the precedent set by T2* (star) myocardial iron quantification measures. Myocardial T2* guided therapy appear to have culminated in lower cardiac mortality for thalassemia patients. T2* CMR measures can allow one to adjust iron chelation treatment based on myocardial siderosis quantification, and match intensity of therapy with disease severity. Mortality rates from cardiac iron overload appear to have improved coincident with the introduction of this capability to clinicians [31]. This scenario of measuring important myocardial tissue changes with CMR parameters vividly illustrates a case where the fundamental promise of CMR, i.e., to match the right treatment to the right patient, appears to have been realized. T1 mapping might have the potential to deliver similar results in the future.

## ECV (extracellular volume fraction) mapping

Extracellular volume fraction (ECV) measures quantify expansion of the interstitial space (including the myocardial vasculature estimated to be ~4.5% [32]) by using Gd contrast as an extracellular space marker [33-35]. ECV maps [3, 36, 37] are typically expressed as a percentage or a decimal that is encoded in the signal intensity of each pixel (Fig. 2). Clinical ECV mapping images are usually derived from a pixelwise parametric fit of a series of images acquired after one or more radiofrequency pulses for T1 mapping pre and post contrast. Coregistration is an important requirement for image quality.

The technique measures the myocardial uptake of Gd relative to plasma, assuming equilibration of Gd contrast between extracellular extravascular and intravascular compartments without any intravascular protein binding that would prevent free dispersion of contrast. The ratio of the relative concentrations in myocardium and whole blood are measured by their changes in relaxivity (i.e., $\Delta R1 = 1 / T1_{postcontrast} - 1 / T1_{precontrast}$) to yield the partition coefficient, $\lambda = \Delta R1_{myocardium} / \Delta R1_{blood}$. Since the Gd concentration in myocardial interstitial fluid is in equilibrium with plasma (not whole blood), one must correct for the displacement of Gd contrast by erythrocytes and multiply λ by (1-hematocrit) to yield ECV, which is expressed as a volume percent: ECV = λ (1-hematocrit). Water exchange effects may introduce some time or concentration dependence especially at high Gd concentrations or early after contrast administration [38-42], but these effects do not appear to represent major barriers to its clinical utility as an important imaging biomarker with significant prognostic potential [27, 43-46].

ECV is a robust measure of myocardial fibrosis assuming that myocardial edema or amyloidosis are absent. Despite the alterations in myocardial tissue that occur with tissue processing, multiple studies have shown high agreement between ECV and histologic measures of myocardial collagen content [39, 47-50]. ECV is also reproducible [38, 51-53] although varying degrees of Gd dose dependence have been observed as well as cross vendor issues [38-40, 42]. Nonetheless, $R^2$ values for correlation of myocardial fibrosis between ECV and histologic collagen volume fraction measures [39, 47, 49, 50, 54] range between 0.69-0.90 [36, 40, 42, 43, 47]. The $R^2$ values for ECV compare favorably to lower $R^2$ ranges of 0.32-0.61 between isolated post contrast T1 measures and collagen volume fraction measures, where isolated post contrast T1 measures are a surrogate for ECV [55, 57]. Isolated post contrast T1 values may be confounded by variations related weight-based gadolinium contrast dosing, renal clearance, time elapsed between contrast bolus and T1 measurement, and displacement of contrast by the hematocrit. Thus, gender, obesity, renal disease, technologist practice, and anemia would be expected to exert greater influence on isolated post contrast T1 measures than ECV.

ECV introduces a new concept in cardiology practice and permits one to dichotomize the myocardium into its cellular compartment (mostly myocytes) and interstitial compartment (mostly collagen, but also amyloid protein or edema depending on the clinical setting). The heart may be like other organs (lung-pulmonary fibrosis, liver-cirrhosis, kidney-glomerular fibrosis) where disruption of its architecture through interstitial expansion leads to organ dysfunction and vulnerability [2, 58]. Importantly, myocardial fibrosis appears to represent a modifiable 'intermediate phenotype' of pathologic remodeling [58-62] and

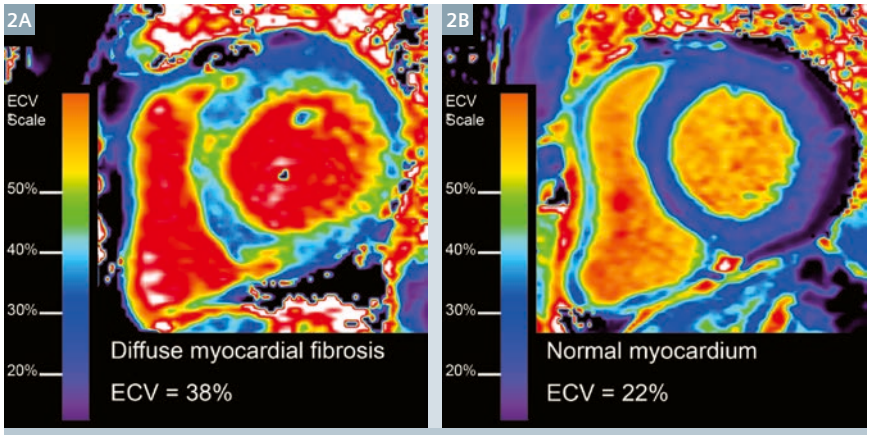


2 Examples of ECV maps quantifying diffuse fibrosis in a patient with nonischemic cardiomyopathy **(2A)**, which contrasts significantly with a patient without fibrosis who demonstrates normal ECV measures **(2B)**.

interstitial heart disease that is potentially treatable [63-66]. Myocardial fibrosis also indicates vulnerability to adverse outcomes [43-46, 67, 68]. Indeed, myocardial fibrosis can be a common disease pathway from a variety of potential insults [2]. Notably, 'antifibrotic' treatment with conventional medications that have been shown to reverse fibrosis [63-66] appears to improve patient outcomes in several large scale trials in select populations [68-74].

Preliminary outcomes data using ECV measures of myocardial fibrosis [43, 44] or amyloidosis [27], suggest that ECV may improve risk stratification [46] and identify therapeutic targets for therapy [2]. Single-center data are encouraging and show that increased ECV is associated with mortality or hospitalization for heart failure. Illustrating the importance of quantifying structural disease in the myocardium, these associations between ECV and outcomes appear stronger than more traditional risk stratifiers such as ejection fraction or disease exposure category (e.g., diabetes) [43, 44, 46]. Furthermore, myocardial ECV appears to predict outcomes better than left ventricular mass [75] suggesting that left ventricular myocardial 'quality' may be more important than its 'quantity'. ECV also appears to be more strongly associated with outcomes than more familiar LGE measures of nonischemic myocardial scar [43]. With risk adjustment for common clinical conditions that relate to outcomes in multivariable Cox regression models, ECV may improve the classification of individual patients at risk and provide added prognostic value beyond age, gender, renal function, myocardial infarction size, ejection fraction, and heart failure stage [46]. Interestingly, cardiac amyloidosis yields typically higher values of ECV than myocardial fibrosis which renders it a promising diagnostic tool and prognostic tool for cardiac amyloidosis [27, 49, 76-79].

## Overlap of T1 or ECV across patient groups for diagnosis versus prognosis

While initial results of T1 and ECV data appear encouraging, concern may arise when the distributions of ECV or other T1 data overlap according to a disease classification scheme (e.g., dilated cardiomyopathy [23, 50]) or a disease 'exposure variable' such as aortic stenosis [53, 80], diabetes [43], heart failure with or without preserved ejection fraction [81, 82], etc. When native T1 or ECV are used as a diagnostic tool to detect that condition or disease classification scheme, this concern is valid. Overlapping distributions of T1 and ECV may pose limitations for their use as a diagnostic tool specifically for that the classification scheme or disease 'exposure variable'. Yet, it is important to put this concern into context. It is expected that the myocardial 'response' to a given stimulus or disease state measured by T1 mapping may overlap across disease categories. For example, the spectrum of myocardial fibrosis measured by histology, is known to vary across individuals [39, 50, 80, 83], reflected in the robust histologic validation data for ECV where one encounters a spectrum of disease [39, 47-50]. Determinants of myocardial fibrosis [2] and amyloidosis accumulation remain incompletely understood.

For prognostic purposes, however, the goal of native T1 or ECV is to measure the myocardial 'response' to a given stimulus from a disease state or classification scheme. This 'response' – or lack thereof – may be more prognostically relevant than the disease state or classification scheme. It is essential to recognize that outcomes data are the final arbiter of what constitutes eventual vulnerability to the patient among the various parameters that can be measured in the genesis of various disease states. Ascertainment of subsequent event rates thus represents the gold standard for vulnerability. Therefore, any overlap of ECV data (or other T1 data) between disease categories do not necessarily limit their clinical assessment of vulnerability. Nor does overlap of any myocardial fibrosis across disease categories relegate its status as a biologically and prognostically meaningful biomarker. Indeed, ECV has robust histological validation data [39, 47-50] and has been shown to have high reproducibility [38, 51, 52]. On the contrary, ECV measures of myocardial fibrosis might be the critical determinant of vulnerability rather than a patient's disease category or classification (e.g., diabetes [43]).

Outcomes data are necessary to compare T1 or ECV measures with more traditional disease states of classification schemes for prognostic purposes. Such data are important because they inform paradigms of disease. In general, the stronger the association with outcomes, the more likely the specific measurement is biologically important. Trials that modify the measurement under investigation can then distinguish whether the measurement is a risk marker or a risk factor. Notably, despite any overlap in disease category or classification scheme, preliminary data demonstrate that ECV may improve the classification of individual patients at risk and provide added prognostic value beyond age, gender, renal function, myocardial infarction size, ejection fraction, and heart failure stage [46]. Additional outcomes data regarding T1 mapping and ECV mapping are undoubtedly forthcoming in work already underway.

## Conclusion

T1 and ECV mapping provide new opportunities to understand myocardial disease. T1 is sensitive to myocardial processes that affect the myocardium globally, i.e., disease specific to the myocyte, the interstitial compartment, or both. Conversely, ECV detects abnormalities limited to expansion of the extracellular compartment, typically fibrosis but also amyloidosis and edema (depending on the clinical context). Emerging work suggests that T1 mapping and ECV mapping have the potential to improve the diagnosis of disease including the burden of disease. Recent work also suggests that T1 mapping and ECV mapping might refine risk stratification. Ultimately, T1 mapping and ECV mapping promise to improve care by matching the right therapy to each patient, but further work is needed to realize this promise.

## References


1 Friedrich MG. There is more than shape and function. J Am Coll Cardiol. 2008;52:1581-1583.
2 Schelbert EB, Fonarow GC, Bonow RO, Butler J, Gheorghiade M. Therapeutic Targets in Heart Failure: Refocusing on the Myocardial Interstitium. J Am Coll Cardiol. 2014;63:2188-2198.
3 Kellman P, Wilson JR, Xue H, Bandettini WP, Shanbhag SM, Druey KM, Ugander M, Arai AE. Extracellular volume fraction mapping in the myocardium, Part 2: Initial Clinical Experience. J Cardiovasc Magn Reson. 2012;14:64.
4 Treibel TA, White SK, Moon JC. Myocardial Tissue Characterization: Histological and Pathophysiological Correlation. Curr Cardiovasc Imaging Rep. 2014;7:9254.
5 Moon JC, Messroghli DR, Kellman P, Piechnik SK, Robson MD, Ugander M, Gatehouse PD, Arai AE, Friedrich MG, Neubauer S, Schulz-Menger J, Schelbert EB. Myocardial T1 mapping and extracellular volume quantification: a Society for Cardiovascular Magnetic Resonance (SCMR) and CMR Working Group of the European Society of Cardiology consensus statement. J Cardiovasc Magn Reson. 2013;15:92.
6 Salerno M, Kramer CM. Advances in parametric mapping with CMR imaging. JACC Cardiovasc Imaging. 2013;6:806-822.
7 Ambale-Venkatesh B, Lima JA. Cardiac MRI: a central prognostic tool in myocardial fibrosis. Nat Rev Cardiol. 2014.
8 Maestrini V, Treibel TA, White SK, Fontana M, Moon JC. T1 Mapping for Characterization of Intracellular and Extracellular Myocardial Diseases in Heart Failure. Curr Cardiovasc Imaging Rep. 2014;7:9287.
9 Jellis CL, Kwon DH. Myocardial T1 mapping: modalities and clinical applications. Cardiovasc Diagn Ther. 2014;4:126-137.
10 Sado DM, Flett AS, Banypersad SM, White SK, Maestrini V, Quarta G, Lachmann RH, Murphy E, Mehta A, Hughes DA, McKenna WJ, Taylor AM, Hausenloy DJ, Hawkins PN, Elliott PM, Moon JC. Cardiovascular magnetic resonance measurement of myocardial extracellular volume in health and disease. Heart. 2012;98:1436-1441.
11 Rogers T, Yap ML, Puntmann VO. Myocardial T1 mapping: a non-invasive alternative to tissue diagnosis? Eur Heart J Cardiovasc Imaging. 2014.
12 Messroghli DM, Schelbert EB. Clinical Applications of Cardiac T1 Mapping. Radiology. 2015;in press.
13 Mewton N, Liu CY, Croisille P, Bluemke D, Lima JA. Assessment of myocardial fibrosis with cardiovascular magnetic resonance. J Am Coll Cardiol. 2011;57:891-903.
14 h-Ici DO, Jeuthe S, Al-Wakeel N, Berger F, Kuehne T, Kozerke S, Messroghli DR. T1 mapping in ischaemic heart disease. Eur Heart J Cardiovasc Imaging. 2014;15:597-602.
15 Wong TC. Cardiovascular Magnetic Resonance Imaging of Myocardial Interstitial Expansion in Hypertrophic Cardiomyopathy. Curr Cardiovasc Imaging Rep. 2014;7:9267.
16 Ferreira VM, Piechnik SK, Dall'Armellina E, Karamitsos TD, Francis JM, Ntusi N, Holloway C, Choudhury RP, Kardos A, Robson MD, Friedrich MG, Neubauer S. Native T1-mapping detects the location, extent and patterns of acute myocarditis without the need for gadolinium contrast agents. J Cardiovasc Magn Reson. 2014;16:36.
17 Ugander M, Bagi PS, Oki AJ, Chen B, Hsu LY, Aletras AH, Shah S, Greiser A, Kellman P, Arai AE. Myocardial edema as detected by pre-contrast T1 and T2 CMR delineates area at risk associated with acute myocardial infarction. JACC Cardiovasc Imaging. 2012;5:596-603.
18 Messroghli DR, Niendorf T, Schulz-Menger J, Dietz R, Friedrich MG. T1 mapping in patients with acute myocardial infarction. J Cardiovasc Magn Reson. 2003;5:353-359.
19 Ferreira VM, Piechnik SK, Dall'armellina E, Karamitsos TD, Francis JM, Ntusi N, Holloway C, Choudhury RP, Kardos A, Robson MD, Friedrich MG, Neubauer S. T Mapping for the Diagnosis of Acute Myocarditis Using CMR: Comparison to T-Weighted and Late Gadolinium Enhanced Imaging. JACC Cardiovasc Imaging. 2013.
20 Ferreira VM, Piechnik SK, Dall'Armellina E, Karamitsos TD, Francis JM, Choudhury RP, Friedrich MG, Robson MD, Neubauer S. Non-contrast T1-mapping detects acute myocardial edema with high diagnostic accuracy: a comparison to T2-weighted cardiovascular magnetic resonance. J Cardiovasc Magn Reson. 2012;14:42.
21 Mahmod M, Piechnik SK, Levelt E, Ferreira VM, Francis JM, Lewis A, Pal N, Dass S, Ashrafian H, Neubauer S, Karamitsos TD. Adenosine stress native T1 mapping in severe aortic stenosis: evidence for a role of the intravascular compartment on myocardial T1 values. J Cardiovasc Magn Reson. 2014;16:92.
22 Bull S, White SK, Piechnik SK, Flett AS, Ferreira VM, Loudon M, Francis JM, Karamitsos TD, Prendergast BD, Robson MD, Neubauer S, Moon JC, Myerson SG. Human non-contrast T1 values and correlation with histology in diffuse fibrosis. Heart. 2013;99:932-937.
23 Puntmann VO, Voigt T, Chen Z, Mayr M, Karim R, Rhode K, Pastor A, Carr-White G, Razavi R, Schaeffter T, Nagel E. Native T1 mapping in differentiation of normal myocardium from diffuse disease in hypertrophic and dilated cardiomyopathy. JACC Cardiovasc Imaging. 2013;6:475-484.
24 Puntmann VO, D'Cruz D, Smith Z, Pastor A, Choong P, Voigt T, Carr-White G, Sangle S, Schaeffter T, Nagel E. Native myocardial T1 mapping by cardiovascular magnetic resonance imaging in subclinical cardiomyopathy in patients with systemic lupus erythematosus. Circ Cardiovasc Imaging. 2013;6:295-301.
25 Fontana M, Banypersad SM, Treibel TA, Maestrini V, Sado DM, White SK, Pica S, Castelletti S, Piechnik SK, Robson MD, Gilbertson JA, Rowczenio D, Hutt DF, Lachmann HJ, Wechalekar AD, Whelan CJ, Gillmore JD, Hawkins PN, Moon JC. Native T1 Mapping in Transthyretin Amyloidosis. JACC Cardiovasc Imaging. 2014.
26 Karamitsos TD, Piechnik SK, Banypersad SM, Fontana M, Ntusi NB, Ferreira VM, Whelan CJ, Myerson SG, Robson MD, Hawkins PN, Neubauer S, Moon JC. Noncontrast T1 mapping for the diagnosis of cardiac amyloidosis. JACC Cardiovasc Imaging. 2013;6:488-497.
27 Banypersad SM, Fontana M, Maestrini V, Sado DM, Captur G, Petrie A, Piechnik SK, Whelan CJ, Herrey AS, Gillmore JD, Lachmann HJ, Wechalekar AD, Hawkins PN, Moon JC. T1 mapping and survival in systemic light-chain amyloidosis. Eur Heart J. 2014.
28 Sado DM, Maestrini V, Piechnik SK, Banypersad SM, White SK, Flett AS, Robson MD, Neubauer S, Ariti C, Arai A, Kellman P, Yamamura J, Schoennagel BP, Shah F, Davis B, Trompeter S, Walker M, Porter J, Moon JC. Noncontrast myocardial T mapping using cardiovascular magnetic resonance for iron overload. J Magn Reson Imaging. 2014.
29 Sado DM, White SK, Piechnik SK, Banypersad SM, Treibel T, Captur G, Fontana M, Maestrini V, Flett AS, Robson MD, Lachmann RH, Murphy E, Mehta A, Hughes D, Neubauer S, Elliott PM, Moon JC. The Identification and Assessment of Anderson Fabry Disease by Cardiovascular Magnetic Resonance Non-Contrast Myocardial T1 Mapping. Circ Cardiovasc Imaging. 2013.
30 Thompson RB, Chow K, Khan A, Chan A, Shanks M, Paterson I, Oudit GY. T1 Mapping with CMR Is Highly Sensitive for Fabry Disease Independent of Hypertrophy and Gender. Circ Cardiovasc Imaging. 2013.
31 Modell B, Khan M, Darlison M, Westwood MA, Ingram D, Pennell DJ. Improved survival of thalassaemia major in the UK and relation to T2* cardiovascular magnetic resonance. J Cardiovasc Magn Reson. 2008;10:42.
32 Jerosch-Herold M, Sheridan DC, Kushner JD, Nauman D, Burgess D, Dutton D, Alharethi R, Li D, Hershberger RE. Cardiac magnetic resonance imaging of myocardial contrast uptake and blood flow in patients affected with idiopathic or familial dilated cardiomyopathy. Am J

Physiol Heart Circ Physiol. 2008;295:H1234-H1242.
33 Arheden H, Saeed M, Higgins CB, Gao DW, Bremerich J, Wyttenbach R, Dae MW, Wendland MF. Measurement of the distribution volume of gadopentetate dimeglumine at echo-planar MR imaging to quantify myocardial infarction: comparison with 99mTc-DTPA autoradiography in rats. Radiology. 1999;211:698-708.
34 Poole-Wilson PA. The Intracellular pH, Potassium and Electrolyte Content of Heart Muscle in Acidosis and Alkalosis. London: University of Cambridge; 1975.
35 Brading AF, Jones AW. Distribution and kinetics of CoEDTA in smooth muscle, and its use as an extracellular marker. J Physiol. 1969;200:387-401.
36 Ugander M, Oki AJ, Hsu LY, Kellman P, Greiser A, Aletras AH, Sibley CT, Chen MY, Bandettini WP, Arai AE. Extracellular volume imaging by magnetic resonance imaging provides insights into overt and sub-clinical myocardial pathology. Eur Heart J. 2012;33:1268-1278.
37 Kellman P, Wilson JR, Xue H, Ugander M, Arai AE. Extracellular volume fraction mapping in the myocardium, Part 1: Evaluation of an automated method. J Cardiovasc Magn Reson. 2012;14:63.
38 Schelbert EB, Testa SM, Meier CG, Ceyrolles WJ, Levenson JE, Blair AJ, Kellman P, Jones BL, Ludwig DR, Schwartzman D, Shroff SG, Wong TC. Myocardial extravascular extracellular volume fraction measurement by gadolinium cardiovascular magnetic resonance in humans: slow infusion versus bolus. J Cardiovasc Magn Reson. 2011;13:16.
39 Miller CA, Naish J, Bishop P, Coutts G, Clark D, Zhao S, Ray SG, Yonan N, Williams SG, Flett AS, Moon JC, Greiser A, Parker GJ, Schmitt M. Comprehensive Validation of Cardiovascular Magnetic Resonance Techniques for the Assessment of Myocardial Extracellular Volume. Circ Cardiovasc Imaging. 2013.
40 Dabir D, Child N, Kalra A, Rogers T, Gebker R, Jabbour A, Plein S, Yu C-Y, Otton J, Kidambi A, McDiarmid A, Broadbent D, Higgins DM, Schnackenburg B, Foote L, Cummins C, Nagel E, Puntmann VO. Reference values for healthy human myocardium using a T1 mapping methodology: results from the International T1 Multicenter cardiovascular magnetic resonance study. J Cardiovasc Magn Reson. 2014;16:69.
41 Coelho-Filho OR, Mongeon FP, Mitchell R, Moreno H, Jr., Nadruz W, Jr., Kwong R, Jerosch-Herold M. The Role of Transcytolemmal Water Exchange in Magnetic Resonance Measurements of Diffuse Myocardial Fibrosis in Hypertensive Heart Disease. Circ Cardiovasc Imaging. 2012.
42 Kawel N, Nacif M, Zavodni A, Jones J, Liu S, Sibley CT, Bluemke DA. T1 mapping of the myocardium: intra-individual assessment of post-contrast T1 time evolution and extracellular volume fraction at 3T for Gd-DTPA and Gd-BOPTA. J Cardiovasc Magn Reson. 2012;14:26.
43 Wong TC, Piehler K, Kang IA, Kadakkal A, Kellman P, Schwartzman DS, Mulukutla SR, Simon MA, Shroff SG, Kuller LH, Schelbert EB. Myocardial Extracellular Volume Fraction Quantified By Cardiovascular Magnetic Resonance is Increased in Diabetes and Associated with Mortality and Incident Heart Failure Admission. Eur Heart J. 2014;35:657-664.
44 Wong TC, Piehler K, Meier CG, Testa SM, Klock AM, Aneizi AA, Shakesprere J, Kellman P, Shroff SG, Schwartzman DS, Mulukutla SR, Simon MA, Schelbert EB. Association between extracellular matrix expansion quantified by cardiovascular magnetic resonance and short-term mortality. Circulation. 2012;126:1206-1216.
45 Wong TC, Piehler KM, Kellman P, Schelbert EB. Extracellular matrix expansion is more strongly associated with cardiovascular outcomes than left ventricular mass. (Abstract). J Am Coll Cardiol. 2014;63:A986.
46 Schelbert EB, Piehler KM, Zareba KM, Moon JC, Ugander M, Messroghli DR, Valeti U, Chang C-CH, Shroff SG, Miller CA, Schmitt M, Kellman P, Butler J, Gheorghiade M, Wong TC. Extracellular matric expansion in non-infarcted myocardium is associated with subsequent death, hospitalization for heart failure, or both across the ejection fraction spectrum (Abstract). J Am Coll Cardiol. 2014;63:A1007.
47 Flett AS, Hayward MP, Ashworth MT, Hansen MS, Taylor AM, Elliott PM, McGregor C, Moon JC. Equilibrium contrast cardiovascular magnetic resonance for the measurement of diffuse myocardial fibrosis: preliminary validation in humans. Circulation. 2010;122:138-144.
48 Fontana M, White SK, Banypersad SM, Sado DM, Maestrini V, Flett AS, Piechnik SK, Neubauer S, Roberts N, Moon J. Comparison of T1 mapping techniques for ECV quantification. Histological validation and reproducibility of ShMOLLI versus multibreath-hold T1 quantification equilibrium contrast CMR. J Cardiovasc Magn Reson. 2012;14:88.
49 White SK, Sado DM, Fontana M, Banypersad SM, Maestrini V, Flett AS, Piechnik SK, Robson MD, Hausenloy DJ, Sheikh AM, Hawkins PN, Moon JC. T1 Mapping for Myocardial Extracellular Volume Measurement by CMR: Bolus Only Versus Primed Infusion Technique. JACC Cardiovasc Imaging. 2013;6:955-962.
50 Aus dem Siepen F, Buss SJ, Messroghli D, Andre F, Lossnitzer D, Seitz S, Keller M, Schnabel PA, Giannitsis E, Korosoglou G, Katus HA, Steen H. T1 mapping in dilated cardiomyopathy with cardiac magnetic resonance: quantification of diffuse myocardial fibrosis and comparison with endomyocardial biopsy. Eur Heart J Cardiovasc Imaging. 2014.
51 Liu S, Han J, Nacif MS, Jones J, Kawel N, Kellman P, Sibley CT, Bluemke DA. Diffuse myocardial fibrosis evaluation using cardiac magnetic resonance T1 mapping: sample size considerations for clinical trials. J Cardiovasc Magn Reson. 2012;14:90.
52 Kawel N, Nacif M, Zavodni A, Jones J, Liu S, Sibley CT, Bluemke DA. T1 mapping of the myocardium: Intra-individual assessment of the effect of field strength, cardiac cycle and variation by myocardial region. J Cardiovasc Magn Reson. 2012;14:27.
53 Chin CW, Semple S, Malley T, White AC, Mirsadraee S, Weale PJ, Prasad S, Newby DE, Dweck MR. Optimization and comparison of myocardial T1 techniques at 3T in patients with aortic stenosis. Eur Heart J Cardiovasc Imaging. 2014;15:556-565.
54 Fontana M, White SK, Banypersad SM, Sado DM, Maestrini V, Flett AS, Piechnik SK, Neubauer S, Roberts N, Moon JC. Comparison of T1 mapping techniques for ECV quantification. Histological validation and reproducibility of ShMOLLI versus multibreath-hold T1 quantification equilibrium contrast CMR. J Cardiovasc Magn Reson. 2012;14:88.
55 Sibley CT, Noureldin RA, Gai N, Nacif MS, Liu S, Turkbey EB, Mudd JO, van der Geest RJ, Lima JA, Halushka MK, Bluemke DA. T1 Mapping in cardiomyopathy at cardiac MR: comparison with endomyocardial biopsy. Radiology. 2012;265:724-732.
56 Iles LM, Ellims AH, Llewellyn H, Hare JL, Kaye DM, McLean CA, Taylor AJ. Histological validation of cardiac magnetic resonance analysis of regional and diffuse interstitial myocardial fibrosis. Eur Heart J Cardiovasc Imaging. 2014.
57 Iles L, Pfluger H, Phrommintikul A, Cherayath J, Aksit P, Gupta SN, Kaye DM, Taylor AJ. Evaluation of diffuse myocardial fibrosis in heart failure with cardiac magnetic resonance contrast-enhanced T1 mapping. J Am Coll Cardiol. 2008;52:1574-1580.
58 Wynn TA, Ramalingam TR. Mechanisms of fibrosis: therapeutic translation for fibrotic disease. Nat Med. 2012;18:1028-1040.
59 Weber KT, Brilla CG. Pathological hypertrophy and cardiac interstitium. Fibrosis and renin-angiotensin-aldosterone system. Circulation. 1991;83:1849-1865.
60 Swynghedauw B. Molecular mechanisms of myocardial remodeling. Physiol Rev. 1999;79:215-262.
61 Mann DL, Barger PM, Burkhoff D. Myocardial recovery and the failing heart: myth, magic, or molecular target? J Am Coll Cardiol. 2012;60:2465-2472.

62 Kong P, Christia P, Frangogiannis NG. The pathogenesis of cardiac fibrosis. Cell Mol Life Sci. 2013.

63 Schwartzkopff B, Brehm M, Mundhenke M, Strauer BE. Repair of coronary arterioles after treatment with perindopril in hypertensive heart disease. Hypertension. 2000;36:220-225.

64 Brilla CG, Funck RC, Rupp H. Lisinopril-mediated regression of myocardial fibrosis in patients with hypertensive heart disease. Circulation. 2000;102:1388-1393.

65 Diez J, Querejeta R, Lopez B, Gonzalez A, Larman M, Martinez Ubago JL. Losartan-dependent regression of myocardial fibrosis is associated with reduction of left ventricular chamber stiffness in hypertensive patients. Circulation. 2002;105:2512-2517.

66 Izawa H, Murohara T, Nagata K, Isobe S, Asano H, Amano T, Ichihara S, Kato T, Ohshima S, Murase Y, Iino S, Obata K, Noda A, Okumura K, Yokota M. Mineralocorticoid receptor antagonism ameliorates left ventricular diastolic dysfunction and myocardial fibrosis in mildly symptomatic patients with idiopathic dilated cardiomyopathy: a pilot study. Circulation. 2005;112:2940-2945.

67 Tamarappoo BK, John BT, Reinier K, Teodorescu C, Uy-Evanado A, Gunson K, Jui J, Chugh SS. Vulnerable Myocardial Interstitium in Patients With Isolated Left Ventricular Hypertrophy and Sudden Cardiac Death: A Postmortem Histological Evaluation J Am Heart Assoc. 2012;1:e001511.

68 Zannad F, Alla F, Dousset B, Perez A, Pitt B. Limitation of excessive extracellular matrix turnover may contribute to survival benefit of spironolactone therapy in patients with congestive heart failure: insights from the randomized aldactone evaluation study (RALES). Rales Investigators. Circulation. 2000;102:2700-2706.

69 Yusuf S, Sleight P, Pogue J, Bosch J, Davies R, Dagenais G. Effects of an angiotensin-converting-enzyme inhibitor, ramipril, on cardiovascular events in high-risk patients. The Heart Outcomes Prevention Evaluation Study Investigators. N Engl J Med. 2000;342:145-153.

70 The SOLVD Investigators. Effect of enalapril on survival in patients with reduced left ventricular ejection fractions and congestive heart failure. N Engl J Med. 1991;325:293-302.

71 Pfeffer MA, Braunwald E, Moye LA, Basta L, Brown EJ, Jr., Cuddy TE, Davis BR, Geltman EM, Goldman S, Flaker GC, et al. Effect of captopril on mortality and morbidity in patients with left ventricular dysfunction after myocardial infarction. Results of the survival and ventricular enlargement trial. The SAVE Investigators. N Engl J Med. 1992;327:669-677.

72 Pitt B, Zannad F, Remme WJ, Cody R, Castaigne A, Perez A, Palensky J, Wittes J. The effect of spironolactone on morbidity and mortality in patients with severe heart failure. Randomized Aldactone Evaluation Study Investigators. N Engl J Med. 1999;341:709-717.

73 Pitt B, Remme W, Zannad F, Neaton J, Martinez F, Roniker B, Bittman R, Hurley S, Kleiman J, Gatlin M. Eplerenone, a selective aldosterone blocker, in patients with left ventricular dysfunction after myocardial infarction. N Engl J Med. 2003;348:1309-1321.

74 Pfeffer MA, McMurray JJ, Velazquez EJ, Rouleau JL, Kober L, Maggioni AP, Solomon SD, Swedberg K, Van de Werf F, White H, Leimberger JD, Henis M, Edwards S, Zelenkofske S, Sellers MA, Califf RM. Valsartan, captopril, or both in myocardial infarction complicated by heart failure, left ventricular dysfunction, or both. N Engl J Med. 2003;349:1893-1906.

75 Wong TC, Piehler KM, Kellman P, Schelbert EB. Extracellular matrix expansion is more strongly associated with cardiovascular outcomes than left ventricular mass. J Am Coll Cardiol. 2014;63:A986.

76 Mongeon FP, Jerosch-Herold M, Coelho-Filho OR, Blankstein R, Falk RH, Kwong RY. Quantification of extracellular matrix expansion by CMR in infiltrative heart disease. JACC Cardiovasc Imaging. 2012;5:897-907.

77 Robbers LF, Baars EN, Brouwer WP, Beek AM, Hofman MB, Niessen HW, van Rossum AC, Marcu CB. T1 mapping shows increased extracellular matrix size in the myocardium due to amyloid depositions. Circ Cardiovasc Imaging. 2012;5:423-426.

78 Banypersad SM, Sado DM, Flett AS, Gibbs SDJ, Pinney JH, Maestrini V, Cox AT, Fontana M, Whelan CJ, Wechalekar AD, Hawkins PN, Moon JC. Quantification of Myocardial Extracellular Volume Fraction in Systemic AL Amyloidosis: An Equilibrium Contrast Cardiovascular Magnetic Resonance Study. Circ Cardiovasc Imaging. 2012;6:34-39.

79 Barison A, Aquaro GD, Pugliese NR, Cappelli F, Chiappino S, Vergaro G, Mirizzi G, Todiere G, Passino C, Masci PG, Perfetto F, Emdin M. Measurement of myocardial amyloid deposition in systemic amyloidosis: insights from cardiovascular magnetic resonance imaging. J Intern Med. 2014.

80 Flett AS, Sado DM, Quarta G, Mirabel M, Pellerin D, Herrey AS, Hausenloy DJ, Ariti C, Yap J, Kolvekar S, Taylor AM, Moon JC. Diffuse myocardial fibrosis in severe aortic stenosis: an equilibrium contrast cardiovascular magnetic resonance study. Eur Heart J Cardiovasc Imaging. 2012;13:819-826.

81 Su MY, Lin LY, Tseng YH, Chang CC, Wu CK, Lin JL, Tseng WY. CMR-Verified Diffuse Myocardial Fibrosis Is Associated With Diastolic Dysfunction in HFpEF. JACC Cardiovasc Imaging. 2014;7:991-997.

82 Mascherbauer J, Marzluf BA, Tufaro C, Pfaffenberger S, Graf A, Wexberg P, Panzenbock A, Jakowitsch J, Bangert C, Laimer D, Schreiber C, Karakus G, Hulsmann M, Pacher R, Lang IM, Maurer G, Bonderman D. Cardiac magnetic resonance postcontrast T1 time is associated with outcome in patients with heart failure and preserved ejection fraction. Circ Cardiovasc Imaging. 2013;6:1056-1065.

83 van Heerebeek L, Borbely A, Niessen HW, Bronzwaer JG, van der Velden J, Stienen GJ, Linke WA, Laarman GJ, Paulus WJ. Myocardial structure and function differ in systolic and diastolic heart failure. Circulation. 2006;113:1966-1973.


## Contact


Erik Schelbert, MD, MS, FACC
Director, Cardiovascular Magnetic Resonance
Assistant Professor of Medicine
Assistant Professor of Clinical and Translational Science
University of Pittsburgh UPMC Heart and Vascular Institute
200 Lothrop Street, PUH A349
Pittsburgh, PA 15213
USA
Phone: +1 412-647-5840
Fax: +1 412-647-4227
schelberteb@upmc.edu

# Clinical Utility of Cardiac T1- and Extracellular Volume (ECV) Mapping. A Brief Review

Magnus Lundin, M.D.; Martin Ugander, M.D., Ph.D.

Department of Clinical Physiology, Karolinska Institutet and Karolinska University Hospital, Stockholm, Sweden

The clinical utility of cardiovascular magnetic resonance (CMR) is rooted in the ability to provide important clinical information on myocardial tissue characterization. Late gadolinium enhancement (LGE) sequences are established routine for detecting myocardial infarction and focal myocardial scarring of non-ischemic origin [1]. However, LGE is based on T1-weighted inversion recovery imaging and entails visual interpretation of relative signal intensities in relation to healthy myocardium.

CMR has been experimentally shown to be able to quantify the distribution of gadolinium-based extracellular contrast agents [2], also known as the extracellular volume fraction (ECV). The basis for measuring ECV is the measurement of T1 before and after the administration of a clinical gadolinium-based extracellular contrast agent at a clinical dose. The inverse of T1 (1/T1) is referred to as R1, and the change in R1 that occurs following contrast administration is proportional to contrast agent concentration. Importantly, blood has a known extracellular space which can be measured by venous blood sampling as 1-hematocrit. Consequently, since extracellular contrast agents distribute into the extracellular space, T1-mapping can be used to quantify relative contrast agents concentrations calibrated to the blood, thus yielding ECV.

ECV is a physiologically intuitive measure insofar as it measures the proportion of tissue comprised of the space between cells. It has recently become possible to generate ECV-maps in clinical routine through automated processing [3]. Myocardial ECV has a normal range of 20-30% [4], but is altered in various myocardial pathologies. These conditions include diffuse fibrosis, acute and chronic myocardial infarction, myocarditis, hypertrophic cardiomyopathy, dilated cardiomyopathy, and amyloidosis [4–6]. A benefit of ECV mapping is that it is measured in absolute units, which allows for a more accurate diagnosis in disease that homogeneously affect the myocardium. Furthermore, this allows for quantitative comparisons both over time in the same patient as well as comparisons between different patients. Importantly, use of mapping allows for visualization of the extent of changes in myocardial ECV.

Native T1-maps alone provide important clinical information, since native T1 is increased in conditions including inflammation [7] and edema in myocardial infarction [8]. T1 is also measured in absolute units as opposed to other sequences that can detect edema, including T2-weighted imaging. Furthermore, T1 is decreased in myocardial iron overload [9] as well as in myocardial glycolipid overload, as seen in Anderson-Fabry disease [10].

1

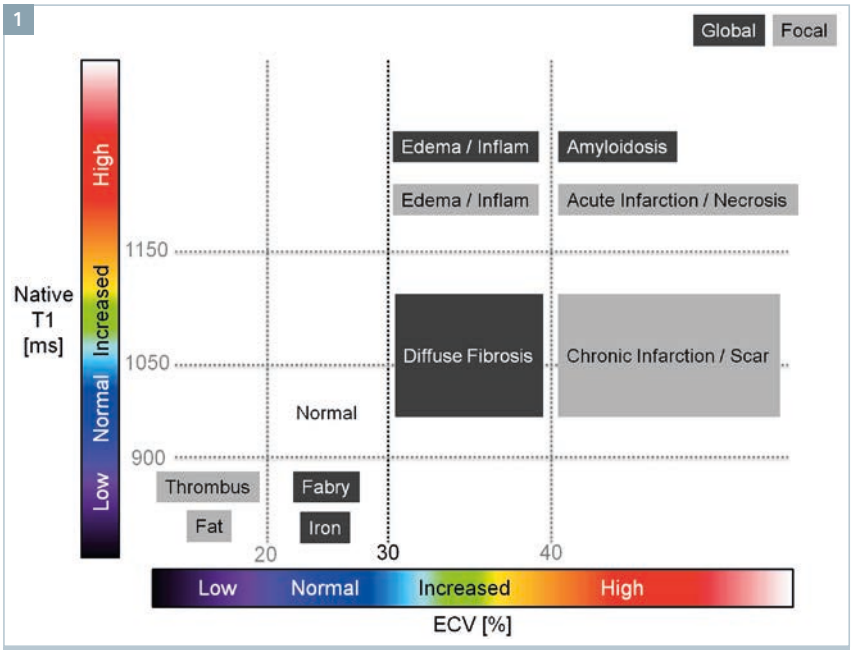


1 Schematic diagram for focal and global myocardial tissue characterization using native T1 measured in milliseconds, and the extracellular volume fraction (ECV) measured in percent. Absolute cutoff values defining normality for native T1 may vary depending on the exact sequence used for T1-mapping.

The combination of ECV-mapping and T1-mapping can provide quantitative characterization of a number of myocardial pathologies. Figure 1 is a schematic illustration that can be used to interpret the clinical results of T1 and ECV. Figures 2-5 show four clinical cases showing: T1-map (left), LGE (middle) and ECV-map (right). T1 is shown using a color scale from black (0 ms) to white (2000 ms), normal range is purple. LGE shows focal lesions as white and remote myocardium as black. ECV is shown using a color scale where blue is normal range (20-30%); turquoise and light green, indicates increased ECV; and red and white is very high ECV.

LGE: Late gadolinium enhancement
ECV: extracellular volume

Notably, ECV imaging has been proven to provide important prognostic information [11], and a first consensus statement on the use of T1 and ECV in CMR has been published [12]. Continued work is underway to enable implementation for optimized clinical workflow, and there is an expanding number of publications in the field.

Taken together, the combination of ECV-mapping and T1-mapping represent a powerful diagnostic tool in CMR. Not only can otherwise undetectable abnormalities be visualized, but findings can also be characterized in absolute units. This feature both improves the diagnostic accuracy and makes it possible to objectively determine the severity of disease.

2

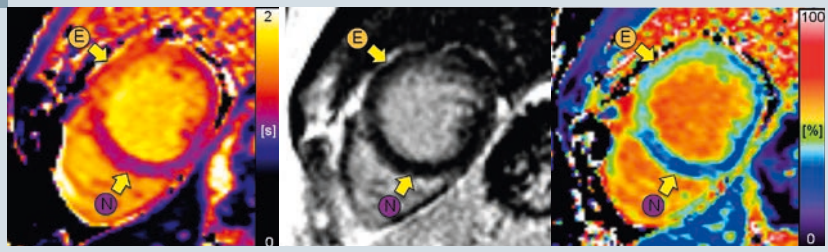


2 A 40-year-old woman presenting with chest pain and ST-elevation, but a normal invasive coronary angiogram. CMR shows segmental edema (E) based on increased T1 (1300 ms) and ECV (40%) compared to normal (N) myocardium (T1 1040 ms, ECV 29%). Note that the edematous segment appears normal on LGE. The case was interpreted as likely segmental stress cardiomyopathy or coronary spasm, and no infarction.

3

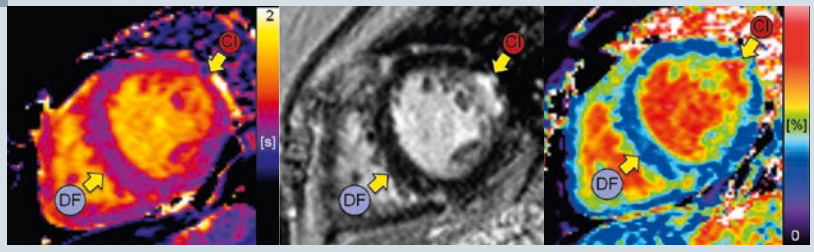


3 A 70-year-old woman with a chronic infarction (CI) that is shown clearly on both LGE and ECV (70%) and less clear on T1-maps (1140 ms). This patient also had diffuse fibrosis (DF) in the septum (T1 1075 ms, ECV 34%).

4

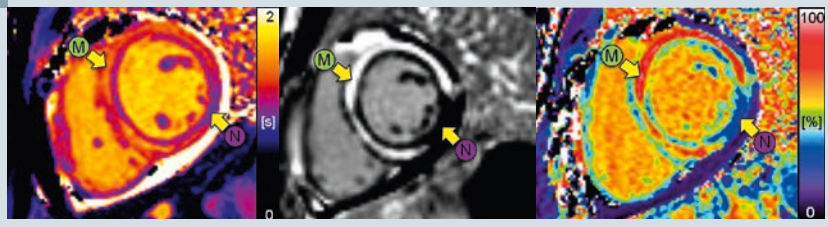


4 A 21-year-old man with acute presentation of myocarditis (M) midmurally in all segments except the inferolateral segment where the myocardium appears normal (N). The affected regions are shown clearly on both ECV (80%), LGE and T1 (1500 ms), in stark contrast to the normal segment (T1 1000 ms and ECV 27%).

5

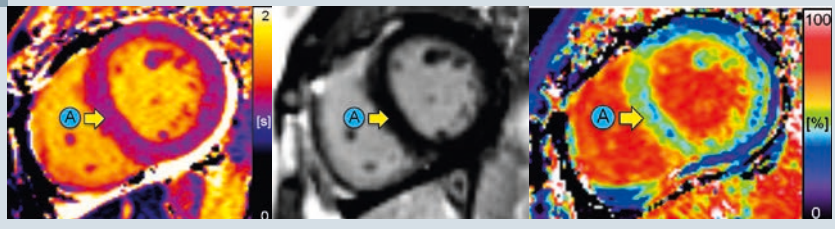


5 A 47-year-old woman with amyloidosis (A) with increased ECV (42%) and slightly increased T1 (1100 ms) but normal appearing LGE.

## References


1 Pennell DJ, Sechtem UP, Higgins CB, Manning WJ, Pohost GM, Rademakers FE, van Rossum AC, Shaw LJ, Yucel EK. Clinical indications for cardiovascular magnetic resonance (CMR): Consensus Panel report. Eur Heart J. 2004 Nov;25(21):1940–65.

2 Arheden H, Saeed M, Higgins CB, Gao D-W, Bremerich J, Wyttenbach R, Dae MW, Wendland MF. Measurement of the Distribution Volume of Gadopentetate Dimeglumine at Echo-planar MR Imaging to Quantify Myocardial Infarction: Comparison with 99mTc-DTPA Autoradiography. Radiology. 1999;211(3):698–708.

3 Kellman P, Wilson JR, Xue H, Ugander M, Arai AE. Extracellular volume fraction mapping in the myocardium, part 1: evaluation of an automated method. J Cardiovasc Magn Reson. 2012 Sep 10;14:63.

4 Kellman P, Wilson JR, Xue H, Bandettini WP, Shanbhag SM, Druey KM, Ugander M, Arai AE. Extracellular volume fraction mapping in the myocardium, part 2: initial clinical experience. J Cardiovasc Magn Reson. 2012 Jan;14:64.

5 Sado DM, Flett AS, Moon JC. Novel imaging techniques for diffuse myocardial fibrosis. Future Cardiol. 2011 Sep;7(5):643–50.

6 Ugander M, Oki AJ, Hsu L-Y, Kellman P, Greiser A, Aletras AH, Sibley CT, Chen MY, Bandettini WP, Arai AE. Extracellular volume imaging by magnetic resonance imaging provides insights into overt and sub-clinical myocardial pathology. Eur Heart J. 2012 May;33(10):1268–78.

7 Wassmuth R, Schulz-Menger J. Cardiovascular magnetic resonance imaging of myocardial inflammation. Expert Rev Cardiovasc Ther. 2011 Sep;9(9):1193–201.

8 Ugander M, Bagi PS, Oki AJ, Chen B, Hsu L-Y, Aletras AH, Shah S, Greiser A, Kellman P, Arai AE. Myocardial edema as detected by pre-contrast T1 and T2 CMR delineates area at risk associated with acute myocardial infarction. JACC Cardiovasc Imaging. 2012 Jun;5(6):596–603.

9 Sado DM, Maestrini V, Piechnik SK, Banypersad SM, White SK, Flett AS, Robson MD, Neubauer S, Ariti C, Arai A, Kellman P, Yamamura J, Schoennagel BP, Shah F, Davis B, Trompeter S, Walker M, Porter J, Moon JC. Noncontrast myocardial T1 mapping using cardiovascular magnetic resonance for iron overload. J Magn Reson Imaging. 2014 Aug 8;00. [Epub ahead of print].

10 Sado DM, White SK, Piechnik SK, Banypersad SM, Treibel T, Captur G, Fontana M, Maestrini V, Flett AS, Robson MD, Lachmann RH, Murphy E, Mehta A, Hughes D, Neubauer S, Elliott PM, Moon JC. Identification and assessment of Anderson-Fabry disease by cardiovascular magnetic resonance noncontrast myocardial T1 mapping. Circ Cardiovasc Imaging. 2013 May 1;6(3):392–8.

11 Wong TC, Piehler K, Meier CG, Testa SM, Klock AM, Aneizi AA, Shakesprere J, Kellman P, Shroff SG, Schwartzman DS, Mulukutla SR, Simon MA, Schelbert EB. Association between extracellular matrix expansion quantified by cardiovascular magnetic resonance and short-term mortality. Circulation. 2012 Sep 4;126(10):1206-16.

12 Moon JC, Messroghli DR, Kellman P, Piechnik SK, Robson MD, Ugander M, Gatehouse PD, Arai AE, Friedrich MG, Neubauer S, Schulz-Menger J, Schelbert EB; Society for Cardiovascular Magnetic Resonance Imaging; Cardiovascular Magnetic Resonance Working Group of the European Society of Cardiology. Myocardial T1 mapping and extracellular volume quantification: a Society for Cardiovascular Magnetic Resonance (SCMR) and CMR Working Group of the European Society of Cardiology consensus statement. J Cardiovasc Magn Reson. 2013 Oct 14;15:92.


## Contact


Martin Ugander, M.D., Ph.D.
Department of Clinical Physiology N2:01
Karolinska Institutet and
Karolinska University Hospital
SE-171 76 Stockholm
Sweden
Phone: +46709850088
martin.ugander@ki.se

# Myocardial T1 Mapping – Comparison of Techniques

Kelvin Chow, Ph.D.; Richard Thompson, Ph.D.

Department of Biomedical Engineering, University of Alberta, Edmonton, Canada

## Introduction

Diffuse myocardial fibrosis and other remodeling of the myocardial extracellular space are common pathological features of many cardiac diseases [1]. These changes can be measured non-invasively using magnetic resonance imaging (MRI) through changes in native (non-contrast) myocardial T1 relaxation times, post-contrast T1 times, and derived estimates of extracellular volume (ECV) using both native and post-contrast T1 values. Numerous clinical studies have found correlations between both myocardial T1 and ECV measurements and various metrics of disease severity in patient populations including heart failure [2], dilated cardiomyopathy [3], and amyloidosis [4]. These findings have also been further validated by histological correlations to MRI fibrosis measurements in human studies of aortic stenosis and hypertrophic cardiomyopathy, as well as infiltrative diseases such as amyloidosis [5-8]. A large single-centre study of myocardial ECV in consecutive patients showed increased ECV to be an independent predictor of short-term mortality [9], demonstrating its prognostic importance.

The ability to quickly and reliably assess diffuse myocardial fibrosis using MRI makes T1 and ECV promising surrogate biomarkers with the potential for widespread clinical utility [10-12]. This optimism has led to the development of a multitude of techniques for their measurement, each with unique properties, advantages, and disadvantages. Three major classes of T1 measurement techniques are reviewed here in order to provide insight into differences in reported T1 and ECV values and determine the most appropriate technique for potential new studies.

## T1 mapping techniques

**Continuous Look-Locker techniques**

The classic Look-Locker experiment consists of a series of measurements using a train of radiofrequency (RF) pulses with a short repetition time (TR) to more efficiently sample the T1 recovery curve [13]. This is commonly implemented using an inversion pulse followed by a continuous spoiled gradient recalled echo (GRE) readout [14] (Fig. 1A). Magnetization perturbation caused by the repeated RF excitations causes a shortening of the apparent relaxation time (T1*) and a reduction in the equilibrium magnetization. However, assuming that the TR << T1 and a flip angle <10° is used, the true T1 value can be calculated when using a standard 3-parameter exponential recovery model by applying the commonly termed "Look-Locker correction factor" [15] (Fig. 2A):

$$\text{Signal} = A - B*\exp(-TI/T1^*) \quad \text{[Eq. 1]}$$

$$T1 = (B/A - 1)T1^* \quad \text{[Eq. 2]}$$

Cardiac Look-Locker implementations typically use gated-segmented imaging readouts, with between 15-30 images acquired at different effective inversion recovery (TI) times and cardiac phases in a single breath-hold (Table 1). This *k*-space segmentation results in images with less temporal blurring compared to single-shot images, but with increased sensitivity to artifacts from poor breath-holding.

## Table 1

| | Continuous Look-Locker [3, 50] | MOLLI (Intermittent Look-Locker) [6, 18, 23, 29, 30, 49] | SASHA (Independently magnetization-preparation) [37, 44, 45] |
|---|---|---|---|
| Readout | GRE | bSSFP | bSSFP |
| *k*-space acquisition | segmented | single-shot | single-shot |
| Preparation pulse | inversion | inversion | saturation |
| Number of images | 15-30 | 7-11 | 11 (variable) |
| Duration | 1 breath-hold | 9-18 heartbeats | 11 heartbeats typical (variable) |
| Base matrix size | 176-192 | 192-256 | 192-256 |
| Flip angle | 10-12° | 35° | 70° |
| Myocardial T1 (1.5T) | Not reported | 939-1011 ms | 1174 ms |
| Normal ECV (1.5T) | 25% | 25-27% | 18-22% |

Comparison of typical pulse sequence parameters between three major classes of myocardial T1 mapping sequences.

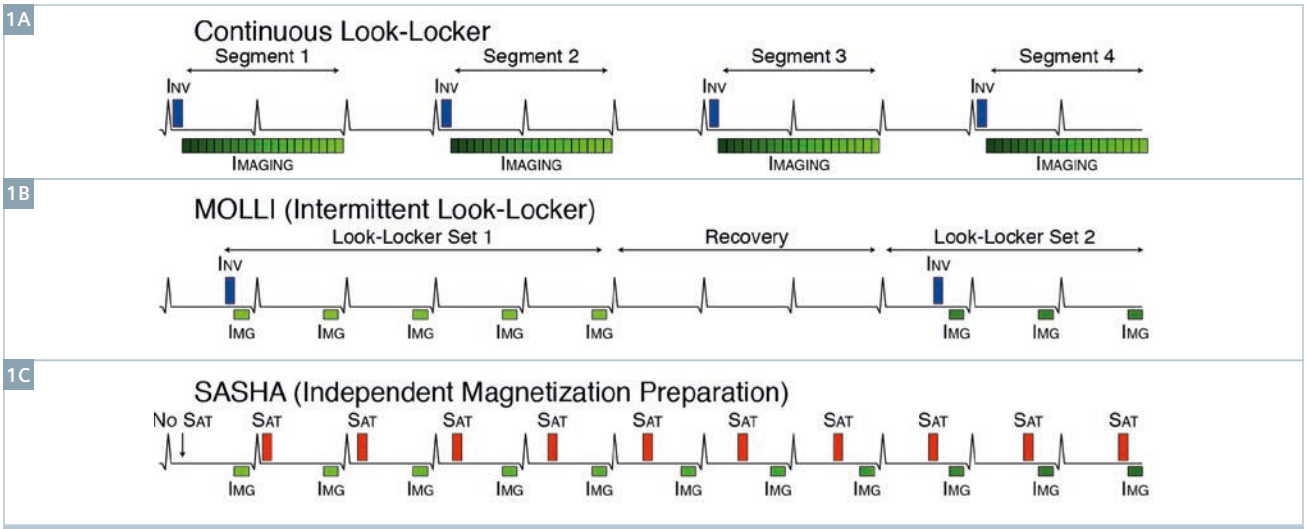


1 Pulse sequence diagram of three major classes of myocardial T1 mapping sequences. **(1A)** A continuous Look-Locker sequence acquires many segmented images following an inversion pulse. **(1B)** The MOLLI sequence consists of Look-Locker sets, each containing multiple single shot images following a single inversion, with recovery periods between sets. **(1C)** The SASHA sequence is composed of a non-saturated single-shot image followed by a series of images at variable saturation recovery times, with only a single image following each saturation pulse.

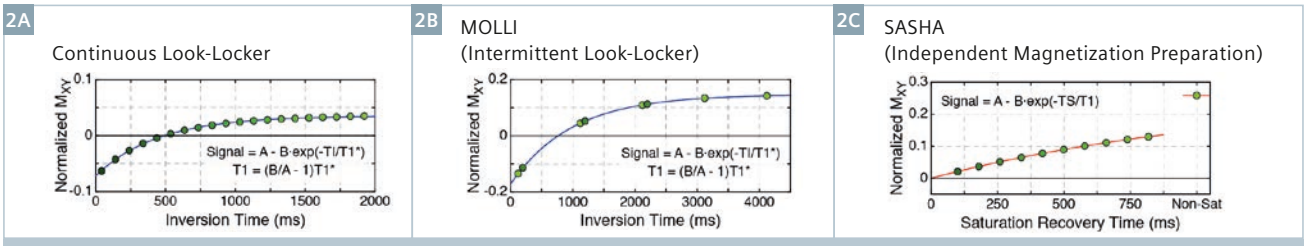


2 Sampling of the T1 recovery curve for three major classes of myocardial T1 mapping sequences. **(2A)** Continuous Look-Locker sequences have many data points along the recovery curve, but have lower SNR due to the low flip angle GRE readout. **(2B)** Samples of the recovery curve in MOLLI are clustered, with the spacing between clusters approximately equal to the R-R interval. The spacing within the clusters is determined by the "TI increment" between Look-Locker sets. Data is shown for a 5(3)3 scheme with an 80 ms TI increment. Both continuous and intermittent Look-Locker techniques generally use the "Look-Locker correction factor" to estimate true T1 values. **(2C)** The SASHA sequence samples a saturation recovery curve instead of an inversion recovery curve, with many data points at comparatively short TS times. A non-saturated image is assigned an infinitely long TS time and acts as an anchor point.

Look-Locker sequences with a continuous balanced steady-state free precession (bSSFP[1]) imaging readout such as the Small Animal Look-Locker Inversion recovery (SALLI) [16] and Multi-Contrast Late Enhancement (MCLE[1]) sequences [17] have been used to improve blood-tissue contrast and overall signal yield compared to GRE. These sequences also utilize the cardiac phase information to generate a cine-like time series for analysis of cardiac function.

Continuous Look-Locker sequences provide excellent sampling of the inversion recovery curve, but the cardiac motion between images that is intrinsic to the sequence design can be problematic for T1 quantification. Continuous through-plane cardiac motion in a typical short-axis slice results in signal enhancement as unexcited spins move into the imaging plane, modulating the shape of the recovery curve and potentially confounding calculated T1 values. Additionally, data analysis is time consuming because the myocardium must be manually contoured for each image separately and parametric T1 pixel maps cannot be readily generated.

### Intermittent Look-Locker techniques

The MOdified Look-Locker Inversion recovery (MOLLI[1]) technique overcomes many of the challenges associated with cardiac and respiratory motion by using 'intermittent' cardiac-gated single-shot readouts instead of continuous readouts [18]. The sequence consists of multiple 'Look-Locker sets', each of which contains an inversion pulse followed by gated single-shot images at a consistent cardiac phase in several sequential heartbeats (Fig. 1B). As sampling of the recovery curve in each set is limited and also determined by the heart rate, Look-Locker sets are repeated with slightly incremented TI values and separated by several heartbeats to allow magnetization recovery. MOLLI images also generally use bSSFP readouts to improve blood-tissue contrast as well

as overall signal yield, although a GRE variant has been used at 7T[2] [19].

Implementations vary in the number of Look-Locker sets and the number of images in each set, which are commonly indicated with a series of numbers such as 3(3)3(3)5. In this naming convention [20], the parentheses indicate the number of recovery heartbeats between sets and all other numbers indicate the number of images in each set. In this example, 3(3)3(3)5 describes the original MOLLI implementation with three Look-Locker sets containing 3, 3, and 5 images and each set separated by 3 heartbeats for recovery. The choice of sampling pattern affects not only the total breath-hold duration, but also the variability of calculated T1 values and potential heart rate dependent T1 errors.

With good breath-holding, the consistent cardiac phase between MOLLI images simplifies data analysis by allowing regions of interest (ROIs) to be drawn for all images simultaneously. Consistent spatial positions between images allows parametric T1 maps to be generated, which provide an invaluable visual tool for identifying spatial patterns of T1 abnormalities. While myocardial T1 mapping was feasible with other techniques prior to MOLLI, the simplicity of a single breath-hold acquisition and straightforward analysis contributed to its success and helped to spur the growth of the T1 mapping field as a whole.

Similar to the continuous Look-Locker techniques, the measured apparent T1 time, termed T1*, from MOLLI data is generally shorter than the true T1 time due to magnetization perturbation by the image readouts. Conventional MOLLI analysis uses the standard Look-Locker correction factor (Eq. 2) to estimate the true T1 value. However, MOLLI's intermittent bSSFP readouts result in notable differences in the magnetization time-course compared to the continuous GRE readouts for which the correction factor was derived. This difference in magnetization progression gives rise to errors in MOLLI T1 values that are systematically dependent on multiple factors and well characterized [20]. Briefly, MOLLI T1 values are generally systematically underestimated with reduced T2 values [21, 22], increased T1 values [18, 23, 24], high heart rates [18, 23], increased off-resonance [25], poor inversion efficiency [26, 27], and magnetization transfer (MT) effects [28]. The magnitude of T1 errors from these factors is dependent on various aspects on the sequence implementation, resulting in a wide range of calculated MOLLI T1 values. For example, various studies of healthy subjects using 3(3)3(3)5 MOLLI at 1.5T have reported average myocardial T1 values of 939±24 ms (n=20) [29], 1011±41 ms (n=10) [30], and 950±21 ms (n=102) [31]. Despite moderate differences in mean T1 values between studies, the coefficient of variation within a given study is 2.2-4.0%, suggesting that healthy myocardial MOLLI T1 values are stable and consistent within a specific sequence implementation.

While a number of MOLLI's systematic dependencies are deeply rooted in the use of the Look-Locker correction factor for an intermittent bSSFP Look-Locker readout, other dependencies have been mitigated through a combination of sequence modifications and alternative image reconstruction algorithms. For example, heart rate dependence in certain MOLLI implementations is largely due to incomplete magnetization recovery between Look-Locker sets. By ordering the Look-Locker sets from longest to shortest, such as the 5(3)3, 4(1)3(1)2, and 5(1)1(1)1 patterns, and defining the recovery durations in seconds instead of heartbeats [32], heart rate dependence is significantly reduced. A conditional fitting algorithm used in the shortened MOLLI (ShMOLLI[1]) sequence, where images from later Look-Locker sets are discarded when fitting long T1 values or if the residual fit error is too great, further improves heart rate insensitivity [23]. An optimized adiabatic inversion pulse was also found to increase the accuracy of the MOLLI sequence [27], and more complex MOLLI T1 calculation techniques utilizing Bloch equation simulations [33] have also been developed to account for other dependencies. However, as these improvements bring MOLLI T1 values closer to the true T1 value, it is important to be mindful that newer implementations are no longer directly comparable to reported literature values from previous, less accurate implementations.

Although systematic errors in MOLLI T1 values are conceptually undesirable when trying to accurately quantify true T1 values, the primary goal of most T1 mapping is to reliably quantify myocardial fibrosis. This more pragmatic view asserts that well characterized systematic errors are tolerable, provided that MOLLI T1 values are a reproducible biomarker that is sensitive to fibrosis. This perspective is supported by extensive published literature using the MOLLI techniques in a wide variety of cardiomyopathies. Furthermore, the influence of T2 values and MT on native MOLLI T1 values may actually increase its sensitivity to overall cardiac disease, as common pathologic changes in T2 and MT also increase native MOLLI T1 values. However, variability in factors such as flip angle and off-resonance is dependent on MRI system design and shimming, but still cause artifactual changes in MOLLI T1 values. Thus MOLLI's systematic dependencies are simultaneously an advantage and a disadvantage. While they may increase sensitivity of MOLLI T1 values as a biomarker for overall cardiac disease, there is the potential for misinterpretation because it may be difficult to rule out non-pathological confounders as the underlying cause of MOLLI T1 derived ECV abnormalities.

Intermittent Look-Locker can also be performed using a saturation recovery preparation, such as in the MLLSR sequence [34]. As an ideal saturation pulse nullifies longitudinal magnetization regardless of the magnetization before it, recovery periods between Look-Locker sets are no longer required and thus more images can be acquired in the same total duration. However, as MLLSR still fundamentally uses an intermittent Look-Locker acquisition, it has similar characteristics to the MOLLI sequences, with underestimated

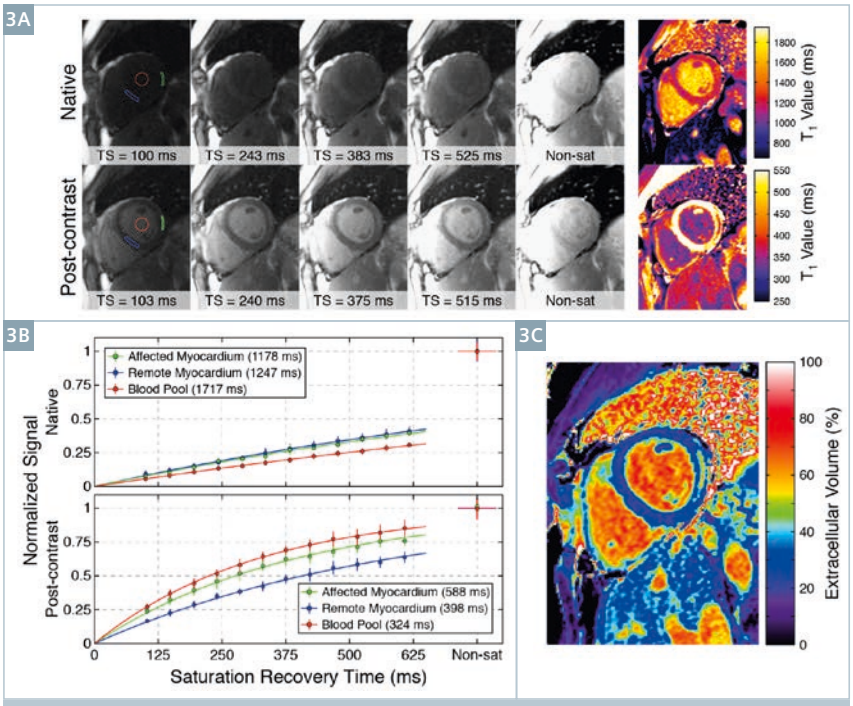


3 T1 and ECV mapping in a subject with myocarditis. **(3A)** Sample raw images from native (top) and post-contrast (bottom) SASHA-VFA T1 mapping and resulting T1 maps (right). Non-saturated images are window-leveled independently to allow better visualization. Images were motion corrected using Siemens HeartFreeze and T1 maps were generated on the scanner. ROIs drawn in the affected myocardium (green), remote myocardium (blue) and blood pool (red) are shown in the shortest TS image only. **(3B)** Signal intensities and 2-parameter best-fit curves are shown for each ROI in native (top) and post-contrast (bottom) data. **(3C)** ECV map was calculated by co-registering native and post-contrast T1 maps. *Data courtesy Drs. Peter Kellman and Andrew Arai at the National Institutes of Health.*

apparent T1* values that cannot be accurately corrected with direct application of the Look-Locker correction factor in Eq. 2.

**Independently magnetization-preparation techniques**

Both continuous and intermittent Look-Locker sequences acquire multiple images after a single magnetization preparation (inversion or saturation) pulse as a means of reducing the total scan time and providing a wide range of sampled recovery times. In comparison, the SR-TFL [35], SAP-T1 [36], and SAturation-recovery single-SHot Acquisition (SASHA[1]) sequences [37] acquire only a single image after each saturation pulse. As ideal saturation pulses reset the longitudinal magnetization regardless of the initial state, each image is independently magnetization prepared, and thus the magnetization time-course in each image readout is independent of other image readouts. The SASHA sequence consists of a non-prepared 'anchor' image, followed by a series of saturation recovery images in sequential heartbeats (Fig. 1C). Images are gated single-shot bSSFP readouts, similar to the MOLLI sequence (Table 1), but have significantly poorer blood-tissue contrast. SASHA images and analysis from a subject with myocarditis are shown in Fig. 3.

T1 values calculated from SASHA data using a 3-parameter model (Eq. 1) have been shown to be highly accurate and robust over a wide range of T1, T2, flip angles, heart rates, off-resonance values, and magnetization transfer effects [20, 28, 37]. However, the dynamic range of signal intensities in SASHA is nearly half that of MOLLI due to its saturation recovery preparation, resulting in significantly higher SASHA T1 variability [20]. SASHA data acquired using a variable flip angle (VFA) readout and using a 2-parameter model for T1 calculation has been recently shown to have coefficients of variation similar to MOLLI measurements while maintaining SASHA's accuracy [38]. VFA images were also shown to consistently reduce image artifacts associated with off-resonance effects. However, VFA readouts further reduce blood tissue-contrast in the anchor image, potentially reducing the effectiveness of motion correction algorithms and impairing visual identification of the myocardial boundaries when contouring on raw images.

The number of acquired SASHA images is flexible and can be reduced in subjects with diminished breath-hold capabilities at the expense of increased variability. The original SASHA sequence used saturation recovery times (TS) linearly spanning the range of values possible while keeping the saturation and imaging in the same heartbeat to maximize the number of acquired images in a fixed duration. Longer TS times may better sample the recovery curve for long T1 values and can be achieved by imaging in a separate heartbeat from the saturation pulse, such as in the SR-TFL sequence [35] and the recent SMART$_1$Map sequence [39]. Recent work numerically optimizing saturation recovery times for 3-parameter [40] and 2-parameter [41] models found clustered sampling patterns with repeated TS times result in moderate reductions in T1 variability.

The robustness of the SASHA sequence to systematic confounders makes it an attractive candidate for T1 mapping in new study protocols. While SASHA is a relatively new sequence with less clinical and histological validation compared to more established techniques, studies with SASHA in patients with heart failure [37], anthracycline cardiotoxicity remodelling [42], and Fabry disease [43] have findings consistent with established literature. Nevertheless, the lack of established values and difficulty comparing values between techniques make SASHA a difficult choice for sites where data has already been acquired with another technique.

## Discussion

Absolute native myocardial T1 values vary significantly between imaging sequences, with 15-20% lower values with MOLLI compared to SASHA [44, 45] due to MOLLI's systematic underestimation [20]. ECV values are derived using both native and post-contrast T1 measurements in the blood and myocardium and thus systematic T1 errors, which may be different between each of these measurements, result in even larger differences between sequences (Table 1). Therefore, caution must be exercised when comparing literature values, and a recent consensus statement on T1 mapping recommends that site-specific normative values be established for any given T1 mapping sequence implementation [46].

In clinical practice, breath-hold motion commonly causes errors in T1 maps as signal intensity changes between images are caused by spatial misalignment instead of magnetization recovery. Although manually adjusting ROIs between images can overcome some motion effects, this process increases analysis time and effort. A robust non-rigid image registration algorithm designed for the large changes in image contrast in MOLLI data was found to significantly reduce apparent motion between images and improve T1 map quality [47]. In the Siemens implementation found in the MyoMaps package, T1 maps are generated from motion corrected images on the scanner console directly. This immediate feedback allows the operator to easily detect poor quality data sets and repeat the acquisition and enables focused investigations within the same study, as T1 abnormalities can be detected in real-time.

By extending the image registration algorithm to co-register native (non-contrast) and post-contrast T1 maps and using hematocrit values with automated blood pool segmentation, parametric ECV maps can also be generated [48, 49]. ECV image maps are more easily interpretable than T1 maps because they represent a physiologically relevant parameter and the ability to generate these in a semi-automated manner greatly improves analysis workflow. The uncertainty in T1 values from fitting measured data to the exponential recovery model can be quantified by converting fit residuals into a standard deviation with the same units as T1 values [32]. This approach can be further extended to calculating uncertainties in derived ECV values. These uncertainty maps provide valuable context in interpreting the likelihood of whether T1 and ECV abnormalities are simply due to measurement noise.

## Conclusions

Myocardial T1 mapping is an active and exciting field of research, driven by a strong clinical motivation to detect diffuse myocardial fibrosis that is so ubiquitous in cardiac disease. A number of techniques are commonly used for T1 mapping, each with unique advantages and disadvantages. While direct comparison of values between these techniques is complicated by different systematic dependencies between sequences, the ability of each technique described here to detect fibrosis is supported by clinical evidence and literature. The most appropriate technique for any given study depends on considerations such as the image quality of single-shot images in subjects with smaller or thinner hearts and fast heart rates, the likelihood of variations in known confounders, and the need to compare values to existing literature. Commercial availability of a T1 mapping sequence in MyoMaps provides broad clinical access to this technology, and is a significant step towards the adoption of T1 mapping as a clinical standard for quantifying myocardial fibrosis.

### References


1 Mewton N, Liu CY, Croisille P, Bluemke DA, Lima JAC. Assessment of myocardial fibrosis with cardiovascular magnetic resonance. J Am Coll Cardiol 2011;57:891–903. doi: 10.1016/j.jacc.2010.11.013.

2 Iles L, Pfluger H, Phrommintikul A, Cherayath J, Aksit P, Gupta SN, Kaye DM, Taylor AJ. Evaluation of diffuse myocardial fibrosis in heart failure with cardiac magnetic resonance contrast-enhanced T1 mapping. J Am Coll Cardiol 2008;52:1574–1580. doi: 10.1016/j.jacc.2008.06.049.

3 Jerosch-Herold M, Sheridan DC, Kushner JD, Nauman D, Burgess D, Dutton D, Alharethi R, Li D, Hershberger RE. Cardiac magnetic resonance imaging of myocardial contrast uptake and blood flow in patients affected with idiopathic or familial dilated cardiomyopathy. Am J Physiol Heart Circ Physiol 2008;295:H1234–H1242. doi: 10.1152/ajpheart.00429.2008.

4 Karamitsos TD, Piechnik SK, Banypersad SM, et al. Noncontrast T1 mapping for the diagnosis of cardiac amyloidosis. JACC Cardiovasc Imaging 2013;6:488–497. doi: 10.1016/j.jcmg.2012.11.013.

5 Flett AS, Hayward MP, Ashworth MT, Hansen MS, Taylor AM, Elliott PM, McGregor C, Moon JC. Equilibrium contrast cardiovascular magnetic resonance for the measurement of diffuse myocardial fibrosis: preliminary validation in humans. Circulation 2010;122:138–144. doi: 10.1161/CIRCULATIONAHA.109.930636.

6 Fontana M, White SK, Banypersad SM, Sado DM, Maestrini V, Flett AS, Piechnik SK, Neubauer S, Roberts N, Moon JC. Comparison of T1 mapping techniques for ECV quantification. Histological validation and reproducibility of ShMOLLI versus multibreath-hold T1 quantification equilibrium contrast CMR. J Cardiovasc Magn Reson 2012;14:88. doi: 10.1186/1532-429X-14-88.

7 Bull S, White SK, Piechnik SK, et al. Human non-contrast T1 values and correlation with histology in diffuse fibrosis. Heart 2013;99:932–937. doi: 10.1136/heartjnl-2012-303052.

8 White SK, Sado DM, Fontana M, et al. T1 Mapping for Myocardial Extracellular Volume Measurement by CMR: Bolus Only Versus Primed Infusion Technique. JACC Cardiovasc Imaging 2013;6:955–962. doi: doi: 10.1016/j.jcmg.2013.01.011.

9 Wong TC, Piehler K, Meier CG, et al. Association between extracellular matrix expansion quantified by cardiovascular magnetic resonance and short-term mortality. Circulation 2012;126:1206–1216. doi: 10.1161/CIRCULATIONAHA.111.089409.

10 Ferrari VA, Witschey WRT, Zhou R. Cardiac magnetic resonance assessment of myocardial fibrosis: honing new clinical tools. Circ Cardiovasc Imaging 2011;4:604–606. doi: 10.1161/CIRCIMAGING.111.969204.

11 Lima JAC. The promise of myocardial fibrosis assessment by T1 mapping. JACC Cardiovasc Imaging 2013;6:485–487. doi: 10.1016/j.jcmg.2012.11.014.

12 Moon JC, Treibel TA, Schelbert EB. T1 Mapping for Diffuse Myocardial Fibrosis. J Am Coll Cardiol 2013;62:1288–1289. doi: 10.1016/j.jacc.2013.05.077.

13 Look D, Locker D. Time Saving in Measurement of NMR and EPR Relaxation Times. Review of Scientific Instruments 1970;41:250–251. doi: 10.1063/1.1684482.
14 Haase A, Matthaei D, Bartkowski R, Dühmke E, Leibfritz D. Inversion recovery snapshot FLASH MR imaging. J Comput Assist Tomogr 1989;13:1036–1040.
15 Deichmann R, Haase A. Quantification of T1 values by SNAPSHOT-FLASH NMR imaging. J Magn Reson 1992;96:608–612. doi: doi: DOI: 10.1016/0022-2364(92)90347-A.
16 Messroghli DR, Nordmeyer S, Buehrer M, et al. Small Animal Look-Locker Inversion Recovery (SALLI) for Simultaneous Generation of Cardiac T1 Maps and Cine and Inversion Recovery–prepared Images at High Heart Rates: Initial Experience. Radiology 2011;261:258–265. doi: 10.1148/radiol.11101943.
17 Connelly KA, Detsky JS, Graham JJ, Paul G, Vijayaragavan R, Dick AJ, Wright GA. Multicontrast late gadolinium enhancement imaging enables viability and wall motion assessment in a single acquisition with reduced scan times. J Magn Reson Imaging 2009;30:771–777. doi: 10.1002/jmri.21907.
18 Messroghli DR, Radjenovic A, Kozerke S, Higgins DM, Sivananthan MU, Ridgway JP. Modified Look-Locker inversion recovery (MOLLI) for high-resolution T1 mapping of the heart. Magn Reson Med 2004;52:141–146. doi: 10.1002/mrm.20110.
19 Rodgers CT, Piechnik SK, DelaBarre LJ, Van de Moortele P-F, Snyder CJ, Neubauer S, Robson MD, Vaughan JT. Inversion recovery at 7 T in the human myocardium: Measurement of T1, inversion efficiency and B1 (+). Magn Reson Med 2013;70:1038–1046. doi: 10.1002/mrm.24548.
20 Kellman P, Hansen MS. T1-mapping in the heart: accuracy and precision. J Cardiovasc Magn Reson 2014;16:2. doi: 10.1186/1532-429X-16-2.
21 Chow K, Flewitt JA, Pagano JJ, Green JD, Friedrich MG, Thompson RB. T2-dependent errors in MOLLI T1 values: simulations, phantoms, and in-vivo studies. J Cardiovasc Magn Reson 2012;14:P281.
22 Gai ND, Stehning C, Nacif M, Bluemke DA. Modified Look-Locker T1 evaluation using Bloch simulations: human and phantom validation. Magn Reson Med 2013;69:329–336. doi: 10.1002/mrm.24251.
23 Piechnik SK, Ferreira VM, Dall'Armellina E, Cochlin LE, Greiser A, Neubauer S, Robson MD. Shortened Modified Look-Locker Inversion recovery (ShMOLLI) for clinical myocardial T1-mapping at 1.5 and 3 T within a 9 heartbeat breathhold. J Cardiovasc Magn Reson 2010;12:69. doi: 10.1186/1532-429X-12-69.
24 Lee JJ, Liu S, Nacif MS, Ugander M, Han J, Kawel N, Sibley CT, Kellman P, Arai AE, Bluemke DA. Myocardial T1 and extracellular volume fraction mapping at 3 tesla. J Cardiovasc Magn Reson 2011;13:75. doi: 10.1186/1532-429X-13-75.
25 Kellman P, Herzka DA, Arai AE, Hansen MS. Influence of Off-resonance in myocardial T1-mapping using SSFP based MOLLI method. J Cardiovasc Magn Reson 2013;15:63. doi: 10.1186/1532-429X-15-63.
26 Chow K, Flewitt JA, Pagano JJ, Green JD, Friedrich MG, Thompson RB. MOLLI T1 Values Have Systematic T2 and Inversion Efficiency Dependent Errors. Proc Intl Soc Magn Reson Med 2012. p. 395.
27 Kellman P, Herzka DA, Hansen MS. Adiabatic inversion pulses for myocardial T1 mapping. Magn Reson Med 2014;71:1428–1434. doi: 10.1002/mrm.24793.
28 Robson MD, Piechnik SK, Tunnicliffe EM, Neubauer S. T1 measurements in the human myocardium: The effects of magnetization transfer on the SASHA and MOLLI sequences. Magn Reson Med 2013. doi: 10.1002/mrm.24867.
29 Messroghli DR, Greiser A, Fröhlich M, Dietz R, Schulz-Menger J. Optimization and validation of a fully-integrated pulse sequence for modified look-locker inversion-recovery (MOLLI) T1 mapping of the heart. J Magn Reson Imaging 2007;26:1081–1086. doi: 10.1002/jmri.21119.
30 Kawel N, Nacif M, Santini F, Liu S, Bremerich J, Arai AE, Bluemke DA. Partition coefficients for gadolinium chelates in the normal myocardium: Comparison of gadopentetate dimeglumine and gadobenate dimeglumine. J Magn Reson Imaging 2012;36:733–737. doi: 10.1002/jmri.23651.
31 Dabir D, Child N, Kalra A, et al. Reference values for healthy human myocardium using a T1 mapping methodology: results from the International T1 Multicenter cardiovascular magnetic resonance study. J Cardiovasc Magn Reson 2014;16:69. doi: 10.1186/s12968-014-0069-x.
32 Kellman P, Arai AE, Xue H. T1 and extracellular volume mapping in the heart: estimation of error maps and the influence of noise on precision. J Cardiovasc Magn Reson 2013;15:56. doi: 10.1186/1532-429X-15-56.
33 Shao J, Nguyen K-L, Natsuaki Y, Spottiswoode B, Hu P. Instantaneous signal loss simulation (InSiL): An improved algorithm for myocardial T1 mapping using the MOLLI sequence. J Magn Reson Imaging 2014. doi: 10.1002/jmri.24599.
34 Song T, Stainsby JA, Ho VB, Hood MN, Slavin GS. Flexible cardiac T(1) mapping using a modified look-locker acquisition with saturation recovery. Magn Reson Med 2012;67:622–627. doi: 10.1002/mrm.24137.
35 Wacker CM, Bock M, Hartlep AW, Beck G, van Kaick G, Ertl G, Bauer WR, Schad LR. Changes in myocardial oxygenation and perfusion under pharmacological stress with dipyridamole: assessment using T*2 and T1 measurements. Magn Reson Med 1999;41:686–695.
36 Higgins DM, Ridgway JP, Radjenovic A, Sivananthan UM, Smith MA. T1 measurement using a short acquisition period for quantitative cardiac applications. Med Phys 2005;32:1738–1746.
37 Chow K, Flewitt JA, Green JD, Pagano JJ, Friedrich MG, Thompson RB. Saturation recovery single-shot acquisition (SASHA) for myocardial T1 mapping. Magn Reson Med 2014;71:2082–2095. doi: 10.1002/mrm.24878.
38 Chow K, Spottiswoode B, Pagano JJ, Thompson R. Improved precision in SASHA T1 mapping with a variable flip angle readout. J Cardiovasc Magn Reson 2014;16:M9.
39 Slavin GS, Hood MN, Ho VB, Stainsby JA. Breath-Held Myocardial T1 Mapping Using Multiple Single-Point Saturation Recovery. Proc Intl Soc Magn Reson Med, Vol. 20. 2012. p. 1244.
40 Akçakaya M, Weingärtner S, Roujol S, Nezafat R. On the selection of sampling points for myocardial T1 mapping. Magn Reson Med 2014. doi: 10.1002/mrm.25285.
41 Kellman P, Xue H, Chow K, Spottiswoode BS, Arai AE, Thompson RB. Optimized saturation recovery protocols for T1-mapping in the heart: influence of sampling strategies on precision. J Cardiovasc Magn Reson 2014;16:55. doi: 10.1186/s12968-014-0055-3.
42 Tham E, Chow K, Spavor M, Pagano JJ, Haykowsky MJ, Thompson RB. Degree of diffuse fibrosis measured by MRI correlates with LV remodelling in childhood cancer survivors after anthracycline chemotherapy. J Cardiovasc Magn Reson 2011;13:P276.
43 Thompson RB, Chow K, Khan A, Chan A, Shanks M, Paterson I, Oudit GY. $T_1$ mapping with cardiovascular MRI is highly sensitive for Fabry disease independent of hypertrophy and sex. Circ Cardiovasc Imaging 2013;6:637–645. doi: 10.1161/CIRCIMAGING.113.000482.
44 Flewitt JA, Chow K, Pagano JJ, Green JD, Friedrich MG, Thompson RB. Effect of Systematic T1 Errors on Lambda Calculations: Comparison of Different T1 Mapping Techniques. Proc Intl Soc Magn Reson Med, Vol. 20. 2012. p. 3370.
45 Roujol S, Weingärtner S, Foppa M, Chow K, Kawaji K, Ngo LH, Kellman P, Manning WJ, Thompson RB, Nezafat R. Accuracy, Precision, and Reproducibility of Four T1 Mapping Sequences: A Head-to-Head Comparison of MOLLI, ShMOLLI, SASHA, and SAPPHIRE. Radiology 2014;272:683–689. doi: 10.1148/radiol.14140296.
46 Moon JC, Messroghli DR, Kellman P, et al. Myocardial T1 mapping and extracellular volume quantification: a Society for Cardiovascular Magnetic Resonance (SCMR) and CMR

Working Group of the European Society of Cardiology consensus statement. J Cardiovasc Magn Reson 2013;15:92. doi: 10.1186/1532-429X-15-92.
47 Xue H, Shah S, Greiser A, Guetter C, Littmann A, Jolly M-P, Arai AE, Zuehlsdorff S, Guehring J, Kellman P. Motion correction for myocardial T1 mapping using image registration with synthetic image estimation. Magn Reson Med 2012;67:1644–1655. doi: 10.1002/mrm.23153.
48 Kellman P, Wilson JR, Xue H, Ugander M, Arai AE. Extracellular volume fraction mapping in the myocardium, part 1: evaluation of an automated method. J Cardiovasc Magn Reson 2012;14:63. doi: 10.1186/1532-429X-14-63.
49 Kellman P, Wilson JR, Xue H, Bandettini WP, Shanbhag SM, Druey KM, Ugander M, Arai AE. Extracellular volume fraction mapping in the myocardium, part 2: initial clinical experience. J Cardiovasc Magn Reson 2012;14:64. doi: 10.1186/1532-429X-14-64.
50 Neilan TG, Coelho-Filho OR, Shah RV, et al. Myocardial extracellular volume fraction from T1 measurements in healthy volunteers and mice: relationship to aging and cardiac dimensions. JACC Cardiovasc Imaging 2013;6:672–683. doi: 10.1016/j.jcmg.2012.09.020.

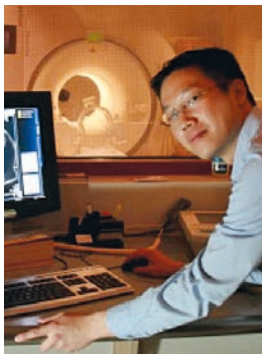

## Contact

Kelvin Chow, Ph.D.
1098 Research Transition Facility
Department of Biomedical Engineering
University of Alberta
Edmonton AB T6G 2V2
Canada
kelvin.chow@ualberta.ca

## Contact

Dr. Richard Thompson, Associate Professor
1098 Research Transition Facility
Department of Biomedical Engineering
University of Alberta
Edmonton AB T6G 2V2
Canada
Phone: +1 (780) 492-8665
richard.thompson@ualberta.ca

[1] The product is still under development and not commercially available yet. Its future availability cannot be ensured.
[2] MAGNETOM 7T is ongoing research. All data shown are acquired using a non-commercial system under institutional review board permission. MAGNETOM 7T is still under development and not commercially available yet. Its future availability cannot be ensured.

# Increasing Productivity in Myocardial and Liver T2* Acquisition and Analysis

Juliano Lara Fernandes, M.D., Ph.D., MBA; José Michel Kalaf, M.D.

Jose Michel Kalaf Research Institute, Radiologia Clinica de Campinas, Campinas, Brazil

Parametric mapping has become one of the key developments in cardiovascular magnetic resonance (CMR) over the last years [1]. Despite more recent applications using T1 and T2 maps, T2* mapping was the first clinical driver of this growth and a landmark for the success of CMR on the assessment of iron overload in different diseases.

The clinical importance of CMR for this purpose was first pointed out in 2001 by Anderson et al. [2]. In this seminal paper, the authors demonstrated a clear association between values of myocardial T2* and left ventricular ejection fraction, identifying the cut-off of 20 ms as a marker of myocardial iron overload with a significant increase in risk of ventricular dysfunction below the 10 ms limit. At this time, they also correlated the values of liver T2* with direct liver iron concentration (LIC) as measured by invasive biopsy.

Since that initial paper, advances in T2* sequences and analysis gained rapid speed with important clinical information following through. In technical aspects, the first T2* sequences for both liver and heart used single echo and multiple breath-holds for the generation of images with different echo times. While providing acceptable interscanner and intercenter reproducibility, breath-hold times were up to 20 seconds and the total exam time was also very long due to the need for multiple respiratory pauses [3]. The first evolution of the method resulted in sequences that provided multiple echoes using a single respiratory pause and significantly shortened total exam time while keeping very good overall interscanner, interpatient and intercenter reproducibility [4]. Myocardial T2* was then further advanced by the use of black blood techniques that maintained the previous advantages of fast acquisition but reduced the coefficient of variation of the exam to 4.1% using diastolic acquisitions and removal of flow compensation allowing for lower initial TEs [5]. Finally, other organs started to be assessed along with the heart and the liver, with special focus on the pancreas and pituitary gland [6, 7].

In terms of clinical applications, more accurate calibration curves of liver T2* and liver iron content became available, allowing for precise determination of LIC [8, 9], comparable to previously validated T2 techniques [9]. Prognostic data started to identify cohorts of patients at high risk for development of heart failure showing that 47% of patients with a cardiac T2* below 6 ms developed heart failure at one year follow-up [10]. The calibration of cardiac T2* and true myocardial iron concentration (MIC) was made possible after the work of Carpenter et al. with twelve human hearts donated after patient's death or transplantation comparing CMR values to plasma atomic emission spectroscopy [11]. This work along with previous validation studies for the liver now permits the classification of severity in both organs using T2*, R2* and final LIC and MIC levels (Table 1).

The impact of T2* mapping along with the development of new iron chelators over the last decade has resulted in a major change in the natural history of thalassemia major and other transfusion-dependent anemias. In countries that applied CMR routinely for these patients along with regular access to chelation, early diagnosis of high MIC allowed for significant changes in management strategies. Reductions in overall mortality of up to 62% and iron overload related deaths of 71% were observed [12] with a shift of the major cause of death in these patients from heart to chronic liver disease and infections [13]. Currently, all major guidelines for the management of iron chelation recommend the use of both liver and myocardial T2* assessment on a yearly basis and

## Table 1

| | Classification | T2* (ms) | R2* (Hz) | Iron Concentration (mg/g dw) |
|---|---|---|---|---|
| Myocardial | Normal | ≥ 20 | ≤ 50 | ≤ 1.16 |
| | Mild/Moderate | 10 to 20 | > 50 – 100 | > 1.16 to 2.71 |
| | Severe | < 10 | > 100 | > 2.71 |
| Liver | Normal | ≥ 11.4 | < 88 | < 2.0 |
| | Mild | 3.8 – 11.4 | 88 – 263 | 2.0 – 7.0 |
| | Moderate | 1.8 – 3.8 | 263 – 555 | 7.0 – 15.0 |
| | Severe | < 1.8 | > 555 | > 15.0 |

Reference values and stratification of liver iron concentration and myocardial iron concentration by T2* at 1.5T.

as the key diagnostic test for therapeutical strategies [14-16].

## Clinical demand: Needs and limitations

Despite the very successful use of T2* mapping for the assessment of iron overload, recent surveys indicate that the adoptance of the technique has been very heterogeneous and that cases of high LIC and/or high MIC are still abundant, especially in developing parts of the world where most of the patients are located [17]. Understanding the limitations that do not allow widespread use of the technique is important in order to move the field further in the right direction.

The first limitation refers to the number of patients in need of the exam. While T2* mapping was initially developed for the study of patients with thalassemia major, it is now recognized that it also plays a significant role in the management of other diseases including myelodisplastic syndromes, sickle cell disease, hemochromatosis, thalassemia intermedia and other rare anemias with regular blood transfusions [18]. While the number of known patients with thalassemia major in the world is only just above 100,000 [19], the total number of patients counting all the other indications for iron overload assessment with MRI is estimated to be at least five times higher, especially with the increase in life span in most of these diseases. This puts significant pressure onto the healthcare system if one considers not only the costs but also the availability of slots in the current MRI installed base. For example, assuming that a standard scanner performs around 500 exams a month, it would require approximately 80 exclusively dedicated centers just to account for all the yearly scans needed to fulfill this unmet need of iron overload evaluation. Since scanners are not available exclusively for this purpose, these patients have to compete with demands from all other MRI indications, significantly limiting actual availability.

The second significant limitation to access is the need for dedicated training for the acquisition and assessment of T2* images of the liver and heart. While the pulse sequences used to generate the images are based on well-known gradient echo techniques, only recently have dedicated protocols been delivered as standard packages on most systems. Not only that, the post-processing step of quantitative analysis of the acquired images and T2* calculations is not automatic and frequently requires the use of a third party commercial software or spreadsheet [20]. Training is also necessary in the correction for some of the intrinsic limitations of the sequence, especially in situations of high LIC where truncation or use of an additional constant on the decay equation is needed [21, 22]. This additional toll results in many centers supposedly capable of performing the exam being unable to offer it on a routine basis, further reducing availability.

Considering the central role that CMR has taken in the assessment of iron overload together with the limitations discussed above, a new approach to improved productivity while maintaining the high quality of the exams was designed using recent product developments provided by Siemens Healthcare with the MyoMaps package.

## All Iron Detected (AID) project

The AID project was developed in order to offer high quality iron overload assessment to the maximum number of patients with a clinical indication for the exam in a multicenter design. The idea was to overcome limitations of (1) cost, (2) availability, (3) need for extensive training and (4) low productivity. To reach these goals, the aim was to develop a CMR protocol where the patient would stay inside the magnet for not more than five minutes, with a total exam time of under ten minutes. This would allow for the evaluation of approximately 70 patients in a 12-hour shift, boosting productivity by 200% with an increase from two to six patients per hour. The protocol was applied in seven different centers in six cities in Brazil (Radiologia Clinica de Campinas, Mater Dei Hospital (Belo Horizonte), Santa Joana Diagnostico (Recife), Sirio Libanes Hospital (São Paulo), CDPI (Rio de Janeiro), DASA (São Paulo) and Ana Nery Hospital (Santa Cruz do Sul)). Three of these centers had very little experience with either T1 or T2* imaging and no specific training was provided except for a one-hour meeting for overall discussion of the project with the principal investigators four months prior to the implementation of the exams. The protocol was transferred to each center's scanner (two 1.5T MAGNETOM Aera scanners with software version *syngo* MR D13 and five 1.5T MAGNETOM Avanto scanners with software version *syngo* MR B17, Siemens Healthcare, Erlangen, Germany) using a prototype version of MyoMaps.

Figure 1 shows the protocol used in the study. While our focus was on T2* we added the assessment of native T1 of the heart and liver using MyoMaps as well for research purposes, actually prolonging the exam time for another one to two minutes but still keeping within the five-minute exam target. For the localizers we chose to use a traditional orthogonal setup followed by a simple 2-chamber prescription used for the positioning of the heart short axis slices.

1

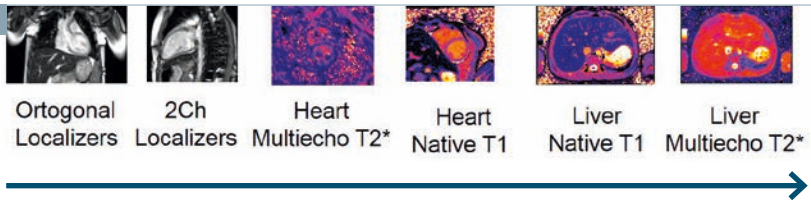


1 Overview of the protocol used in the AID project with the MyoMaps prototype[1] product.

Next, a multi-echo black-blood gradient echo sequence in the mid portion of the left ventricle acquired 12 short-axis images with different TEs (2.3 to 18.9 ms, with 1.5 ms intervals). The same short-axis slice position was copied in order to obtain eight images using a Modified Look-Locker Inversion Recovery (MOLLI[1]) sequence with 5 (3 s) 3 design as previously published for native T1 of the heart [23]. The same sequence was used for the axial single slice acquisition of the liver and also for T1 mapping. The position of the liver was copied for the final multi-echo gradient echo sequence consisting of twelve images with TEs from 1.1 to 11.0 ms with 0.9 ms intervals. As an optional acquisition, a complete set of ten short-axis slices covering the entire left ventricle was obtained in two centers that also performed a free breathing prototype cine sequence with sparsely sampled iterative reconstruction for rapid evaluation of left ventricular function in less than one minute.

While special care was taken to acquire images in reduced time, we were also careful to guarantee that the results would be accurate and consistent among all centers, especially the ones with least experience. This was planned in the MyoMaps product by automatic application of Inline Motion Correction and pixel-based quantification of both T1 and T2* based on the raw images generated. Inline processing removed the need for further analysis of the images with additional post-processing reducing also the overall time for reporting the final values for both organs in addition to the shortened acquisition intervals. Furthermore, it also allowed us to avoid the need for training the different sites in manual analysis: This was skipped altogether, since previous results with inline processing showed good correlation between the automatic measures and manual analysis [24].

The preliminary results of the project allowed us to scan 179 patients with

[1] WIP, the product is currently under development and is not for sale in the US and in other countries. Its future availability cannot be ensured.

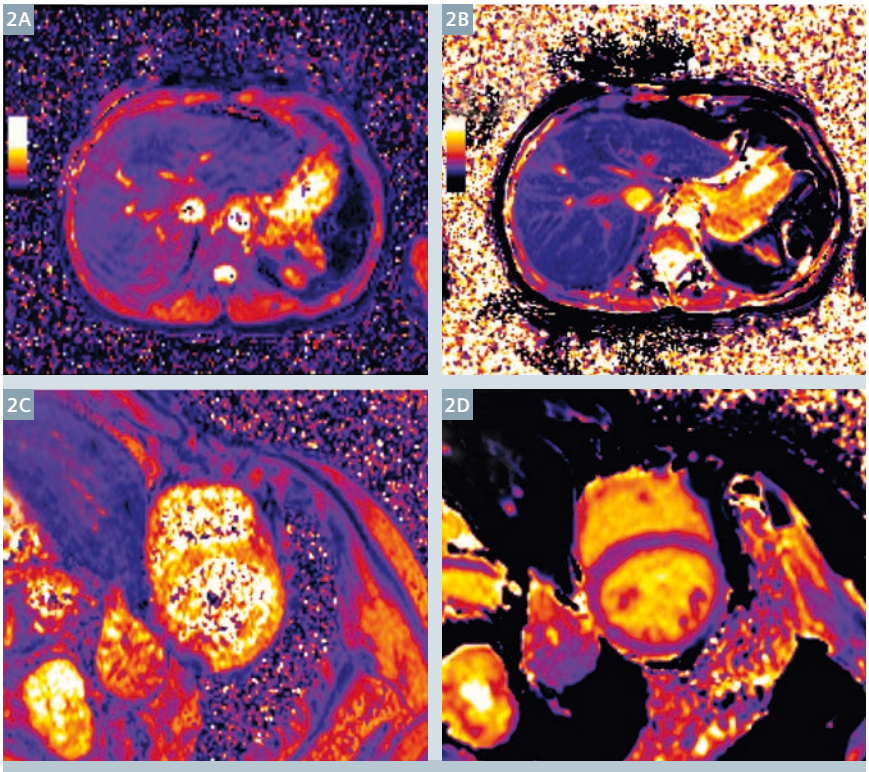


2 Inline pixel fit images automatically generated for T2* and T1 of the liver **(2A, B respectively)** as well as the heart **(2C, D).** Both organs had normal T1 and T2* values in this 41-year-old female patient with sickle cell disease.

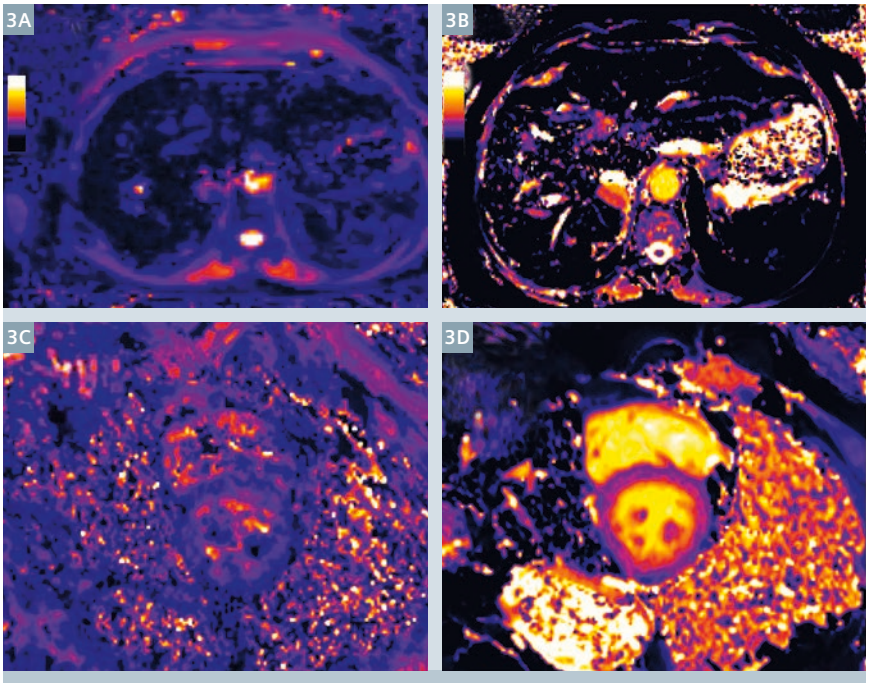


3 A 35-year-old female patient with severe iron overload in the liver and heart with a T2* of 1.7 ms and 9.8 ms **(3A, C respectively).** T1 values for both organs were also low calculated at 320 ms and 751 ms **(3B, D respectively).** The window and level used are the same as in figure 2 and demonstrate the differences in the color maps for both variables when assessing normal and pathological organs.

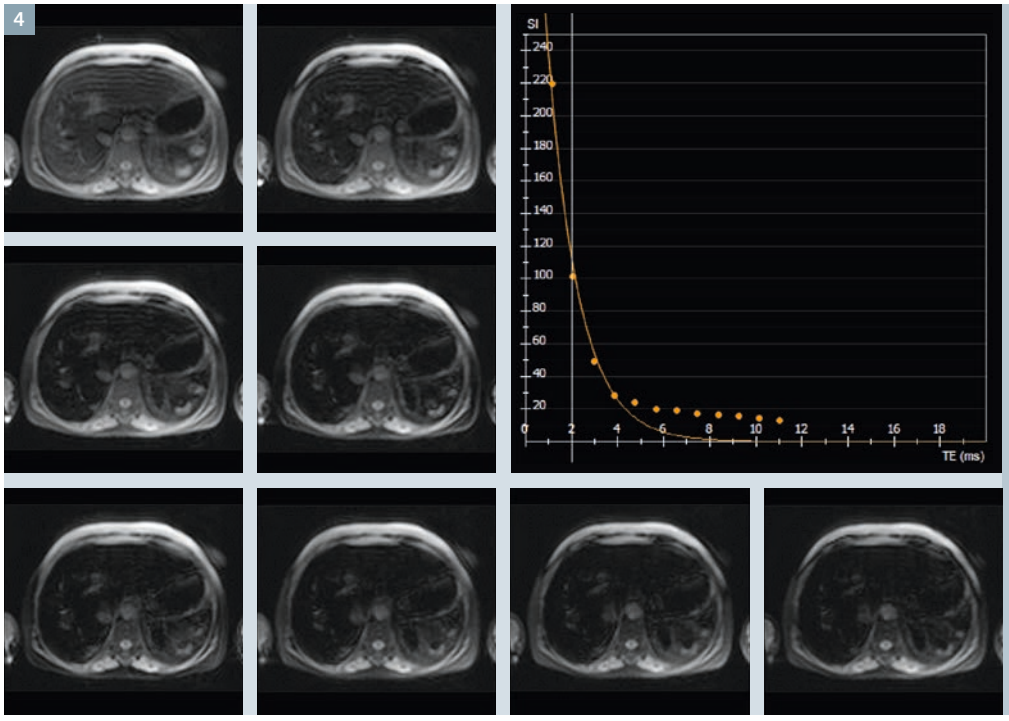


**4** Original gradient echo raw images used for the inline calculation of the liver T2* map in figure 3 with the first eight images with different echoes represented. The manual post-processing fitting of the T2* decay curve with the truncation of the last points after the fourth dataset is also shown.

a median scan time of 5.2 minutes (IQR 4 to 7 minutes) in patients with a wide age range (2 to 91 years old, 44% children[2]/adolescents) and varying myocardial T2* values (4.2 to 61 ms) and liver T2* values (0.7 to 32.4 ms). An example of a patient with normal T1 and T2* values of the heart and liver is shown in figure 2. These images are automatically generated by the scanner as DICOM images and each pixel represents the calculated T1/T2* values without any need for further post-processing. Figure 3 shows severe iron deposition in the liver and heart. In figure 4 the first eight original raw images used for the offline calculation of the T2* of the liver are shown along a manual fitting curve that was used for the comparison with the inline generated T2* map. In this case, truncation had to be used to account for the plateau observed in the images with longest TEs after the fifth echo.

## Further clinical applications

While T2* mapping of the heart and liver might apparently be limited only to assessment of iron overload, the technique has much broader potential clinical applications in which MyoMaps may provide significant insights. Blood oxygen level-dependent (BOLD) CMR has been proposed for almost twenty years as an accurate technique to assess myocardial perfusion [25]. In particular T2* imaging has been considered one of the most sensitive methods for this assessment as it is dependent on the paramagnetic properties of deoxygenated hemoglobin [26, 27]. However, previous studies used relatively simple imaging techniques and did not assess the myocardium with more current tools using parametric T2* mapping with higher resolution imaging and possible improvement in accuracy. The use of MyoMaps for stress-induced changes in BOLD CMR might be therefore helpful in this area [28].

Another potential use of T2* mapping also derives from previous observations of myocardial edema and hemorrhage characterized during the acute phase of myocardial infarction [29]. This also opens the possibility of using pixel-fit automatically generated images maps for identifying and monitoring tissue changes along different phases of the disease providing a roadmap for understanding physiological and pathological changes, which might influence treatment strategies.

## Conclusion

In summary, T2* imaging with CMR has experienced significant technical advances over recent years and has been proven to positively affect the management of iron overload diseases. The use of the prototype MyoMaps package[1] with automatic motion correction and inline quantification of T2* as well as T1 and T2 allowed us to further increase productivity, decrease training needs and offer more exams to patients with high demand for these scans with total imaging time around five minutes. The application of T2* mapping with MyoMaps might allow us to investigate other aspects of cardiovascular disease using BOLD imaging and edema and hemorrhage characterization.

[1] WIP, the product is currently under development and is not for sale in the US and in other countries. Its future availability cannot be ensured.

[2] Siemens disclaimer: MR scanning has not been established as safe for imaging fetuses and infants less than two years of age. The responsible physician must evaluate the benefits of the MR examination compared to those of other imaging procedures.

## Acknowledgements

We would like especially to thank RT Luciana Andrea Barozi Fioravante for all the analysis work and effort put into making the development of this project possible. We would also like to acknowledge the principal investigators in each of the sites that participated in the AID project: Maria Helena Albernaz Siqueira, Karina Nobrega, Jose Francisco Avila, Ilan Gottlieb, Marly Maria Uellendahl Lopes and Andre Mauricio Fernandes. Finally, we are grateful for the continuous support from the development team from Siemens Healthcare: Ralph Strecker and Andreas Greiser.

### References

1 Salerno M, Kramer CM. Advances in parametric mapping with CMR imaging. JACC Cardiovascular imaging 2013; 6:806-822.
2 Anderson LJ, Holden S, Davis B, et al. Cardiovascular T2-star (T2*) magnetic resonance for the early diagnosis of myocardial iron overload. Eur Heart J 2001; 22:2171-2179.
3 Westwood MA, Anderson LJ, Firmin DN, et al. Interscanner reproducibility of cardiovascular magnetic resonance T2* measurements of tissue iron in thalassemia. J Magn Reson Imaging 2003; 18:616-620.
4 Tanner MA, He T, Westwood MA, Firmin DN, Pennell DJ, Thalassemia International Federation Heart TI. Multi-center validation of the transferability of the magnetic resonance T2* technique for the quantification of tissue iron. Haematologica 2006; 91:1388-1391.
5 He T, Gatehouse PD, Kirk P, et al. Black-blood T2* technique for myocardial iron measurement in thalassemia. J Magn Reson Imaging 2007; 25:1205-1209.
6 Wood JC, Noetzl L, Hyderi A, Joukar M, Coates T, Mittelman S. Predicting pituitary iron and endocrine dysfunction. Ann N Y Acad Sci 2010; 1202:123-128.
7 Au WY, Lam WW, Chu W, et al. A T2* magnetic resonance imaging study of pancreatic iron overload in thalassemia major. Haematologica 2008; 93:116-119.
8 Hankins JS, McCarville MB, Loeffler RB, et al. R2* magnetic resonance imaging of the liver in patients with iron overload. Blood 2009; 113:4853-4855.
9 Wood JC, Enriquez C, Ghugre N, et al. MRI R2 and R2* mapping accurately estimates hepatic iron concentration in transfusion-dependent thalassemia and sickle cell disease patients. Blood 2005; 106:1460-1465.
10 Kirk P, Roughton M, Porter JB, et al. Cardiac T2* magnetic resonance for prediction of cardiac complications in thalassemia major. Circulation 2009; 120:1961-1968.
11 Carpenter JP, He T, Kirk P, et al. On T2* magnetic resonance and cardiac iron. Circulation 2011; 123:1519-1528.
12 Modell B, Khan M, Darlison M, Westwood MA, Ingram D, Pennell DJ. Improved survival of thalassaemia major in the UK and relation to T2* cardiovascular magnetic resonance. J Cardiovasc Magn Reson 2008; 10:42.
13 Voskaridou E, Ladis V, Kattamis A, et al. A national registry of haemoglobinopathies in Greece: deducted demographics, trends in mortality and affected births. Ann Hematol 2012; 91:1451-1458.
14 Fernandes JL. Iron chelation therapy in the management of transfusion-related cardiac iron overload. Transfusion 2012; 52:2256-2268.
15 Hoffbrand AV, Taher A, Cappellini MD. How I treat transfusional iron overload. Blood 2012; 120:3657-3669.
16 Cappellini MD, Cohen A, Eleftheriou A, Piga A, Porter J, Taher A. Iron Overload. In: Guidelines for the clinical management of thalassemia. Nicosia, Cyprus: Thalassemia International Federation, 2008:33-63.
17 Carpenter JP, Taigang H, Kirk P, et al. Worldwide survy of T2* cardiovascular magnetic resonance in Thalassaemia. Journal of Cardiovascular Magnetic Resonance 2011; 13(Suppl 1):O15.
18 Fleming RE, Ponka P. Iron overload in human disease. N Engl J Med 2012; 366:348-359.
19 Modell B, Darlison M. Global epidemiology of haemoglobin disorders and derived service indicators. Bull World Health Organ 2008; 86:480-487.
20 Fernandes JL, Sampaio EF, Verissimo M, et al. Heart and liver T2 assessment for iron overload using different software programs. Eur Radiol 2011; 21:2503-2510.
21 Ghugre NR, Enriquez CM, Coates TD, Nelson MD, Jr., Wood JC. Improved R2* measurements in myocardial iron overload. J Magn Reson Imaging 2006; 23:9-16.
22 He T, Gatehouse PD, Smith GC, Mohiaddin RH, Pennell DJ, Firmin DN. Myocardial T2* measurements in iron-overloaded thalassemia: An in vivo study to investigate optimal methods of quantification. Magn Reson Med 2008; 60:1082-1089.
23 Kellman P, Hansen MS. T1-mapping in the heart: accuracy and precision. Journal of Cardiovascular Magnetic Resonance : official journal of the Society for Cardiovascular Magnetic Resonance 2014; 16:2.
24 Alam MH, Baksi AJ, He T, et al. Validation of Siemens T2* inline WIP package for quantification of cardiac and hepatic loading at 1.5T and 3T. Journal of Cardiovascular Magnetic Resonance 2014; 16(Suppl 1):P323.
25 Li D, Dhawale P, Rubin PJ, Haacke EM, Gropler RJ. Myocardial signal response to dipyridamole and dobutamine: demonstration of the BOLD effect using a double-echo gradient-echo sequence. Magn Reson Med 1996; 36:16-20.
26 Friedrich MG, Niendorf T, Schulz-Menger J, Gross CM, Dietz R. Blood oxygen level-dependent magnetic resonance imaging in patients with stress-induced angina. Circulation 2003; 108:2219-2223.
27 Wacker CM, Hartlep AW, Pfleger S, Schad LR, Ertl G, Bauer WR. Susceptibility-sensitive magnetic resonance imaging detects human myocardium supplied by a stenotic coronary artery without a contrast agent. Journal of the American College of Cardiology 2003; 41:834-840.
28 Stalder AF, Schmidt M, Greiser A, Speier P, Guehring J, Friedrich MG, Mueller E. Robust cardiac BOLD MRI using an fMRI-like approach with repeated stress paradigms. Magn Reson Med. 2014 Mar 10. doi: 10.1002/mrm.25164.
29 Zia MI, Ghugre NR, Connelly KA, et al. Characterizing myocardial edema and hemorrhage using quantitative T2 and T2* mapping at multiple time intervals post ST-segment elevation myocardial infarction. Circulation Cardiovascular Imaging 2012; 5:566-572.

## Contact

Juliano Lara Fernandes
R. Antonio Lapa 1032
Campinas-SP – 13025-292
Brazil
Phone: +55-19-3579-2903
Fax: +55-19-3252-2903
jlaraf@terra.com.br

# Cardiac Dot Engine: Significant Time Reduction at Cardiac Magnetic Resonance Imaging

Jesús Ciro Pueyo, M.D., Ph.D.[1]; Paula García-Barquín, M.D.[1]; Laura Romina Zalazar, M.D.[1]; José Miguel Madrid, M.D.[1]; Jon Etxano, M.D.[1]; Efrén Ojeda, M.Sc.[2]; Óscar Fernández[3]

[1] Department of Radiology, Clínica Universidad de Navarra, Pamplona, Spain
[2] Siemens Healthcare, Erlangen, Germany
[3] Siemens Healthcare Getafe (Madrid), Spain

## Introduction

Cardiac Magnetic Resonance (CMR) has rapidly developed and is now the technique of choice in the study of multiple heart diseases and an important tool for planning revascularization strategies in patients with coronary artery disease [1]. It allows the assessment of cardiac morphology and function. Therefore, it provides important information about tissue characterization by detecting the first steps of the ischemic cascade through perfusion sequences. An appropriate assessment of myocardial viability can be performed with delayed enhancement sequences [2].

However, CMR is not without certain limitations. Firstly, it requires skilled personnel with a good knowledge of cardiac anatomy and cardiac planes. Secondly, the scan times for CMR studies are substantially longer than for other types of study (with up to more than an hour on stress heart exams) and remain a limiting factor in the recruitment of patients suffering from claustrophobia.

In order to reduce CMR scan times, the Cardiac Dot Engine has been developed. It is a new software technology from Siemens Healthcare, which offers a review of CMR fully guided and suited to the needs of the patient.

The system guides you through a series of graphical illustrations selecting some anatomical reference points on the heart. The software then performs an automatic planning of the different cardiac planes without the need for user intervention. It also allows you to obtain superimposable slices in all sequences of the study, increasing confidence in our diagnoses [3].

## Clinical experience

Our experience with the Dot software began in June 2013. To date, we have performed in our center over 272 CMR studies of which 60% are stress studies after administration of adenosine. All studies have been performed under medical supervision and have been reproducible and high-quality diagnostic scans.

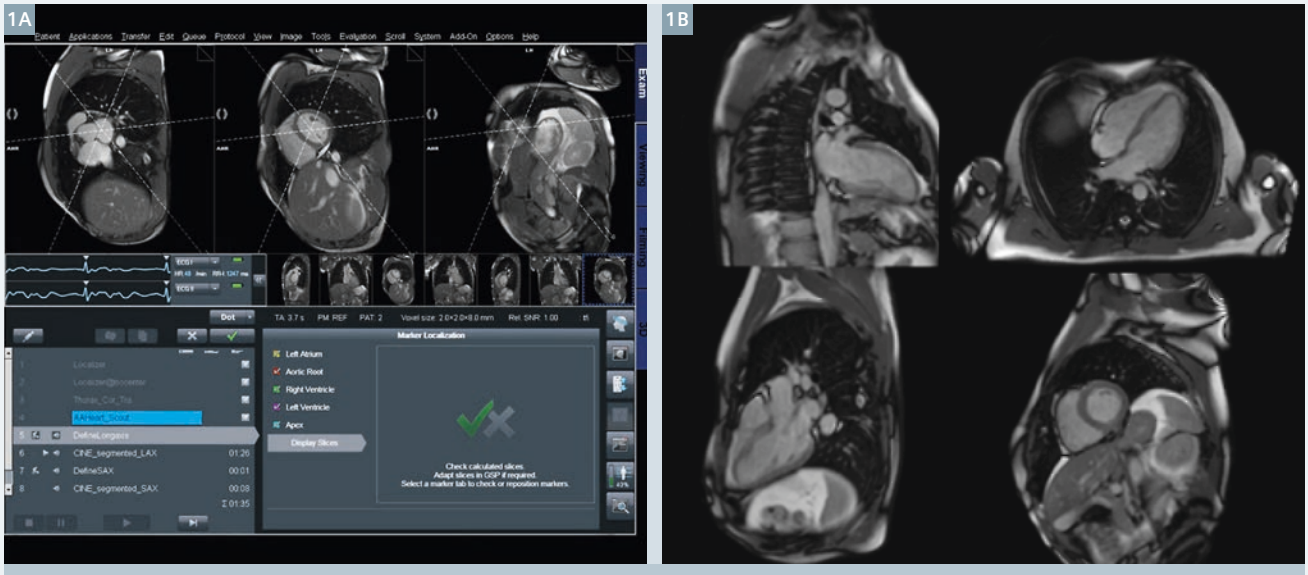


1 Automatic planning of the different cardiac axis with Cardiac Dot Engine.

During this time, we have observed a significant reduction of the average scan time.

We therefore proposed the following study to assess the time saved by using the Cardiac Dot Engine in both conventional and stress studies, compared to standard cardiac scans.

## Materials and methods

**Study design and patients**
We have retrospectively reviewed a total of 194 patients consecutively between October 2012 and March 2014 with CMR studies performed at our Siemens 1.5T system (MAGNETOM Aera XQ) with an 18-channel body matrix coil.

For the correct categorization of the study we took into account some variables:

- First, the type of study of stress or conventional CMR. The technical specifications of both protocol studies are summarized in Table 1.
- Second, the use of Short Tau Inversion Recovery (STIR) sequences. We usually use this sequence for patients with suspected acute disease or suspicion of infiltrative heart disease.
- Third, the use of the Cardiac Dot Engine or conventional software.

Depending on the different variables, we obtained eight groups comparing the average scan time with the Cardiac Dot Engine and without it (conventional software).

The total examination time comprises the time from the beginning until the end of each scan.

The image quality of the studies has been assessed by a radiologist with over 20 years of experience on a 10-point scale (1 = poor to 10 = excellent).

The statistical analysis has been performed using a Student's T-test for independent samples to compare means. SPSS Statistics software 20.0 (IBM corporation, Armonk, NY, USA) has been used.

## Table 1

| Conventional CMR | Stress CMR |
|---|---|
| Localizer | Localizer |
| HASTE | HASTE |
| AAHeart-Scout | AAHeart-Scout |
| Function 4-chamber | Function 4-chamber |
| Dynamic rest (Gadovist® 0.1 mmol/kg, 4 ml/s) | Dynamic stress adenosine (Gadovist® 0.1 mmol/kg, 4 ml/s) |
| Function 2 + 3-chamber | Function 2 + 3-chamber |
| Function short-axis | Function short-axis |
| Delayed enhancement | Delayed enhancement |
| | Dynamic rest (Gadovist® 0.1 mmol/kg, 4 ml/s) |

Specifications of both study protocols (stress and conventional CMR) performed at our Siemens 1.5T MAGNETOM Aera XQ.

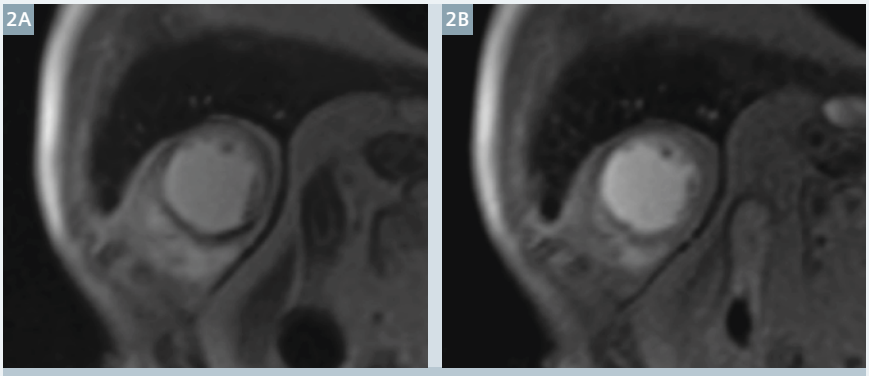


**2** MR images show positive findings on stress study in a 53-year-old man with chest pain. The inferolateral wall stress-induced perfusion shows a defect **(2A)** that corresponds with a stenosis involving the left circumflex artery (LCX), disappearing in the dynamic perfusion study **(2B)**.These findings were confirmed on subsequent invasive angiography with successful coronary stenting of the stenosis.

## Results

The image quality of all studies obtained a result between 9 and 10.

For conventional CMR studies with STIR sequences (58 patients) statistically significant differences in the average examination time using the Cardiac Dot Engine (t = 39.1 min +/- 12.1) have been observed, reducing the average examination time by 26.5 minutes compared to examination times using conventional software (t = 65.6 min +/- 14.1) (P = .003).

For stress CMR studies with STIR sequences (27 patients) a statistically significant decrease of the examination time has been observed with a reduction of 19.7 minutes (t = 45.11 min +/- 14.7) using the Cardiac Dot Engine compared to (t = 64.9 min +/- 7.8) examination times using conventional software (P = .001).

Furthermore, for CMR studies without STIR sequences (31 patients) a significant mean reduction of the examination time of 15.5 minutes has been found, which has been also statistically significant (t = 57.7 min +/- 14.7) compared to (t = 42.2 min +/- 16.1) (P= .001).

Stress CMR studies without STIR sequences (78 patients) have also shown mean examination times of (t = 44.6 min +/- 16.8) using the Cardiac Dot Engine compared to (t = 65.1 min +/- 22.3) using the conventional software, which means a time reduction of 20.4 min (P = .002) (Table 2).

## Discussion and limitations

Our study is not without limitations.

First of all, it is a retrospective study, which has inherent disadvantages.

There are also independent variables that may alter the average examination time. For example, at the time of infusion of adenosine, as a rule, there is a cardiologist present. The mean arrival time of the cardiologist is (t = 4.8 min +/- 7.1), which introduces a considerable delay.

There may also be glitches that force the study to be repeated, although this is very rare. This process, however, rarely extends beyond 5 minutes.

Another factor that may have extended the examination times at the beginning of this study is the universal training of all MRI personnel. It has been observed that during the initial learning phase, after the introduction of the Cardiac Dot Engine, the average examination times have been longer than afterwards. However, once the basic handling of the Dot Engine has been learned, the Cardiac Dot Engine has a fast learning curve without requirement of highly specialized technologists.

## Conclusion

The Cardiac Dot Engine introduces patient benefit by providing systematically reproducible and efficient studies that consistently reduce examination time, resulting in increased efficiency, reduced costs and improved patient satisfaction without ever sacrificing high-quality diagnostic images.

## Table 2

**Time reduction in cardiac magnetic resonance**

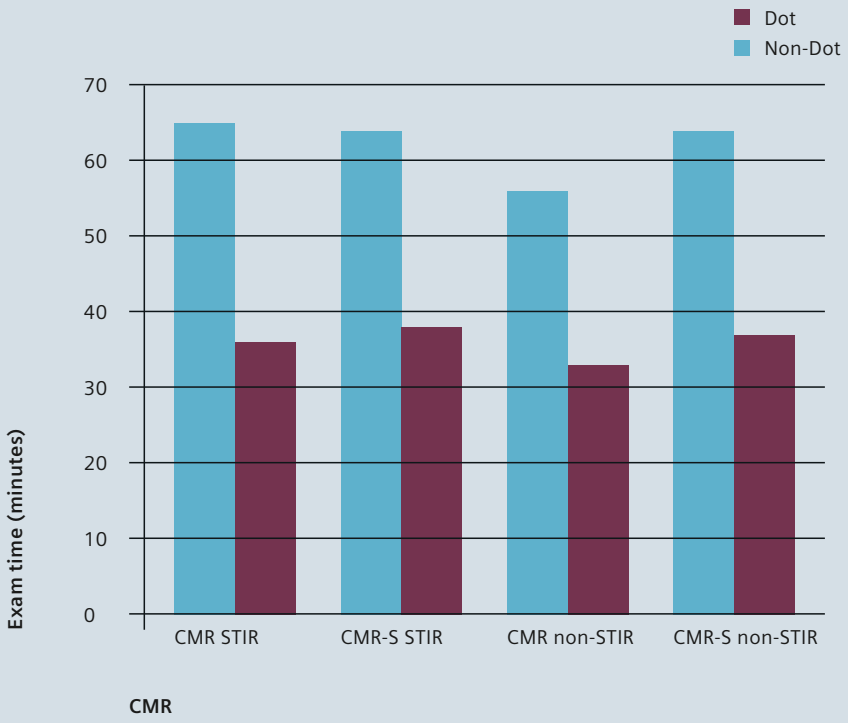


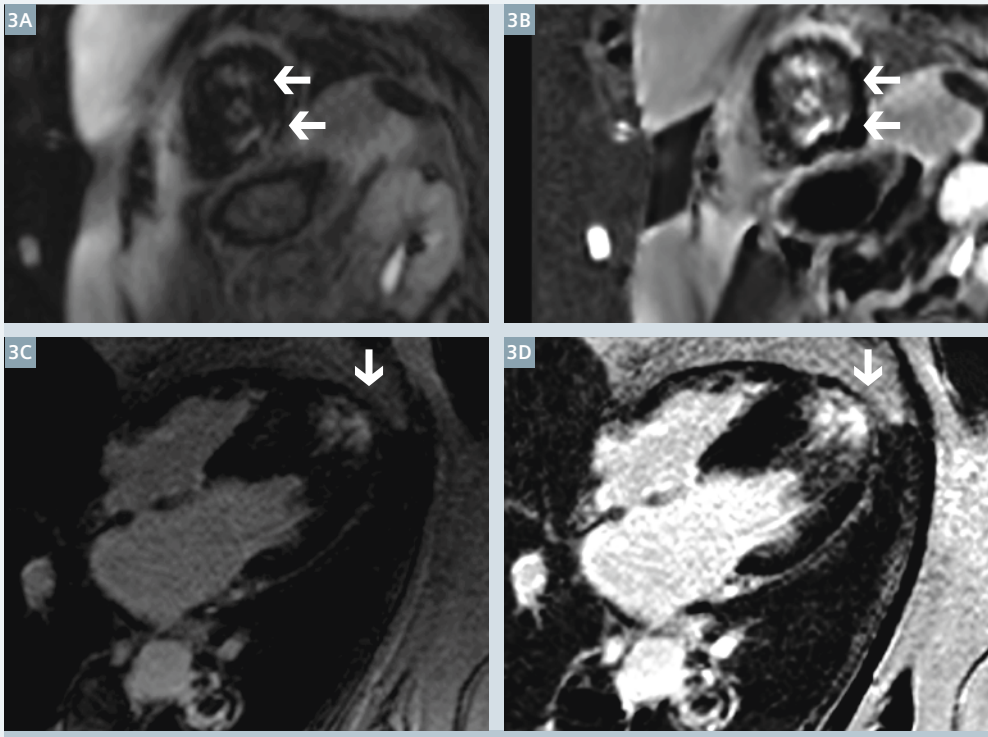


3 Short axis **(3A, B)** and four-chamber-view **(3C, D)** demonstrates hypertrophic changes as well as delayed contrast enhancement in the apex in a 43-year-old man with hypertrophic cardiomyopathy.

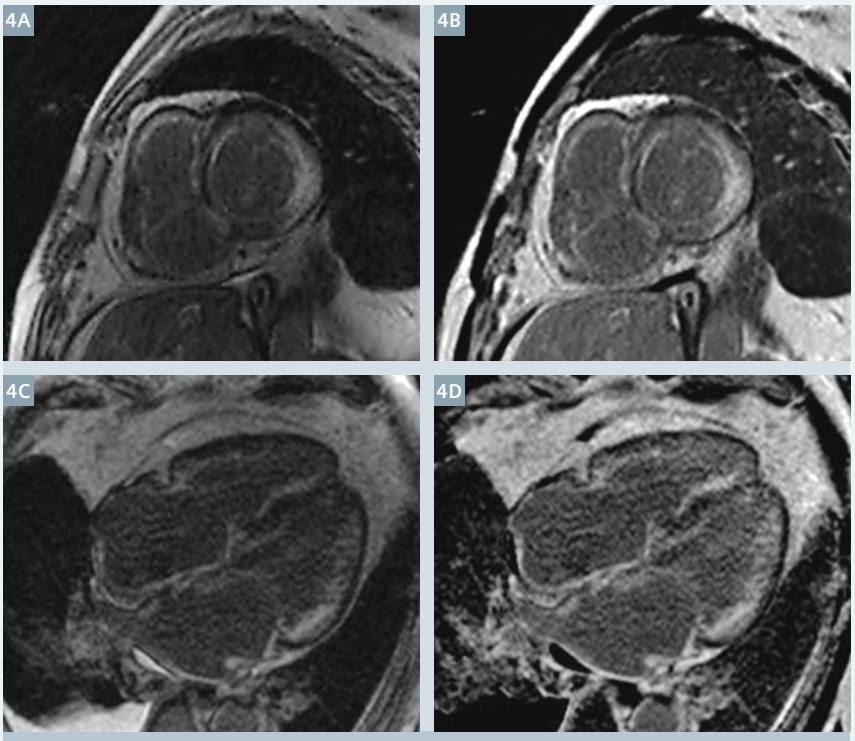


4 Delayed enhancement in the short axis **(4A, B)** and four-chamber-view **(4C, D)** reveals the presence of a diffuse patchy enhancement pattern, very suggestive of cardiac amyloidosis in a patient with congestive heart failure. A cardiac biopsy confirmed the diagnosis.

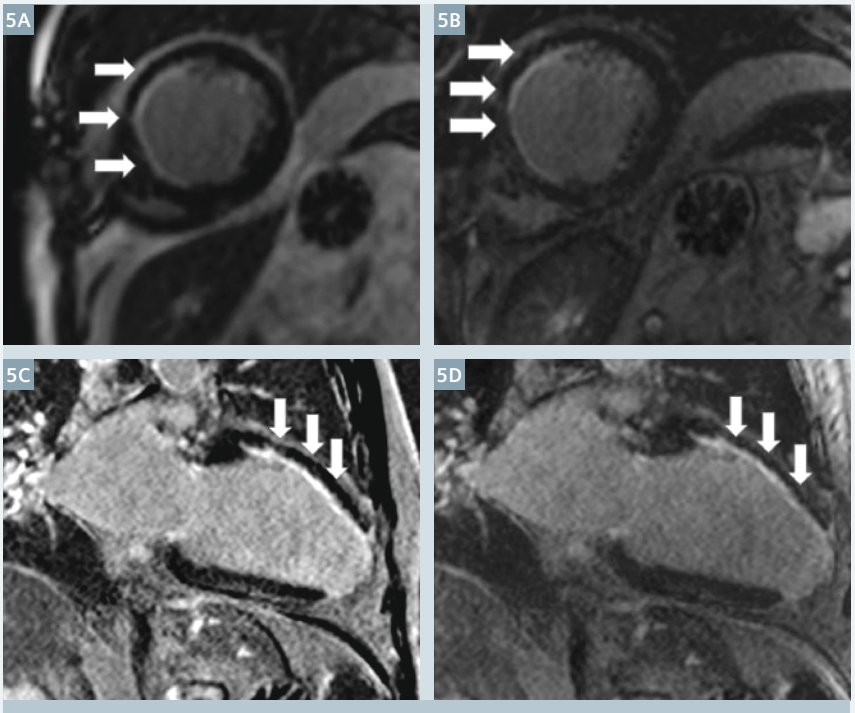


5 **(5A, B)** Short axis and **(5C, D)** two-chamber-view of delayed enhancement sequences. Arrows point to the septal wall of this patient, showing a severe subendocardial hyperenhancement that represents the region of myocardial infarction in the territory of left anterior descending (LAD) and the left circumflex artery (LCX).

## Acknowledgements

The authors would like to thank all the members of the Cardiac MRI team from the Clínica Universidad de Navarra (CUN) and the MRI nurses for their valuable participation, helpfulness and support during the study, and also a very important acknowledgment to our colleagues from Siemens Healthcare, especially Efrén Ojeda, for his continuous support and contribution.

### References

1 McMurray JJ, Adamopoulos S, Anker SD, Auricchio A, Böhm M, Dickstein K et al. ESC guidelines for the diagnosis and treatment of acute and chronic heart failure 2012. Eur J Heart Fail. 2012 Aug;14(8):803-69.
2 Montalescot G, Sechtem U, Achenbach S, Andreotti F, Arden C, Budaj A et al. 2013 ESC guidelines on the management of stable coronary artery disease: the Task Force on the management of stable coronary artery disease of the European Society of Cardiology. Eur Heart J. 2013 Oct;34(38):2949-3003.
3 Moenninghoff C, Umutlu L, Kloeters C, Ringelstein A, Ladd ME, Sombetzki A et al. Workflow efficiency of two 1.5 T MR scanners with and without an automated user interface for head examinations. Acad Radiol. 2013 Jun;20(6):721-30.

## Contact

Jesús Ciro Pueyo, M.D., Ph.D.
Department of Radiology
Clínica Universidad de Navarra
Av. Pio XII, 36
31008 Pamplona
Spain
Phone: +34 948255400
Fax: +34 948296500
jpueyo@unav.es

# Cardiac MRI on MAGNETOM ESSENZA

Ilan Gottlieb, M.D., Ph.D.; Gabriel Camargo, M.D.

Radiology Department, Casa de Saúde São José, Rio de Janeiro, Brazil

## Introduction

Of course you would prefer to drive to work every day in a state-of-the-art convertible sports car, with the top down, feeling the autumn breeze on your face. But for most people, reality dictates otherwise, and you must settle for something less grand. However, even at a lower budget, you can still have what matters most on your daily commute: Comfort and reliability. This is the fairest picture we could draw from working with a MAGNETOM ESSENZA. It's definitely not a top-of-the-range sports car, but it will get you almost anywhere. Due to its hardware configuration, the ESSENZA has some limitations for cardiac imaging, but after some adjustments, it can absorb most of the routine cardiac workload. We will try to delineate some adjustments in sequence design and exam strategy, which may enhance image quality and overcome some pitfalls.

## 1. System configuration

The MAGNETOM ESSENZA is a 1.5T system that comes with built-in cardiac capability in all system configurations. This includes cine functional imaging, perfusion sequences, inversion-recovery late gadolinium enhancement with PSIR (phase sensitive inversion recovery), TSE-based morphologic sequences, and phase contrast for flow measurement. There is no 3D gated (to account for cardiac motion) and navigated (to account for respiratory motion) acquisition in any configuration. It has a bore size of 60 cm and gradient strength of 30 mT/m @ 100 T/m/s. Although the magnetic field homogeneity is somewhat limited on the z-axis, cardiac imaging needs small fields-of-view, making this a non-issue for this application. Interestingly, perhaps due to the low gradients and smaller bore size, field homogeneity confined to the heart is rather good, compared to other systems. The system allows up to 16 independent analog RF channels, although we feel 8 channels are enough, given that the small FOV doesn't usually allow for large body areas to be covered at once.

## 2. Improving signal-to-noise

Parallel acquisition acceleration (iPAT) is available (GRAPPA) but should be limited to a minimum, as signal-to-noise ratio is pulled back by the low gradients, limited number of channels and analog coil acquisition. We routinely turn iPAT off for cine imaging, morphologic TSE sequences and segmented late gadolinium enhancement, but we use it for single shot sequences due to temporal resolution constraints. One option would be to increase the number of reference lines (for example to 48), as a middle ground in SNR and acquisition time, but we find that in practice this is somewhat cumbersome and doesn't help much.

We usually work with slice thickness of 8 mm, which can go up to 10 mm in perfusion sequences. Additionally, matrix size for segmented cine and late gadolinium enhancement are 224 to 240, as opposed to 256 commonly used in other systems. We also usually work with FOV of 34 cm or higher, even in smaller patients. These measures are done as a way to improve SNR, but will lower the spatial resolution, which we find can be safely done resulting in good diagnostic images, but can be a problem in infants*, whom we prefer not to image in this system.

Using SSFP[1] instead of s-GRE readout for late gadolinium enhancement also enhances SNR. SSFP has inherent T2/T1-weighting, so theoretically it's not as good for LGE as s-GRE (pure T1-weighting), but in practice the inversion pre-pulse adequately weighs for T1, and enhancement can be depicted as consistently in SSFP as in s-GRE [1].

*Siemens disclaimer: MR scanning has not been established as safe for imaging fetuses and infants less than two years of age. The responsible physician must evaluate the benefits of the MR examination compared to those of other imaging procedures.

[1] The product is still under development and not commercially available yet. Its future availability cannot be ensured.

## Table 1: Sequence overview

| Sequence | Cine | Perfusion | Late Gadolinium Enhancement | Phase contrast | Morphological turbo spin echo |
|---|---|---|---|---|---|
| Matrix | 224 | 160 | 224 | 204 | 224 |
| Phase resolution | 80% | 60% | 80% | 90% | 90% |
| Readout | SSFP | SSFP | SSFP | GRE | TSE |
| iPAT | No | Yes | No | Yes | No |
| Slice thickness | 8 mm | 10 mm | 8 mm | 8 mm | 8 mm |

## 3. Myocardial perfusion

Perfusion sequences are perhaps the most hardware demanding. They can have spoiled gradient echo, steady state free precession or echoplanar readouts. There is the need for a saturation pre-pulse for T1-weighting and entire *k*-space filling in a continuously cartesian manner in every RR interval. Ideally, one should be able to acquire at least three short-axis images of the heart in one heartbeat, at the base, mid and apical levels. Unless matrix size is very small and heart rate is very slow, iPAT needs to be turned on. SSFP readout allows for better SNR and slightly faster acquisition than s-GRE [2]. Individualized pre-pulses before every slice generate homogenous contrast among all slices. Echoplanar readout is faster but renders too noisy images in all systems, especially in the ESSENZA. In order to increase SNR further, 10 mm slice thickness should be considered (8 mm minimum), and matrix size should vary from 160 to 192 mm according to acquisition heart rate. Increasing the receiver bandwidth will decrease minimum TR and speed up the acquisition [3], but should be done cautiously (it is set to high levels already), testing each increase until you feel comfortable with the images. Inversion time (TI) is usually set to the minimum value allowed, around 100 ms.

## 4. Examination strategies

Since breath-hold times are usually long due to iPAT off and low segmentation, a frequent mistake is to demand too much of the patient before contrast injection, and then acquire late gadolinium enhancement images blurred by respiratory motion artifacts. We set up the scanning protocol to have the lowest number of apneas possible. Our scouts are free-breathing, only the short-axis scout is breath-held. We use HASTE and SSFP single shots for overall anatomic evaluation of the aorta, pulmonary artery and heart, asking the patient to take slow and shallow breaths, but not holding. Additionally, we mind segmentation when the heart rate is too slow (or obviously too fast) – as a rule of thumb, one cine slice in the ESSENZA should last 7-8 seconds.

While we usually avoid working with a FOV below 34 cm regardless of patient size due to SNR concerns, on first-pass perfusion sequences where matrix size is considerably reduced, we believe all efforts should focus on keeping the FOV as small as possible. Since the left arm is frequently aligned with the short-axis planes, this upper limb or both should be placed above the patient's head if he/she can tolerate this position. Also, wrapping artifacts should be tolerated as long as they

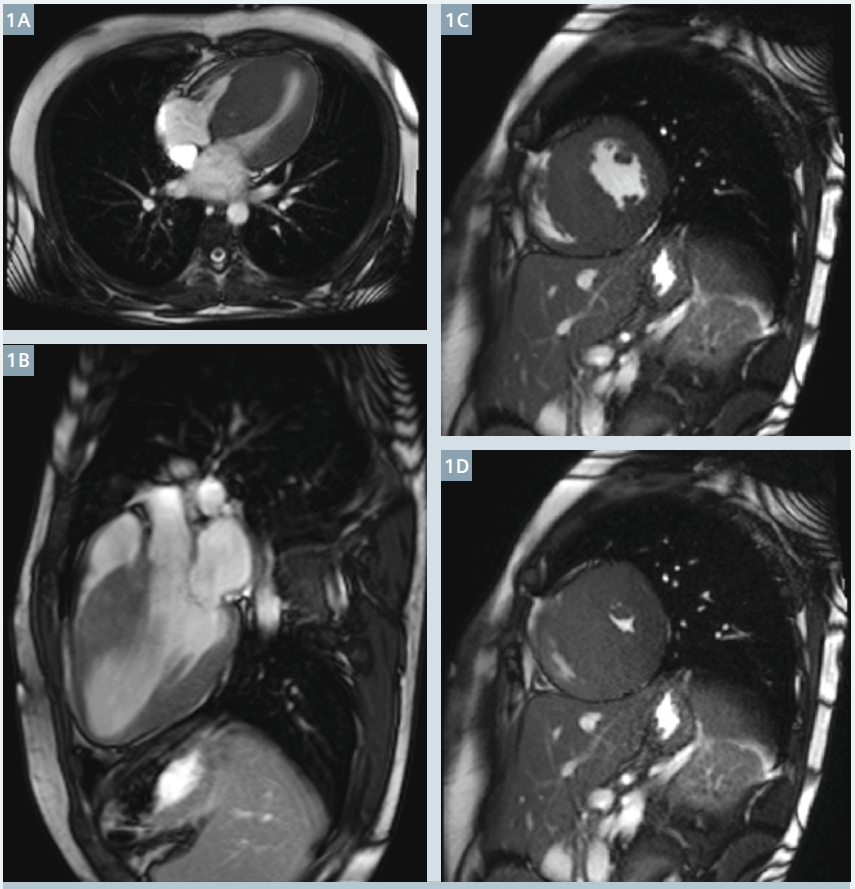


1 SSFP cine images of a patient with hypertrophic obstructive cardiomyopathy (HOCM), on four-chamber-view **(1A)**, longitudinal long-axis-view **(1B)** and short-axis-view in diastole **(1C)** and systole **(1D)**.

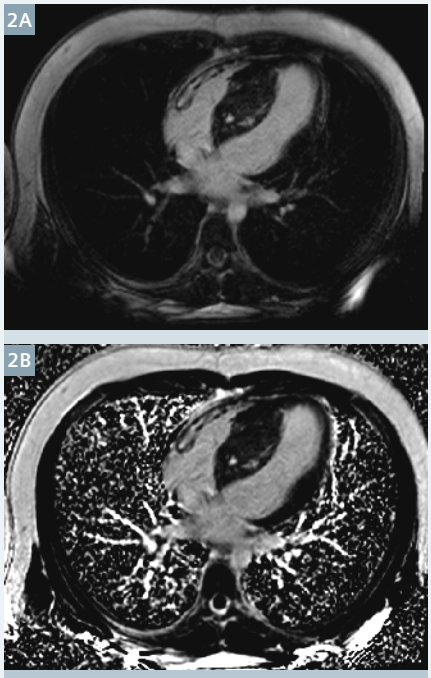


2 Inversion-recovery segmented late gadolinium enhancement images from the patient in figure 1, exhibiting non-ischemic septal fibrosis on magnitude **(2A)** and phase-sensitive **(2B)** reconstructions.

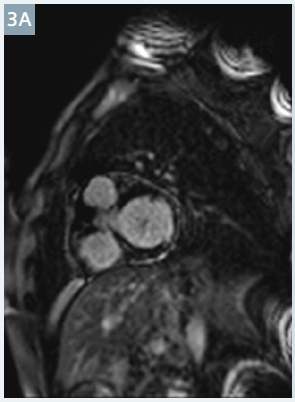


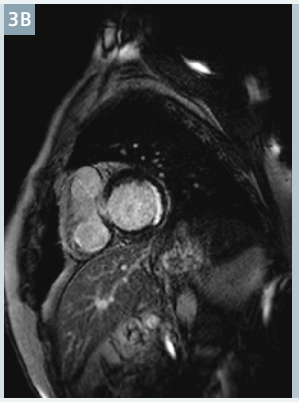


3 Single-shot **(3A)** and segmented **(3B)** inversion-recovery late gadolinium enhancement images from a patient with previous myocardial infarction with subendocardial lateral fibrosis.

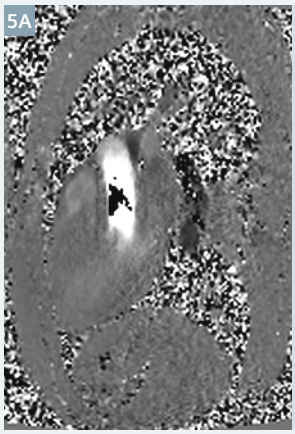



5 In-plane phase contrast image from the HOCM patient in figure 1 exhibiting increased velocities in the ascending aorta with aliasing at 1.5 m/s venc **(5A)**, and corresponding GRE image reconstruction **(5B)**.


4 Stress first pass myocardial perfusion of a patient with obstructive coronary disease, depicting a subendocardial perfusion defect at the inferior and septal walls.

occur distant from the heart, which can be checked on pre-contrast scouts.

## 5. Limitations

For a normal patient with stable sinus rhythm who can hold his/her breath for 10 seconds, MAGNETOM ESSENZA performs quite nicely. But it does not come with arrhythmia detection, and the cine realtime used for patients incompatible with prospective gating is poor, as temporal and spatial resolutions are too low. For the same reason, late gadolinium enhancement single shot images are sub-optimal. We choose not to image small infants*, due to the combination of low SNR in small FOVs and unavailability of gated 3D images for anatomic delineation of congenital abnormalities.

*Siemens disclaimer: MR scanning has not been established as safe for imaging fetuses and infants less than two years of age. The responsible physician must evaluate the benefits of the MR examination compared to those of other imaging procedures.

## Conclusion

MAGNETOM ESSENZA delivers good diagnostic cardiac imaging and seems to have good cost/benefit ratio for a general radiology clinic with some volume of cardiac studies. It is able to handle most of the routine work, is easy to operate and, with some adjustments, delivers excellent image quality.


References

1 Li W, Li BS, Polzin JA, Mai VM, Prasad PV, Edelman RR. Myocardial delayed enhancement imaging using inversion recovery single-shot steady-state free precession: initial experience. J Magn Reson Imaging. 2004 Aug;20(2):327-30.

2 Wang Y, Moin K, Akinboboye O, Reichek N. Myocardial first pass perfusion: steady-state free precession versus spoiled gradient echo and segmented echo planar imaging. Magn Reson Med. 2005 Nov;54(5):1123-9.

3 Kellman P, Arai AE. Imaging sequences for first pass perfusion - a review. J Cardiovasc Magn Reson. 2007;9(3):525-37.


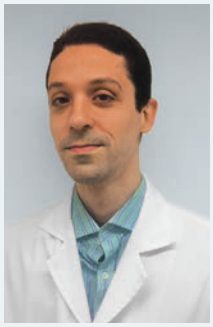

Gabriel Camargo

Ilan Gottlieb


## Contact

Ilan Gottlieb, M.D., Ph.D.
Radiology Department
Casa de Saúde São José
R. Macedo Sobrinho, 21
Rio de Janeiro - RJ, 22271-080
Brazil
ilangottlieb@gmail.com

# An Approach to Semi-Automated Cardiac MR Post-Processing Using *syngo*.via MR Cardiac Analysis

Ryan Avery, M.D.; Puneet Sharma, Ph.D.

University of Arizona Health Network, Department of Medical Imaging, Tucson, AZ, USA

## Introduction

Cardiac MRI (CMR) has become the definitive examination for numerous pathologies due to unique pulse sequences that MRI provides to evaluate both cardiac function and tissue. In order to optimize CMR scanning, the introduction of standardized protocols provide an optimal balance between essential pulse sequences and scan time efficiency [1]. CMRI efficiency has been further advanced with the introduction of shorter MR sequences and automated scanning techniques, such as the Cardiac Dot Engine.

Despite these advances, CMR is still encumbered with time-intensive post-processing of these sequences. Manual techniques, such as Argus workflow (Siemens Multi-Modality WorkPlace) and other commercial post-processing software, perform quantitative analysis by user identification and contouring of anatomic structures; i.e., contouring the ventricular myocardium in short axis cine-gated sequences and evaluating vascular flow with phase contrast sequences, which continue to be a tedious component of CMR interpretation.

Siemens' *syngo*.MR Cardio Engine *in syngo*.via offers a semi-automatic workflow that provides an alternative to manual post-processing by utilizing computer-aided detection of the left ventricle and mitral valve position to provide automatic contouring of the left ventricular throughout the cardiac cycle.

The transition from manual cardiac post-processing to a semi-automatic format requires an adaption of the user's previous manual skill-set to the new semi-automatic workflow. In my clinical experience, most user difficulty relates to the adjustment to the more 'hands-off' workflow of automated post-processing. But with direction, users begin to adapt to the new workflow and are able to fully utilize *syngo*.via's semi-automated processing to acquire maximum efficiency.

In order to further propagate this instruction, I will outline a basic CMR post-processing session using *syngo*.via MR Cardiac Analysis with a notable emphasis regarding changes from traditional manual post-processing, and furthermore, how to maneuver out of potential pitfalls.

## Technique

CMR scanning requires attention to proper image acquisition in relation to long-axis (LAX) and short-axis (SAX) views and central positioning of the heart within the image (Fig. 1). At our institution, the Cardiac Dot Engine ability to efficiently reproduce long- and shot-axis views of the heart is utilized in conjunction with SCMR protocols [1].

Within *syngo*.via, the MR Cardiac Analysis workflow steps are displayed as rectangular tiles (Fig. 2) notifying the performance of multiple steps of processing, which is a departure from

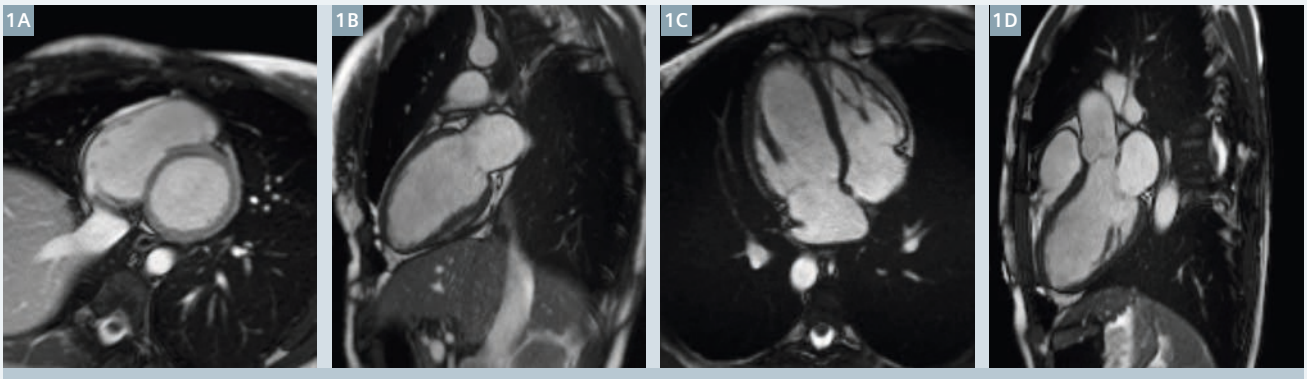


1 Representative SAX and LAX TrueFISP ECG-gated sequences demonstrating proper image orientation and central positioning of the heart.

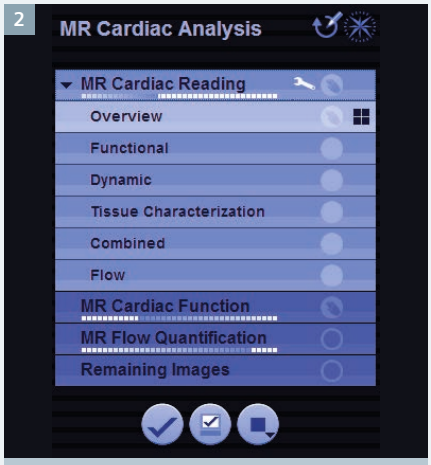


2 MR Cardiac workflow tiles demonstrate progress bars indicating automated processing.

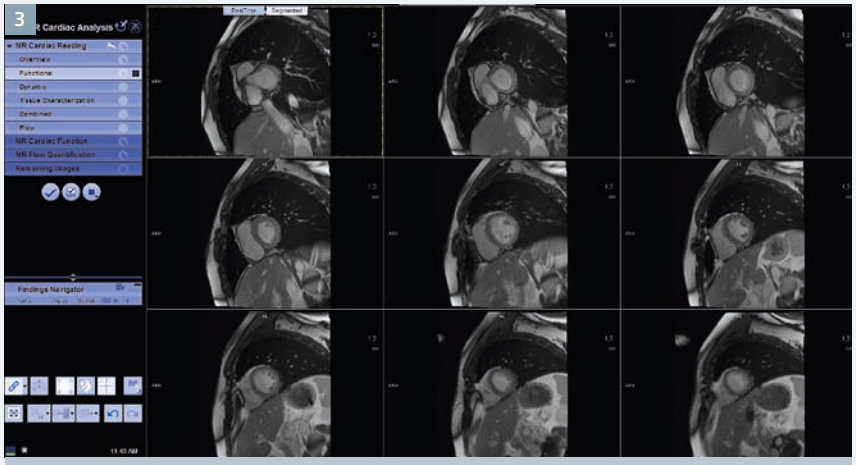


3 Functional workflow displays the SAX and LAX gated sequences in a cine loop. A representative set of SAX is displayed.

manual techniques because *syngo*.via identifies and sorts the sequences necessary for each workflow step and begins post-processing by automatic production of left ventricular base plane and myocardial contouring.

The Overview tile displays all sequences in the order acquired, allowing access to any desired sequence. Progressing to the second tile, Functional, will display the gated sequences for identification wall motion abnormalities (Fig. 3).

Each segmental wall motion abnormality can be display in a color-coded diagram (Fig. 4), which can be archived upon post-processing completion.

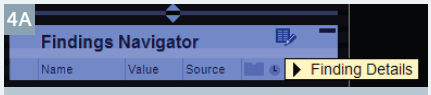


4A Within the Functional step's Finding Details, a color-coded segmental map of wall motion abnormalities can be produced.

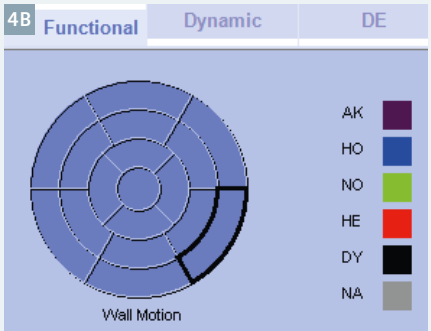


4B Wall segment motion is labeled by clicking on the segment, and then on the color box demarcating the wall motion visualized.


4C With a right click, all unlabeled segments may be labeled as normal.

The Dynamic, Tissue Characterization, and Flow tiles allow directed analysis of perfusion, late gadolinium enhancement, and phase contrast, respectively. Additionally, the Findings section of both Dynamic and Tissue Characterization allow for color-coded diagram production. (It is felt that these steps are similar enough to Functional that a step-by-step discussion is beyond the scope of this article.)

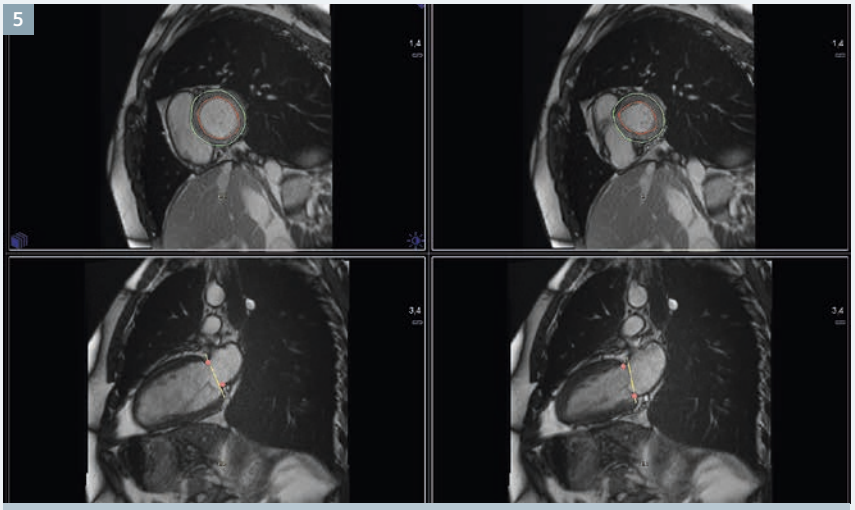

5 First monitor of MR Cardiac Function. The top row is dedicated to SAX views, and the bottom is dedicated to available LAX views. Automated myocardial contours are produced for the SAX (top row), and the designated position of the mitral valve base plane is displayed in the LAX views (bottom row).

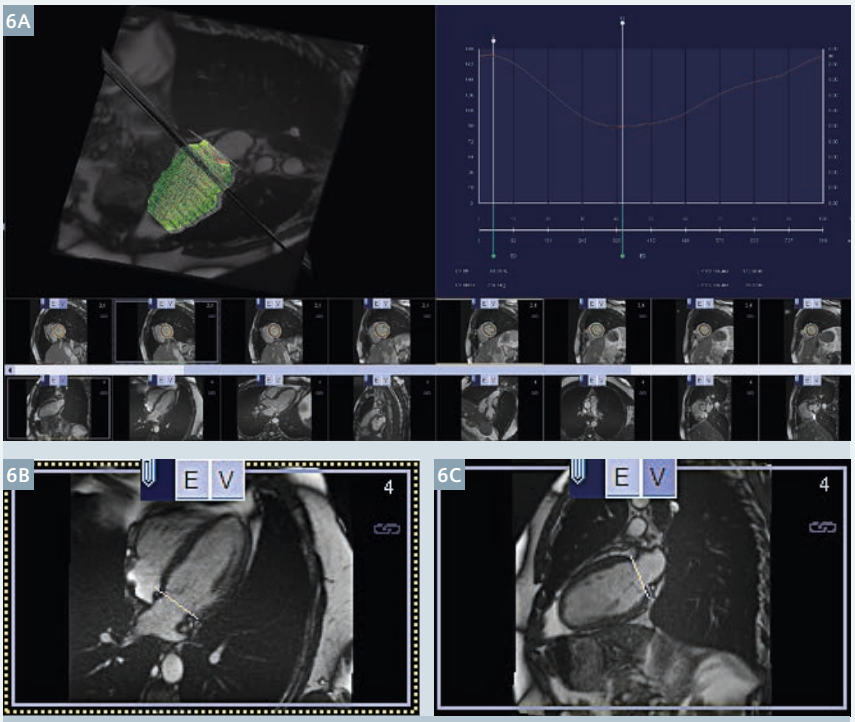


6 Second monitor of MR Cardiac Function. SAX and LAX views can be selected for further processing on monitor 1. A dashed yellow outline designates the image being processed, and any view displayed on monitor 1 has a light blue outline.

The discussion of MR Cardiac Function will assume a 2-monitor display. Monitor 1 is used for active post-processing and displays a 2 x 2 layout with SAX and LAX slices displayed in end-diastole (ED) and end-systole (ES) (Fig. 5).

Monitor 2 displays a row of all SAX views, and a separate row of additional gated-images, which contains the LAX views. Further evaluation of these views on monitor 1 can be performed with left and right arrow keys or mouse-clicking on the preferred slice (Fig. 6).

*syngo*.via's processing is performed by anatomic localization of key structures including the LV apex, the anterior RV insertion point, and LV blood pool, which are demonstrated by a series of automatically positioned color-coded dots (Fig. 7). If necessary, these localization dots may be modified within their respective tile.

The gated-image chosen to denote ED and ES appear on the image. To modify the image designated as ED or ES, the user can drag ED or ES pin on the volume curve (Fig. 8).

The user can quickly evaluate if the processed SAX contours and anatomic locations are correct, and if so, the apical localization, blood pool, and RV insertion steps can be considered accurate, and the user can proceed directly to the Refine Segmentation step (Fig. 9).

During SAX review, it is recommended that the left column of the first monitor be kept in ED, and the second column in ES (Fig. 10). Since the calculated changes between ED and ES are utilized for quantitative analysis, it is recommended that modification be kept to the ED and ES positions to minimize the amount of manual segmentation and processing data points.

The automated position of the mitral valve base plane uses the LAX views to localize the base of the left ventricle in both ED and ES (Fig. 11). Modification of the base plane can be performed in any LAX view by moving the localization dots.

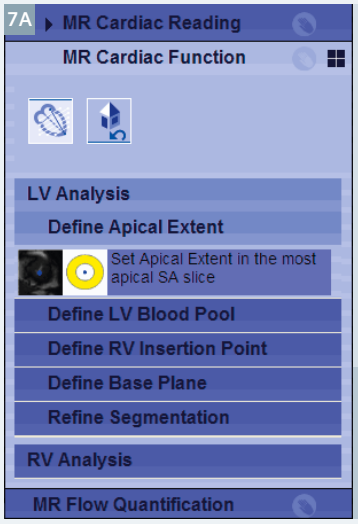


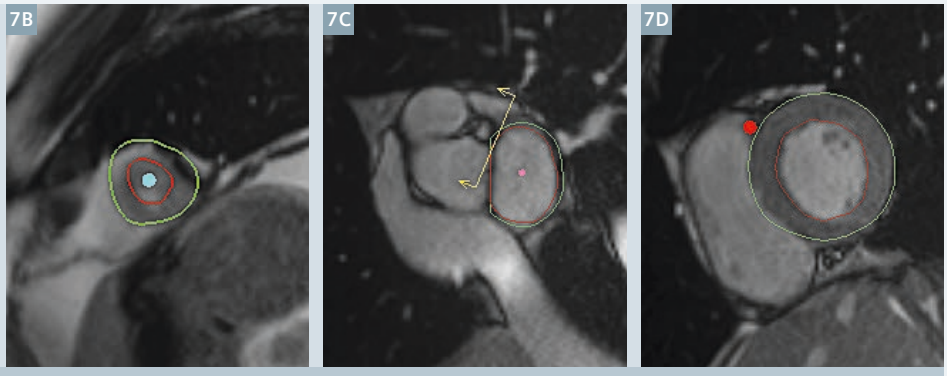


7 MR Cardiac Function interface starts with defining the apical extent, blood pool, and, RV insertions. A single blue dot denotes the position detected as the LV apex. A pink dot placed at the basal LV localizes the central LV blood pool. A red dot outside of the basal LV indicates the location of the RV insertion.

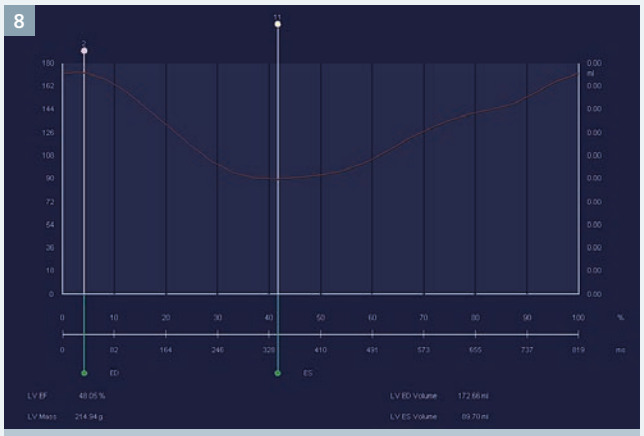


8 A volume curve displays the calculated ventricular volumes throughout the cardiac cycle. Pins designating ED and ES are automatically chosen by *syngo*.via. The image designated as ED or ES can by modified by dragging the pin left or right to the desired curve position.

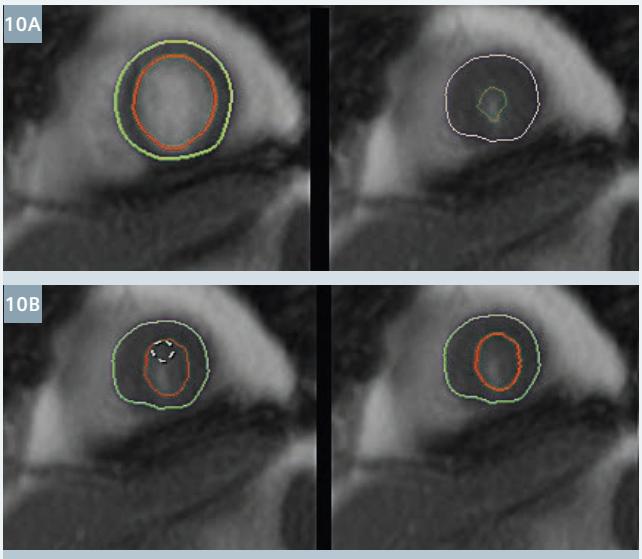


10 A myocardial contour used for processing of all images in series will be shown as a thick line. Initial processing is done in ED, but if the user modifies a contour it will change the line from thin to thick and will be used for contour processing.

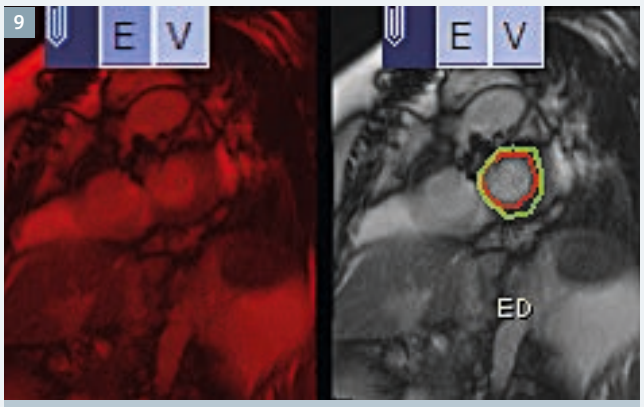


9 The SAX contours can be assessed by right-clicking through the SAX display row. If an image is degraded or unnecessary it may be excluded by clicking the E, which will turn the image red denoting that it's data will not be used in quantitative analysis.

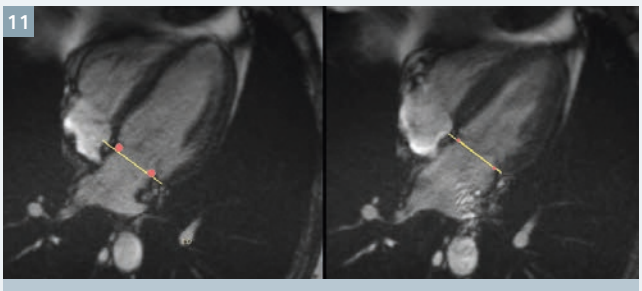


11 Automatic positioning of the mitral valve base plane uses pink localization dots depicting the septal and lateral position of the base plane. Big pink dots are displayed near ED and ES denoting that the image was used for automated processing of the entire cardiac cycle. The user is recommended to only modify the large dots thus decreasing manual post-processing.

Base plane position can be visualized in SAX views as a yellow line with an arrow at the superior and inferior aspects (Fig. 12).

For most CMRs performed, post-processing is complete at this point. Optimally, *syngo*.via should reduce post-processing to a series of visual quality checks confirming proper left ventricle localization and contouring, and mitral valve base plane placement. Manual post-processing, if necessary, should be reduced to simple nudging of portions of the contours and optimization of base plane position.

Some CMRs will require an advanced level of post-processing including RV evaluation and vascular flow quantification, which can also be performed with *syngo*.via using additional steps included in MR Cardiac Analysis.

## Right ventricle assessment

The first step of RV Analysis requires manual contouring of each SAX position in ED. With the manual production of a single contour in ED, *syngo*.via will automatically generate contours for the remainder of the cardiac cycle.

Drawing a contour in a single motion using the free-hand tool is recommended because the processing time required for multiple steps may become tedious. After each contour generation, evaluation of the processed ES contour is recommended to assess accuracy and the possible need for editing (Fig. 13).

To produce the tricuspid valve base plane, the 4-chamber view is used to manually identify the RV base plane margins in ED. After the RV base plane is produced in ED, the RV basal margins must again be localized in the ES view to complete RV base plane processing (Fig. 14).

To complete ventricular processing, using the Join Function tool within Refine Segmentation will smoothly join the contours of both ventricles throughout the cardiac cycle (Fig. 15) producing a more accurate anatomic assessment.

## Flow quantification

The MR Flow Quantification tile is used for phase contrast post-processing. This workflow step can perform vessel contouring with one step with the use of the auto-contour tool (Fig. 16).

If multiple phase contrast views are performed, the additional sequences dragged into the MR Flow Quantification layout from the sequence browser by clicking on the arrow on the right side of the display on the first monitor.

12

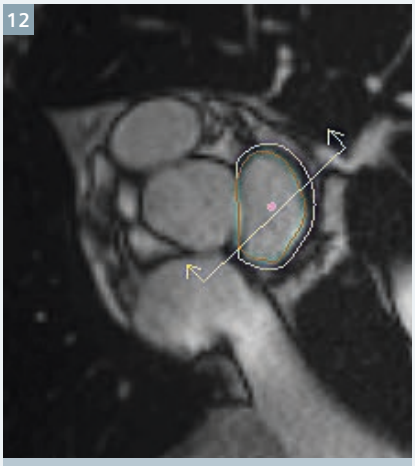

12 Base plane in SAX. The arrows arising from the LV base plane line denote the contour volumes included in the ventricular volume and mass.

13

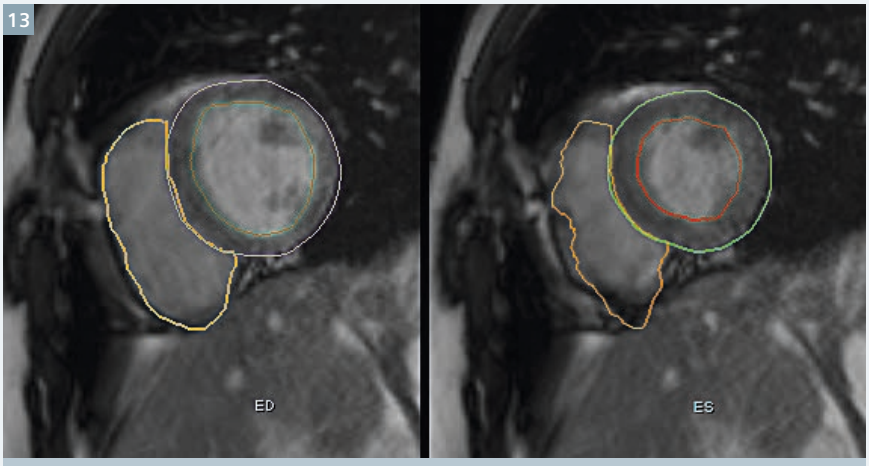


13 The RV contour is drawn for each slice of the SAX in ED. The processed ES contour should be visually assessed after ED contouring. Any refinement of the ES should be performed before moving to the next SAX position.

14

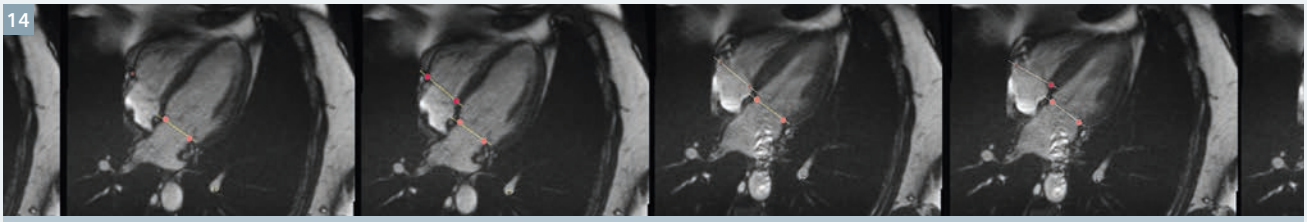

14 Sequential demonstration of Semi-Automated production of the RV base plane. Starting in the ED 4-chamber view, the user will click on the lateral and septal margins of the RV base producing 2 large dots, and the RV base plane line will then form between the dots. Next, in ES the dots are dragged to the proper position of the RV base allowing *syngo*.via to complete processing for the RV base plane throughout the cardiac cycle.

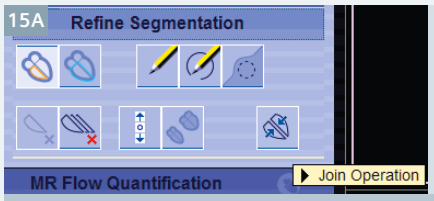


15 Clicking the Join Function tool will combine the septal portion of the RV contours with the LV contours.

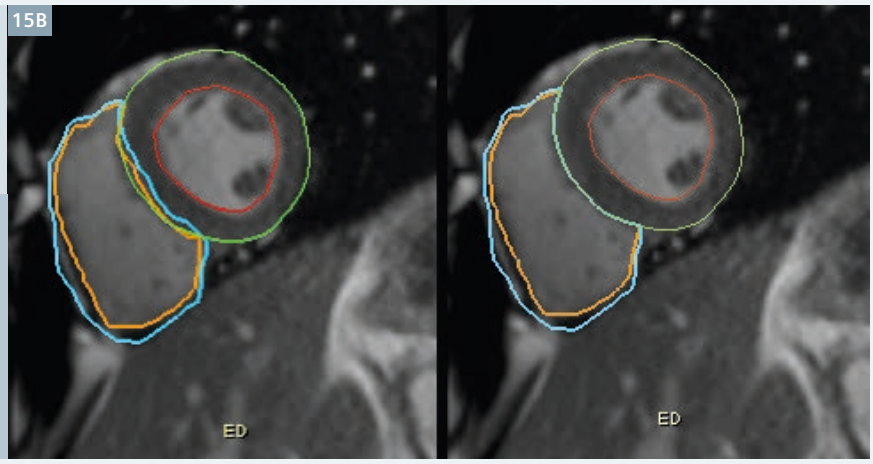


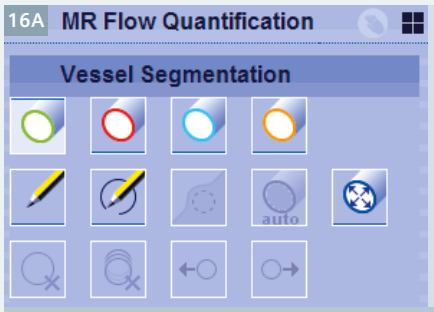


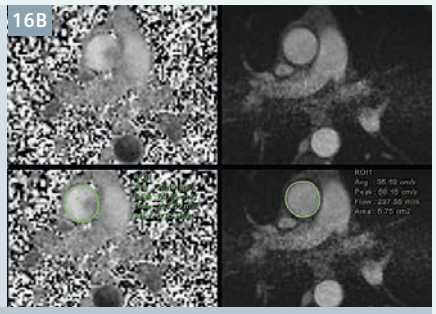


16 The One-Click Vessel Segmentation tool allows MR Flow Quantification to be performed in a single step by a clicking once in the vessel center of an in-plane phase contrast view, which produces an accurate contour of the vessel throughout all images in the sequence.

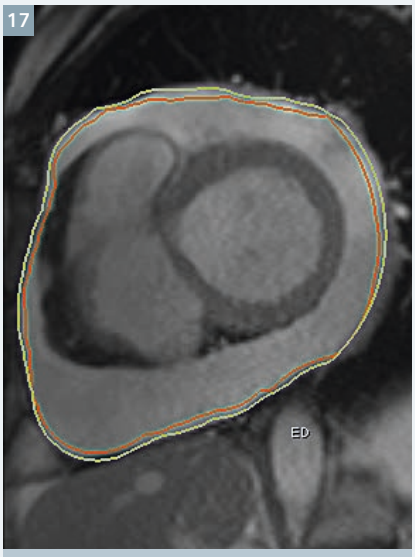


17 Miscalculation of the LV contours is often related to the entire heart being seen as the LV due to an excessively large image acquisition window during MR scanning.

At this stage, post-processing for even more advanced CMRs is completed, and the Finding Details icon can be clicked so ventricular and vessel quantitative data can be saved by clicking on the Create Findings button, which will allow the results to be archived upon completion of the study.

## Pitfalls

Given the variability of cardiac anatomy and image acquisition, *syngo*.via post-processing can falter. Solving these miscalculations can be quite tedious if the user applies manual troubleshooting techniques. However, if approached with an appreciation of semi-automated processing, *syngo*.via can be leveraged to correctly redraw the LV in a short series of steps.

Since most miscalculations result from automated contouring of the wrong anatomic structure or the entire heart (Fig. 17), most cases can be solved by insuring that the SAX stack images are well centered within an appropriate sized acquisition window.

Within *syngo*.via, the first step to correct an LV miscalculation is to reposition the apical dot while in the Apical Localization step. Repositioning the blue dot will result in repeat auto-segmentation producing a new set of myocardial contours and repositioning the LV base plane.

If repositioning of the apical dot does not succeed, I recommend deleting all LV contours with the Delete Contours tool (Fig. 18A), and redrawing in ED the contours for a single SAX slice in the middle of the LV, which automatically produces contours throughout the cardiac cycle for the single SAX image (Fig. 18B). Next, clicking the Spatial Propagation tool will produce automated contours for the remaining SAX stack images (Fig. 18C).

After redrawing the LV contours, the LV base plane position should

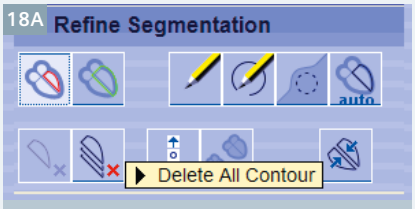


18A Delete Contours in both endocardial (red contour) and epicardial mode (green contour) to remove all LV contours.

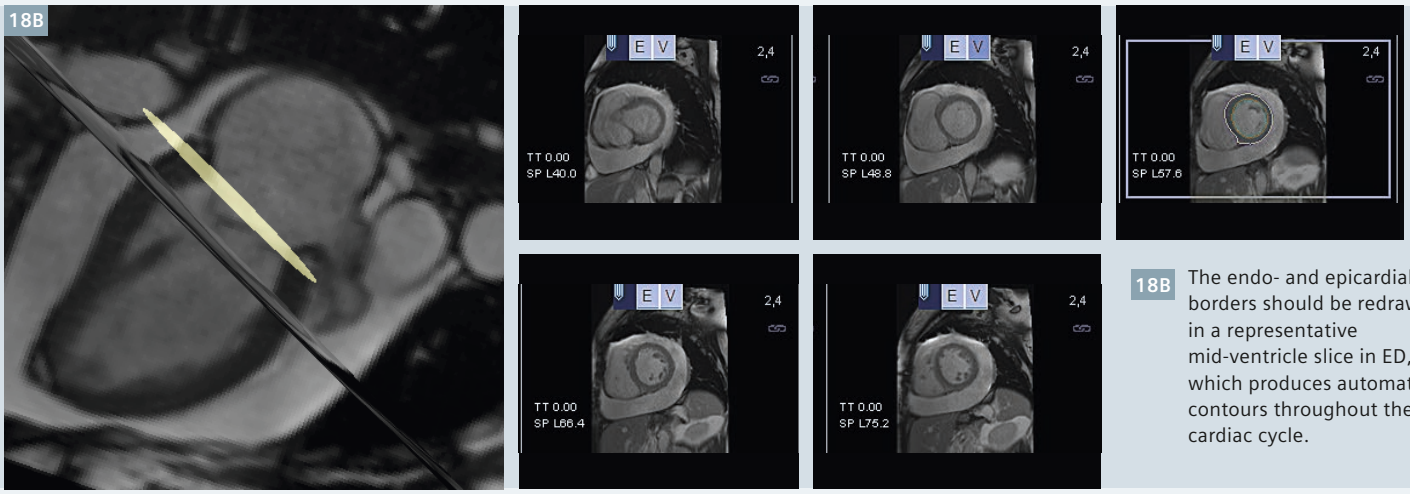


**18B** The endo- and epicardial borders should be redrawn in a representative mid-ventricle slice in ED, which produces automated contours throughout the cardiac cycle.

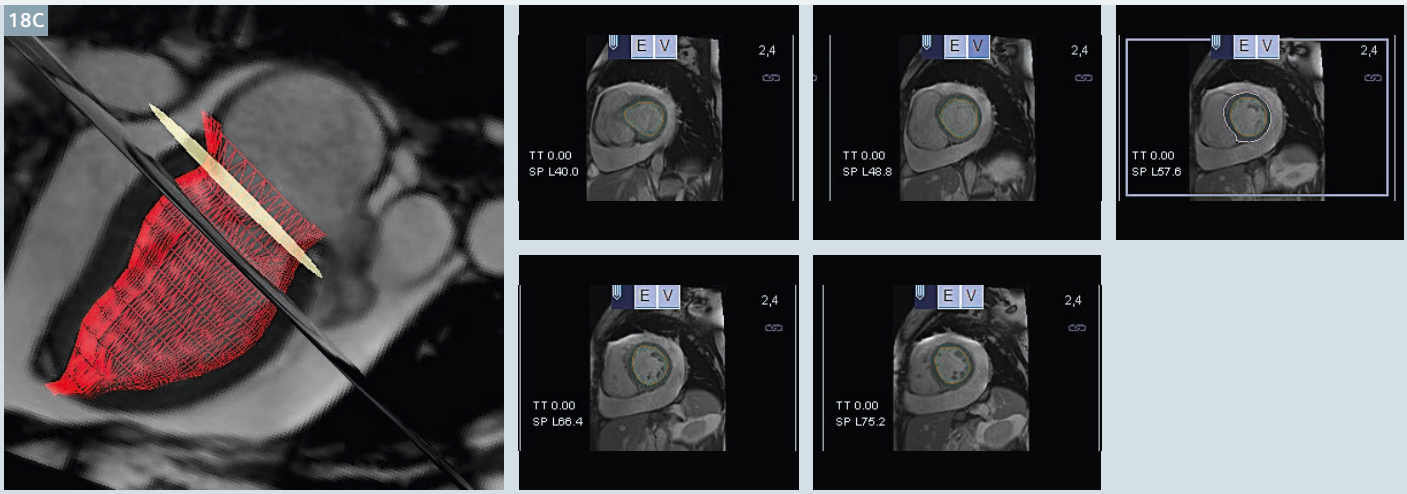


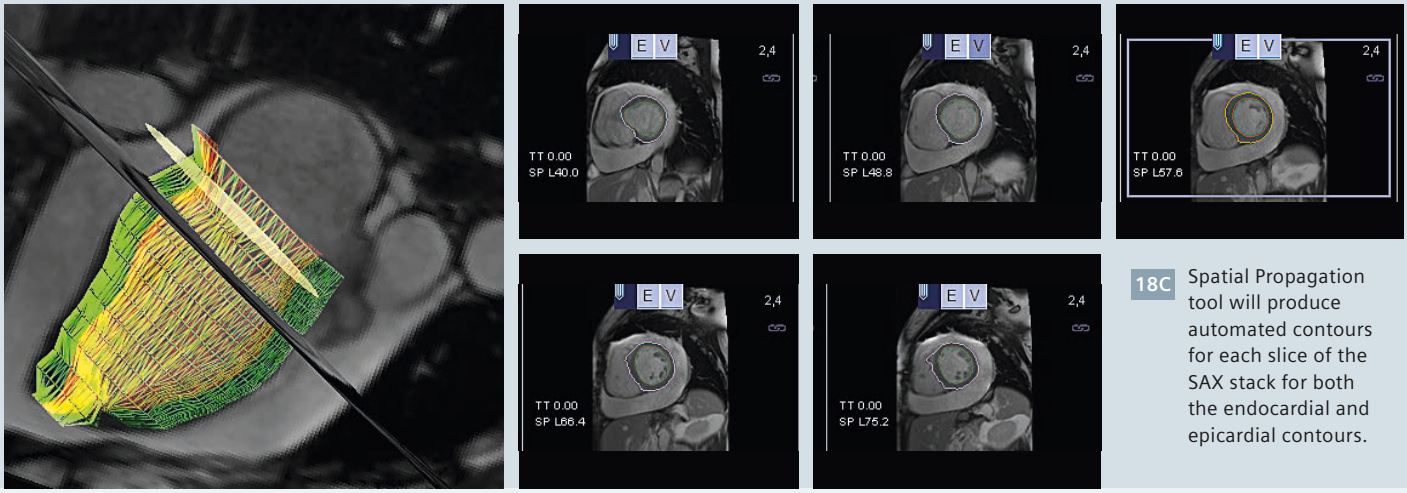


**18C** Spatial Propagation tool will produce automated contours for each slice of the SAX stack for both the endocardial and epicardial contours.

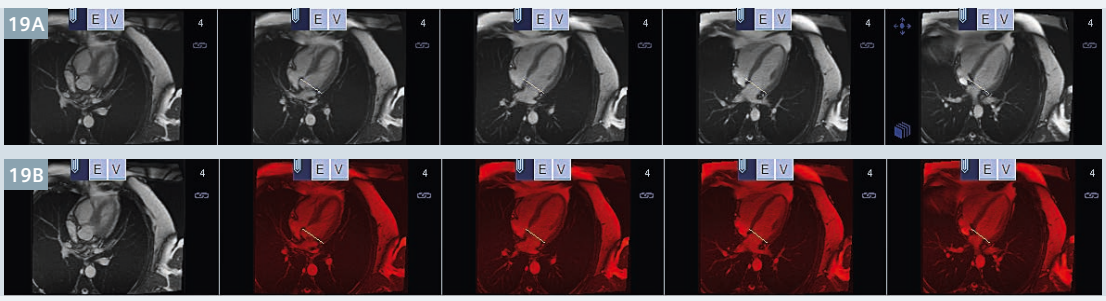


**19** Exclusion of extraneous LAX images, and retention of the 2-, 3-, and 4-chamber LAX views will optimize automated LV base plane localization.

be checked in the LAX views and modified, if necessary, by optimal placement of the large dots.

Some CMR protocols require multiple LAX gated-cine images. If these sequences become accidentally integrated into MR Cardiac Function, the unnecessary LAX views should be excluded with the E button (Fig. 19).

If the LV base plane continues to be incorrect, use the ED/ES tool to restrict contouring to ED and ES thus requiring manual contouring to account for the mitral valve in SAX views. The ED/ES tool will convert *syngo*.via's processing software to a more manual workflow using only ED and ES contouring for quantitative analysis.

## Conclusion

The semi-automatic post-processing offered by *syngo*.via provides an essential step forward in CMR efficiency. Complete post-processing automation is desirable for efficient clinical workflows. However, although single fully automated inline post-processing applications already demonstrated clinical value with respect to "higher interobserver and intraobserver reliability as well as a better time efficiency" [2], the complete semi-automated post-processed reading workflow offered by *syngo*.via provides an essential step forward in CMR efficiency.

To optimize semi-automatic post-processing, the user's manual skill set needs to be modified to the 'hands-off' semi-automated approach, which encourages less direct software interaction. As users transition their skill-set, it has been my experience that post-processing time dramatically improves while retaining high quantitative accuracy, which overall facilitates the movement of CMR into wider clinical application.

### References


1 Kramer CM, Barkhausen J, Flamm SD, et al. Standardized cardiovascular magnetic resonance (CMR) protocols 2013 update. J Cardiovasc Magn Reson 2013. Oct 15:91.

2 Doesch C., et al. Detection of Myocardial Ischemia by Automated, Motion-Corrected, Color-Encoded Perfusion Maps Compared With Visual Analysis of Adenosine Stress Cardiovascular Magnetic Resonance Imaging at 3 T Invest Radiol 2013. 48:678.



## Contact

Ryan Avery, M.D.
University of Arizona Health Network
Dept. of Medical Imaging
1501 N Campbell Ave
PO Box 245068
Tucson, AZ 85724
USA
ravery@radiology.arizona.edu

# Quiescent-Interval Single-Shot Magnetic Resonance Angiography

Robert R. Edelman[1,2]; Shivraman Giri[3]; Eugene Dunkle[1]; Ioannis Koktzoglou[1,4]

[1] NorthShore University HealthSystem, Evanston, IL, USA
[2] Feinberg School of Medicine, Northwestern University, Chicago, IL, USA
[3] Siemens Medical Solutions USA, Inc., Chicago, IL, USA
[4] The University of Chicago Pritzker School of Medicine, Chicago, IL, USA

## Introduction

More than 200 million people worldwide are afflicted by peripheral arterial disease (PAD) [1, 2]. Over the last decade, the incidence of PAD has risen by approximately 13% in high-income countries and 29% in low-income countries [3]. Patients with PAD have a high 10-year risk of death of 40%, 3-fold higher risk of all cause death and 6-fold higher risk of cardiovascular-related death than patients without PAD [4]. Accurate diagnosis is thus critical for disease management and for improving patient outcomes.

The availability of accurate non-invasive imaging tests has decreased the need for preoperative digital subtraction angiography (DSA) in the evaluation of PAD. The ankle brachial index (ABI) is an excellent screening test for hemodynamically significant PAD and can be performed in conjunction with Doppler waveform analysis and segmental pressure measurement in an effort to increase accuracy [5]. However, its sensitivity is low in elderly patients and those with diabetes [6]. Moreover, additional imaging is often needed to help plan for interventional procedures. Computed tomographic angiography (CTA) offers high spatial resolution and short scan times without the risks associated with DSA [7]. For ≥50% stenosis, the reported sensitivity of peripheral CTA is on the order of 89%-100%, with specificity reported at 92%-100% [8]. However, the clinical utility of peripheral CTA is diminished by the presence of vessel wall calcifications, which are associated with diabetes, heart dis-

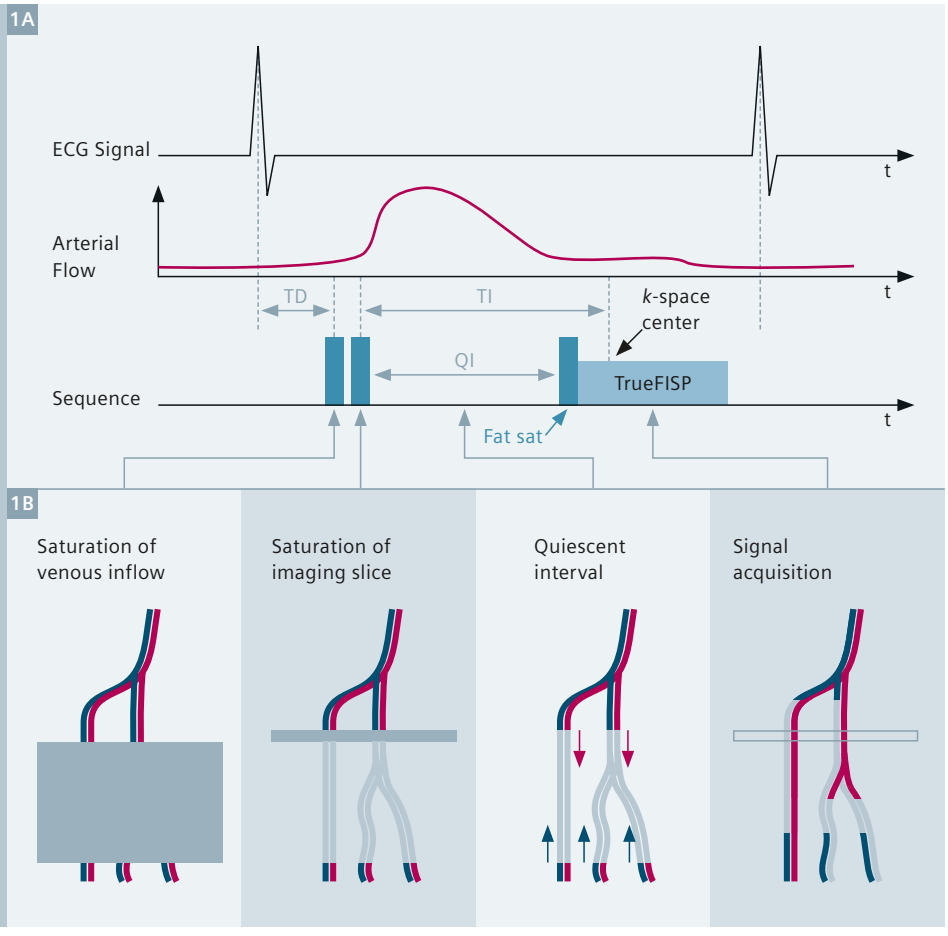


**1** QISS* pulse sequence diagram **(1A, top)** and schematic of vasculature (**1B, bottom**) showing the effect of pulse-timings on signal manipulation to maximize arterial conspicuity. In-plane saturation and tracking venous saturation RF pulses are applied TD ~ 100 ms after the R-wave; these pulses suppress background and venous signal. Following a preset quiescent interval (QI) of 228 ms, during which unsaturated arterial blood flows into the imaging slice, a fat suppression RF pulse is applied, followed by single-shot TrueFISP readout. This process is repeated in subsequent heart-beats to acquire other slices, usually in foot-to-head direction. In the basic configuration used for survey examinations, one 3 mm-thick slice is acquired per RR interval with 1 x 1 mm in-plane spatial resolution.

ease, and advanced age [9]. CT angiography has the disadvantage of exposing patients to ionizing radiation and there is also the associated risk of contrast-induced nephropathy (CIN), which is of particular concern because nearly 40% of patients with PAD have significant renal dysfunction [10]. Contrast-enhanced magnetic resonance angiography (CEMRA) has also been shown to be highly accurate for the detection of stenoses ≥50% within the lower extremity arterial tree [11]. Unfortunately, the administration of gadolinium-based contrast agents in patients with severely impaired renal function is contraindicated due to the risk of nephrogenic systemic fibrosis (NSF) [12].

## Non-enhanced MRA Techniques

Non-enhanced MRA (NEMRA, i.e. MRA without contrast agents) avoids the potential risks of NSF and CIN, as well as ionizing radiation. Two-dimensional time-of-flight NEMRA methods have been available for decades [13, 14]. However, lengthy acquisition times (typically approaching an hour or more) and image artifacts have limited their routine use in favor of contrast-enhanced techniques. Newer subtractive approaches for NEMRA of the peripheral arteries have been proposed which allow efficient depiction of arteries over large fields-of-view and suppress venous signal. These include ECG-gated subtractive 3D turbo spin echo (TSE) imaging such as fresh blood imaging (FBI) [15] and NATIVE SPACE (NATIVE = Non-contrast angiography of the arteries and veins; SPACE = Sampling perfection with application optimized contrast by using different flip angle evolution) [16], as well as variants predicated on 3D balanced steady-state free precession (bSSFP[1]) imaging such as flow-sensitive dephasing [17]. Of these, subtractive TSE MRA techniques have the most clinical validation and are commercially available. However, subtractive TSE MRA is not robust due to its sensitivity to patient motion, pulse wave timing, and abnormal flow patterns [16].

The Quiescent-Interval Single-Shot* (QISS) NEMRA technique was developed as a safer, simple 'push button' non-enhanced alternative to CTA and CEMRA (Fig. 1) [18]. Moreover, QISS MRA eliminates the need for point-of-service blood draws to determine eGFR and yields significant cost savings ($180 per study at our institution) compared with CEMRA by eliminating the MR contrast agent and injector kit. QISS offers several advantages over previously described NEMRA techniques (Fig. 2) [19]. It is highly robust with minimal sensitivity to patient motion and cardiac arrhythmias. It has the particular advantage of enabling a simple and efficient workflow, thereby eliminating the need for special technologist expertise.

*QISS is pending 510(k) clearance and is not commercially available in the US.

[1] The product is still under development and not commercially available yet. Its future availability cannot be ensured.

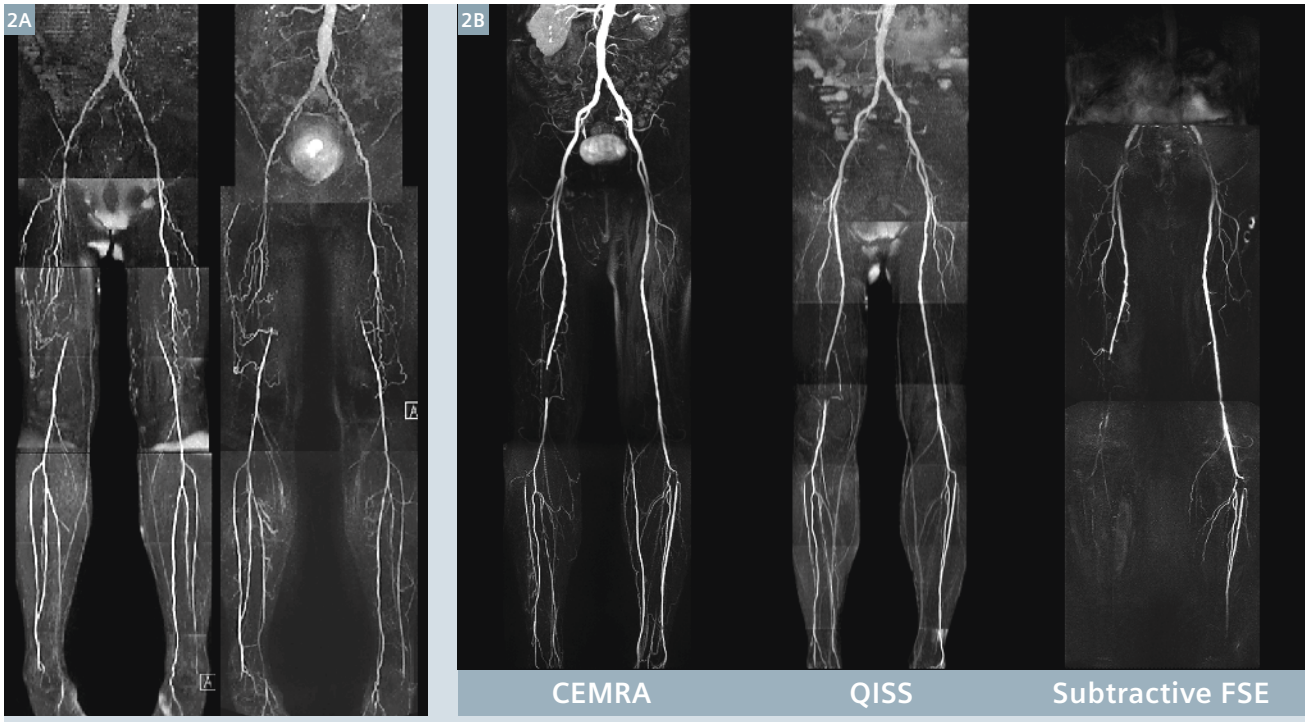


2 **(2A)** 91-year-old smoker with bilaterally occluded superficial femoral arteries (SFA). QISS MRA (left) and CEMRA (right) appear comparable. **(2B)** CEMRA, QISS, and subtractive TSE MRA (Native SPACE) in a patient with PAD. Multiple ≥50% stenoses in the right anterior and posterior tibial arteries and occlusion of the left posterior tibial artery are identified on CEMRA and QISS MRA. Subtractive TSE MRA shows extensive artifactual signal dropout in the abdomen, upper pelvis and right calf. (Signal dropout in the mid-right SFA is due to a stent.) *Adapted with permission from ref. 19*

## Clinical Validation

QISS MRA has been evaluated at field strengths ranging from 1.5 Tesla to 7 Tesla*, with the reported accuracy at 1.5 Tesla and 3 Tesla generally approaching or matching that of CEMRA.[20-26] The technique has also been specifically evaluated in a diabetic patient population in whom CTA may be problematic due to the frequent presence of vascular calcifications and poor renal function.[27] Using CEMRA as the reference standard, QISS showed excellent diagnostic performance with sensitivity of 89.8%, specificity of 96.4%, positive predictive value of 92.4%, and negative predictive value of 95.0%. An example illustrating the advantage of QISS MRA over CTA for the evaluation of diabetic PAD patients is given in Figure 3.

*MAGNETOM 7T is ongoing research. All data shown are acquired using a non-commercial system under institutional review board permission. MAGNETOM 7T is still under development and not commercially available yet. Its future availability cannot be ensured.

## QISS as scout and backup for CEMRA

Currently, many sites use a multi-station, multi-planar scout acquisition to plan the volume placements for stepping table CEMRA. This procedure can be cumbersome since the full extent of the arteries is not visible on the scout images. For such situations, QISS acquisition can potentially serve as a scout image for CEMRA; although it will take longer than the regular scout, it offers more complete and detailed visualization of arterial tree for CEMRA, providing diagnostic information in case of a technical failure with CEMRA. For instance, the patient might move between the time that the pre-contrast mask images and post-contrast images are acquired, resulting in misregistration artifact on the subtracted CEMRA images. Being a non-subtractive single shot technique with very short scan time (<1/3 second per slice), QISS is resistant to motion artifacts. Moreover, the timing for the CEMRA may be inaccurate, resulting in poor arterial opacification or venous overlap (e.g. due to asymmetric atherosclerotic disease causing slower flow on one side, or due to human error). In all these situations, QISS can be a fallback option to salvage patient exam despite non-diagnostic CEMRA (Fig. 4).


3 88-year-old male with claudication and type-2 diabetes. **(3A)** CTA; **(3B)** QISS MRA. The CTA was non-diagnostic due to the presence of extensive vascular calcifications. However, QISS MRA was completely unaffected by the vascular calcifications and demonstrated the patency of proximal vessels and occlusions of calf vessels. In this case, note that QISS MRA image quality was adequate despite the fact that the patient had atrial fibrillation. *Adapted with permission from ref. 20*

## QISS at 3 Tesla

Until QISS, no NEMRA technique had proven effective at 3 Tesla, which is widely considered the optimal field strength for CEMRA. Imaging at 3 Tesla will be necessary to unlock the full clinical potential of NEMRA and to compete with the excellent spatial resolution provided by CTA. In order to take advantage of the large signal-to-noise ratio (SNR) boost at 3 Tesla, one must overcome challenges relating to high specific absorption rate (SAR) and worsened $B_1$ field homogeneity (Table 1).

Shortening the bSSFP shot length, which proportionately reduces RF power deposition, can ameliorate the impact of increased SAR at 3 Tesla. At 1.5 Tesla, we found that GRAPPA acceleration factors in excess of two degraded QISS image quality. Higher GRAPPA acceleration factors (3 to 4) can be used to reduce the shot length at 3 Tesla. With the SNR boost from the higher field strength, one can further reduce the shot length by increasing the sampling bandwidth (~962 Hz/pixel at 3 Tesla vs. 658 Hz/pixel at 1.5 Tesla). The higher sampling bandwidth has the further advantage of reducing bowel-related magnetic susceptibility artifacts in the pelvic region.

We have found that the combination of a GRAPPA factor of 3 and sampling bandwidth of 962 Hz/pixel are sufficient to permit a 90° flip angle to be maintained from the level of the feet through the mid-thigh level. However, this imaging strategy by itself is insufficient for the pelvic and abdominal regions, where SAR limitations are more pronounced due to larger body dimensions. Degradation of image quality from using a flip angle <90° is maximal in the pelvic region because of the additional impact of $B_1$ field inhomogeneity. Unfortunately, a flip angle less than 90° in the pelvis often

results in unilateral loss of arterial conspicuity with QISS MRA. One straightforward solution is to trigger to every other R-wave, which halves the time-averaged power deposition at the expense of doubling scan time. Since SAR limitations only come into play from the upper thigh region through the abdomen, triggering to every other R-wave is only used for the top three stations. Total scan time for a whole-leg study is increased by ~2-3 minutes (e.g. total scan time ~10 minutes**) which is still reasonable.

A final $B_1$ field-related issue is that the pre-scan image filters typically used to correct for RF coil-dependent signal intensity variations do not adequately normalize signal variations caused by $B_1$ field inhomogeneity at 3 Tesla. This signal variation will tend to obscure the arterial signal on a full-thickness MIP, even when the vessel is apparent on a thin MIP. The effectiveness of the pre-scan filter in the pelvis is impeded by noise amplification in the central portions of the body resulting from the use of a high GRAPPA acceleration factor. This limitation is largely avoided by using the 'broad' pre-scan filtering option. Figure 5 illustrates the image quality improvements that can be obtained when several pulse sequence optimizations are combined (e.g. high GRAPPA acceleration factor, high sampling bandwidth, FOCI venous suppression, triggering to every other R-wave for upper stations, and optimized image filtering).

**Developing clinical applications**

Although most clinical efforts using QISS MRA have been directed towards the lower-extremity peripheral arteries, there are several other areas where the technique appears promising. For instance, QISS MRA can be used to evaluate the arteries of the upper extremities and the veins of the lower extremities (Fig. 6). For imaging of the lower extremity veins, we typically place the traveling saturation pulse above the slice and turn off the in-plane saturation pulse (e.g. by setting the RF voltage to zero). Other potential applications include imaging of visceral arteries and veins, pulmonary vessels, and the extracranial carotid arteries. However, additional technical development and clinical validation will be needed for other vascular territories.

** This number indicates the image acquisition time, not including the time for frequency and shimming adjustments. These adjustments are performed once per station for every patient.

## Table 1: Summary of challenges and solutions for 3T QISS

| Challenges at 3T | Solutions |
|---|---|
| Increased SAR | • Shortened shot length using high GRAPPA acceleration factor (3-4) and high sampling bandwidth<br>• Triggering to every other R-wave<br>• QISS with FLASH readout |
| $B_0$ inhomogeneity | • Arterial spin labeled (ASL) QISS |
| $B_1$ inhomogeneity | • $B_1$-robust saturation RF pulses<br>• FOCI inversion RF pulses<br>• $B_1$-dependent image filtering<br>• High permittivity pad |

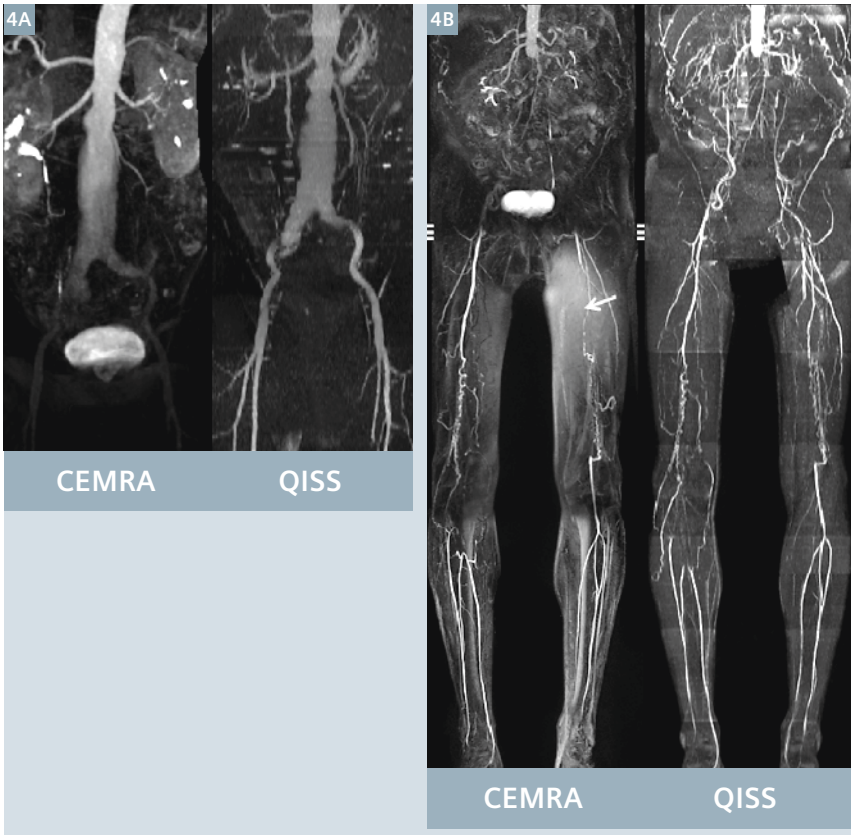


4 Cases where QISS MRA helped to salvage a non-diagnostic CEMRA.
**(4A)** Patient with an abdominal aortic aneurysm. Slow flow in the aneurysm delayed the contrast enhancement of the pelvic arteries, resulting in a non-diagnostic CEMRA exam. However, the pelvic arteries are well shown on the QISS scout study.
**(4B)** Patient with aorto-iliac and bilateral superficial femoral artery occlusive disease. Left leg motion caused misregistration artifact in part of the CEMRA (arrow), whereas the QISS scout images are diagnostic. *Adapted with permission from ref. 20*

**Potential Pitfalls**

Although QISS MRA has proven to be a robust imaging technique, there are potential limitations that should be kept in mind in order to avoid artifacts:

1. **Cardiac rhythm:** The default acquisition window for QISS is approximately 700 ms. In patients with medium or slow heart rates, one slice is acquired per RR interval. With rapid heart rates where the RR interval is less than 700 ms, one slice will be acquired every 2 RR intervals. It is possible to trigger to every RR interval, despite the fast heart rate, by reducing the acquisition window. This can be accomplished by slightly decreasing both the TD (in the special card, default value of 100 ms) and TI (in the contrast card, default value of 350 ms). However, if these values are reduced excessively then loss of flow signal may occur from inadequate inflow or data acquisition during the systolic phase of the cardiac cycle.

   In general, QISS is fairly insensitive to arrhythmias. However, with highly irregular heart rhythms (or with poor triggering due to an inadequate ECG signal), image quality may suffer. Work is currently under way to develop versions of QISS that do not require the use of ECG gating.

2. **Fat suppression:** QISS relies upon uniform fat suppression for optimal vessel depiction. In some areas where fat suppression is imperfect (e.g. groin area), a simple expedient is to edit out the affected region in the maximum intensity projection. However, in certain regions (e.g. the feet) it can be quite difficult to adequately shim so that fat suppression and hence QISS image quality may be suboptimal. For the pedal vessels, we have found that image quality is further improved by placing a small cushion between the top of each foot and the Peripheral Angio 36 coil, since having the coil touching the foot tends to impair the quality of the shim.

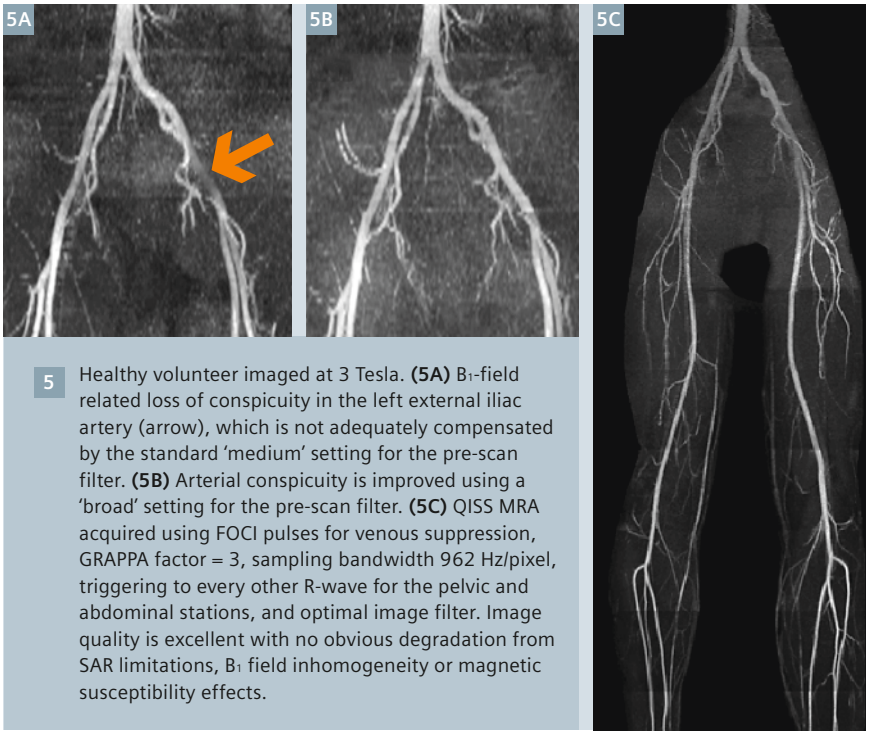


5 Healthy volunteer imaged at 3 Tesla. **(5A)** $B_1$-field related loss of conspicuity in the left external iliac artery (arrow), which is not adequately compensated by the standard 'medium' setting for the pre-scan filter. **(5B)** Arterial conspicuity is improved using a 'broad' setting for the pre-scan filter. **(5C)** QISS MRA acquired using FOCI pulses for venous suppression, GRAPPA factor = 3, sampling bandwidth 962 Hz/pixel, triggering to every other R-wave for the pelvic and abdominal stations, and optimal image filter. Image quality is excellent with no obvious degradation from SAR limitations, $B_1$ field inhomogeneity or magnetic susceptibility effects.

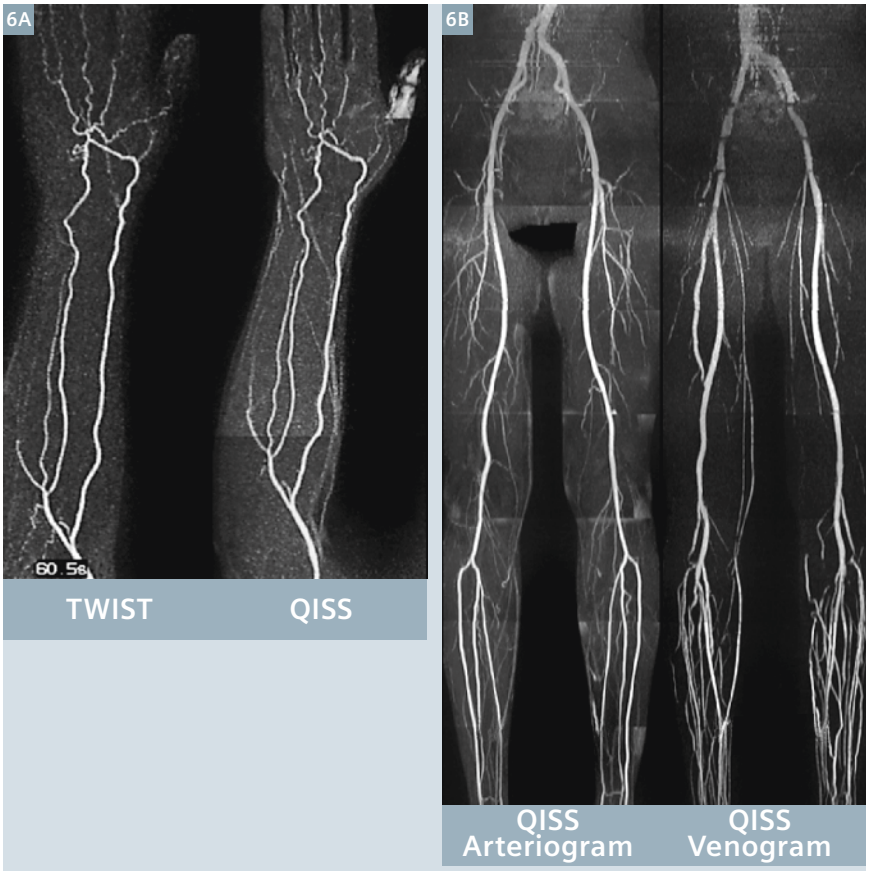


6 Developing potential future clinical applications for QISS MRA.
**(6A)** Healthy subject. QISS MRA (acquired with 1.2 mm thick slices) depicts the forearm arteries comparably to TWIST CEMRA.
**(6B)** Comparison of QISS arteriography (inferior saturation) with QISS venography (superior saturation).

3. **Susceptibility artifact:** The TrueFISP readout along with fat suppression makes QISS more sensitive to magnetic susceptibility artifacts (e.g. from joint prostheses or bowel gas) than CEMRA (which uses a 3D acquisition with short TE). Using a high readout bandwidth without fat suppression minimizes such artifacts.
4. **Flow direction:** The use of venous saturation impairs the ability of QISS to depict reversed arterial flow, particularly when the flow reversal extends over a long vessel segment. In cases where flow reversal is suspected, one may acquire an additional QISS data set using arterial saturation instead of venous saturation. These images will show reversed arterial flow (but will also show veins).
5. **Spatial resolution:** For most peripheral arterial segments, the default slice thickness of 3 mm with no slice overlap is sufficient to show stenotic disease. Thinner slices (e.g. 1.2 mm with 20% slice overlap) are helpful for avoiding partial volume averaging in horizontally oriented vessel segments (e.g. proximal anterior tibial artery) and for imaging small caliber vessels (e.g. in the foot).

**Future Developments**

1. **Alternative *k*-Space Trajectories:** The current implementation of QISS uses a Cartesian *k*-space trajectory. However, it is also possible to acquire QISS using a radial *k*-space trajectory [30]. There are potential advantages and disadvantages to a radial trajectory. One advantage for radial is that the number of views, and hence scan duration within each cardiac cycle, can be reduced almost arbitrarily with minimal impact on spatial resolution. This approach may be beneficial for imaging of patients with fast heart rates. However, the signal-to-noise ratio (SNR) is also reduced and radial streak artifacts may become objectionable if the number of views is excessively decreased. By using a golden view angle increment with a radial *k*-space trajectory, it becomes feasible to sample data throughout the cardiac cycle. One can then generate a cine series of time-resolved QISS images showing the progression of the arterial pulse wave within the arterial tree [31].
2. **Alternative Sampling Strategies:** Although the TrueFISP readout maximizes acquisition speed and SNR, using other pulse sequences for the readout can prove beneficial in certain circumstances. For instances, the use of a fast low angle shot (FLASH) readout in conjunction with a reduced flip angle excitation avoids SAR limitations at 3 Tesla. The use of an ultra-short TE readout might prove beneficial to reduce susceptibility artifacts around joint prostheses.
3. **Alternative Gating Strategies:** Currently, QISS images of the pelvis and abdomen are acquired using breath holding. In order to further enhance, patient comfort, it should be feasible to implement non-breathhold acquisitions by respiratory gating with a belt device, with a navigator technique applied to the anterior abdominal wall, or by self-gating [32].
4. **3D QISS:** Very thin slices (e.g. 0.3 mm can be obtained by using a thin-slab 3D implementation of the QISS technique. Although still early in development, the technique has the potential to exceed the spatial resolution available with CEMRA and nearly match that of CTA.

## Conclusions

QISS MRA provides a robust, rapid, and easy-to-use technique for imaging of the peripheral arteries at both 1.5 and 3 Tesla. There is generally no need to tailor any of the imaging parameters for individual patients. Additionally it can serve as a backup for CEMRA, or function as a standalone technique. Despite similarities in the appearances of the projection angiograms, QISS and CEMRA are predicated on fundamentally different principles and care must be taken to avoid pitfalls specific to each technique. Future developments promise shorter scan times, reduced artifacts, and new clinical applications.

**References**


1. Leng GC, Lee AJ, Fowkes FG, Whiteman M, Dunbar J, Housley E, et al. Incidence, natural history and cardiovascular events in symptomatic and asymptomatic peripheral arterial disease in the general population. Int J Epidemiol. 1996 Dec;25(6):1172-81.
2. Selvin E, Erlinger TP. Prevalence of and risk factors for peripheral arterial disease in the United States: results from the National Health and Nutrition Examination Survey, 1999-2000. Circulation. 2004 Aug 10;110(6):738-43.
3. Hirsch AT, Duval S. The global pandemic of peripheral artery disease. Lancet. 2013 Oct 19;382(9901):1312-4. doi: 10.1016/S0140-6736(13)61576-7. Epub 2013 Aug 1.
4. Arain FA, Cooper LT. Peripheral Arterial Disease: Diagnosis and Management. Mayo Clin Proc. 2008;83(8):944-950.
5. Hirsch AT, Haskal ZJ, Hertzer NR, Bakal CW, Creager MA, Halperin JL, et al. ACC/AHA 2005 guidelines for the management of patients with peripheral arterial disease (lower extremity, renal, mesenteric, and abdominal aortic. J Am Coll Cardiol. 2006 Mar 21;47(6):1239-312.
6. Dachun Xu, Jue Li, Liling Zou, Yawei Xu, Dayi Hu, Pagoto SL, Yunsheng Ma. Sensitivity and specificity of the ankle-brachial index to diagnose peripheral artery disease: a structured review. Vasc Med. 2010 Oct;15(5):361-9. doi: 10.1177/1358863X10378376.
7. Hessel SJ, Adams DF, Abrams HL. Complications of angiography. Radiology. 1981; 138(2): 273-281.
8. Catalano C, Fraioli F, Laghi A, Napoli A, Bezzi M, Pediconi F, Danti M, Nofroni I, Passariello R. Infrarenal aortic and lower-extremity arterial disease: diagnostic performance of multi-detector row CT angiography. Radiology. 2004;231:555–563.
9. Ouwendijk R, Kock MC, van Dijk LC, van Sambeek MR, Stijnen T, Hunink MG. Vessel wall calcifications at multi-detector row CT angiography in patients with peripheral arterial disease: effect on clinical utility and clinical predictors. Radiology. 2006 Nov;241(2):603-8.
10. Tranche-Iparraguirre S, Marín-Iranzo R, Fernández-de Sanmamed R, Riesgo-García A, Hevia-Rodríguez E, García-Casas JB. Peripheral arterial disease and kidney failure: a frequent association. Nefrologia. 2012 May 14;32(3):313-20. doi: 10.3265/Nefrologia.pre2011.Nov.11172. Epub 2012 Jan 27.
11. Menke J, Larsen J. Meta-analysis: Accuracy of contrast-enhanced magnetic resonance angiography for assessing steno-occlusions in peripheral arterial disease. Ann Intern Med. 2010 Sep 7;153(5):325-34. doi: 10.7326/0003-4819-153-5-201009070-00007.

12. Prince MR, Zhang H, Morris M, MacGregor JL, Grossman ME, Silberzweig J, DeLapaz RL, Lee HJ, Magro CM, Valeri AM. Incidence of nephrogenic systemic fibrosis at two large medical centers. Radiology. 2008 Sep;248(3):807-16. doi: 10.1148/radiol.2483071863.
13. Koelemay MJ, Lijmer JG, Stoker J, Legemate DA, Bossuyt PM. Magnetic resonance angiography for the evaluation of lower extremity arterial disease: a meta-analysis. JAMA. 2001 Mar 14;285(10):1338-45.
14. Owen RS, Carpenter JP, Baum RA, Perloff LJ, Cope C.. Magnetic resonance imaging of angiographically occult runoff vessels in peripheral arterial occlusive disease. N Engl J Med. 1992 Jun 11;326(24):1577-1581.
15. Miyazaki M, Takai H, Sugiura S, Wada H, Kuwahara R, Urata J. Peripheral MR angiography: separation of arteries from veins with flow-spoiled gradient pulses in electrocardiography-triggered three-dimensional half-Fourier fast spin-echo imaging. Radiology. 2003 Jun;227(3):890-896. Epub 2003 Apr 17.
16. Lim RP, Hecht EM, Xu J, Babb JS, Oesingmann N, Wong S, Muhs BE, Gagne P, Lee VS. 3D nongadolinium-enhanced ECG-gated MRA of the distal lower extremities: preliminary clinical experience. J Magn Reson Imaging. 2008 Jul;28(1):181-189. doi: 10.1002/jmri.21416.
17. Fan Z, Sheehan J, Bi X, Liu X, Carr J, Li D. 3D noncontrast MR angiography of the distal lower extremities using flow-sensitive dephasing (FSD)-prepared balanced SSFP. Magn Reson Med. 2009 Dec;62(6):1523-32. doi: 10.1002/mrm.22142.
18. Edelman RR, Sheehan JJ, Dunkle E, Schindler N, Carr J, Koktzoglou I. Quiescent-interval single-shot unenhanced magnetic resonance angiography of peripheral vascular disease: technical considerations and clinical feasibility. Magn Reson Med. 2010;63:951–958.
19. Ward EV, Galizia MS, Usman A, Popescu AR, Dunkle E, Edelman RR. Comparison of quiescent inflow single-shot and native space for nonenhanced peripheral MR angiography. J Magn Reson Imaging. 2013;38:1531–1538.
20. Hodnett PA, Koktzoglou I, Davarpanah AH, Seanlon TG, Collins JD, Sheehan JJ, Dunkle E, Gupta N, Carr JC, Edelman RR. Evaluation of Peripheral Arterial Disease with Nonenhanced Quiescent-Interval Single Shot MR Angiography. Radiology. July 2011: 260(1):282-93. R01 HL096916; PMCID: PMC3121010
21. Klasen J, Blondin D, Schmitt P, Bi X, Sansone R, Wittsack HJ, et al. Nonenhanced ECG-gated quiescent-interval single-shot MRA (QISS-MRA) of the lower extremities: comparison with contrast-enhanced MRA. Clin Radiol. 2012 May;67(5):441-6. doi: 10.1016/j.crad.2011.10.014. Epub 2011 Dec 3.
22. Amin P, Collins JD, Koktzoglou I, Molvar C, Markl M, Edelman RR, Carr JC. Evaluating peripheral arterial disease with unenhanced quiescent-interval single-shot MR angiography at 3 T. AJR Am J Roentgenol. 2014 Apr;202(4):886-93. doi: 10.2214/AJR.13.11243. PMID: 24660721
23. Knobloch G, Gielen M, Lauff MT, Romano VC, Schmitt P, Rick M, et al. ECG-gated quiescent-interval single-shot MR angiography of the lower extremities: initial experience at 3 T. Clin Radiol. 2014 May;69(5):485-91. doi: 10.1016/j.crad.2013.12.006. Epub 2014 Mar 7. PMID:24613581.
24. Thierfelder KM, Meimarakis G, Nikolaou K, Sommer WH, Schmitt P, Kazmierczak PM, et al. Non-contrast-enhanced MR angiography at 3 Tesla in patients with advanced peripheral arterial occlusive disease. PLoS One. 2014 Mar 7;9(3):e91078. doi: 10.1371/journal.pone.0091078. eCollection 2014. PMID:24608937.
25. Hansmann J, Morelli JN, Michaely HJ, Riester T, Budjan J, Schoenberg SO, Attenberger UI. Nonenhanced ECG-gated quiescent-interval single shot MRA: image quality and stenosis assessment at 3 tesla compared with contrast-enhanced MRA and digital subtraction angiography. J Magn Reson Imaging. 2014 Jun;39(6):1486-93. doi: 10.1002/jmri.24324. Epub 2013 Oct 10. PMID:24338813.
26. Johst S, Orzada S, Fischer A, Schäfer LC, Nassenstein K, Umutlu L, et al. Sequence comparison for non-enhanced MRA of the lower extremity arteries at 7 Tesla. PLoS One. 2014 Jan 16;9(1):e86274. doi: 10.1371/journal.pone.0086274. eCollection 2014.
27. Hodnett PA, Ward EV, Davarpanah AH, Scanlon TG, Collins JD, Glielmi CB, Bi X, et al. Peripheral arterial disease in a symptomatic diabetic population: prospective comparison of rapid unenhanced MR angiography (MRA) with contrast-enhanced MRA. AJR Am J Roentgenol. 2011 Dec;197(6):1466-73. doi: 10.2214/AJR.10.6091. PMID:22109304.
28. Ordidge RJ, Wylezinska M, Hugg JW, Butterworth E, Franconi F. Frequency offset corrected inversion (FOCI) pulses for use in localized spectroscopy. Magn Reson Med. 1996;36(4):562-566.
29. Payne GS, Leach MO. Implementation and evaluation of frequency offset corrected inversion [FOCI) pulses on a clinical MR system. Magn Reson Med. 1997;38:828-833.
30. Edelman RR, Giri S, Dunkle E, Galizia M, Amin P, Koktzoglou I. Quiescent-inflow single-shot magnetic resonance angiography using a highly undersampled radial *k*-space trajectory. Magn Reson Med. 2013;70(6):1662-1668.
31. Koktzoglou I, Mistretta CA, Giri S, Dunkle EE, Amin P, Edelman RR. Simultaneous static and cine nonenhanced MR angiography using radial sampling and highly constrained back projection reconstruction. Magn Reson Med. 2013 Nov 11. doi: 10.1002/mrm.25008. [Epub ahead of print]
32. Larson AC, Kellman P, Arai A, Hirsch GA, McVeigh E, Li D, Simonetti OP. Preliminary investigation of respiratory self-gating for free-breathing segmented cine MRI. Magn Reson Med. 2005 Jan;53(1):159-68.


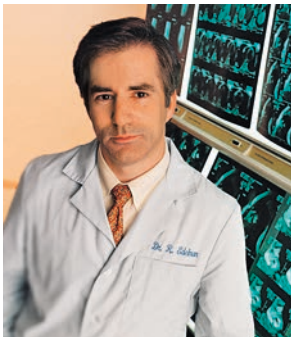

## Contact


Robert R. Edelman, M.D.
Dept. of Radiology
NorthShore University HealthSystem
Feinberg School of Medicine
Northwestern University
Chicago, IL
USA
REdelman@northshore.org

# Expert Talks

## Quantification and Speed.
## What Else Drives CMR Into Broader Clinical Use?

**Don’t miss the talks of experienced and renowned experts at siemens.com/magnetom-world**


### Emerging Contributions of CMR in Cardiology

**Dudley Pennell**
Royal Brompton & Harefield (London, UK)


### Pixel-Based Myocardial Mapping

**Jeanette Schulz-Menger**
Charité Campus Buch / HELIOS Krankenhaus Berlin-Buch (Berlin, Germany)


### Need for Speed in CMR

**James Carr**
Northwestern Memorial Hospital (Chicago, IL, USA)


### Advances in Non-CE MR Angiography

**Robert R. Edelman**
NorthShore University HealthSystem (Evanston, IL, USA)


### Integrated Cardiac PET/MRI

**Felix Nensa**
Essen University Hospital (Essen, Germany)

Visit us at **www.siemens.com/magnetom-world**

Go to **Clinical Corner > Clinical Talks**

# QISS Non-Contrast MR Angiography: A Study of Three Cases with Peripheral Vascular Disease

Maria L. Carr[1]; Shivraman Giri[2]; Sven Zuehlsdorff[2]; Oisin Flanagan[4]; Heron E. Rodriguez[5]; Mark K. Eskandari[5]; Jeremy D. Collins[1]; Robert R. Edelman[3]; James C. Carr[1]

[1] Northwestern University, Department of Radiology, Feinberg School of Medicine, Chicago, IL, USA
[2] Siemens Medical Solutions USA, Inc., Chicago, IL, USA
[3] Northshore University HealthSystem, Evanston, IL, USA
[4] University of Toronto, Department of Medical Imaging, Ontario, Canada
[5] Northwestern Medicine, Division of Vascular Surgery, Chicago, IL, USA

## Introduction

Peripheral arterial disease (PAD) is a common progressive vasculopathy that causes disabling symptoms in the lower extremities, such as diminished arterial pulses, intermittent claudication, rest pain, and can lead to tissue loss. PAD is a common manifestation of the atherosclerotic disease process, affecting from 12% to 14% of the general population [1]. CT angiography (CTA) and contrast-enhanced MR angiography (CEMRA) are the imaging approaches commonly used to evaluate PAD. Many of these patients suffer from renal dysfunction, thus making both CTA and CEMRA less useful due to concerns about contrast-induced nephropathy (CIN) with iodinated contrast or nephrogenic systemic fibrosis (NSF) with gadolinium-based agents [2], respectively. Quiescent-interval single-shot* (QISS) imaging employs a stack of 2D TrueFISP images to cover the entire lower extremity and has recently been described as a non-contrast MR angiography technique for assessment of the lower extremity vasculature that demonstrated clinical utility at 1.5T and 3T [3, 4]. In this article we review three cases with QISS MRA demonstrating the clinical utility of this non-contrast technique for lower extremity arterial evaluation.

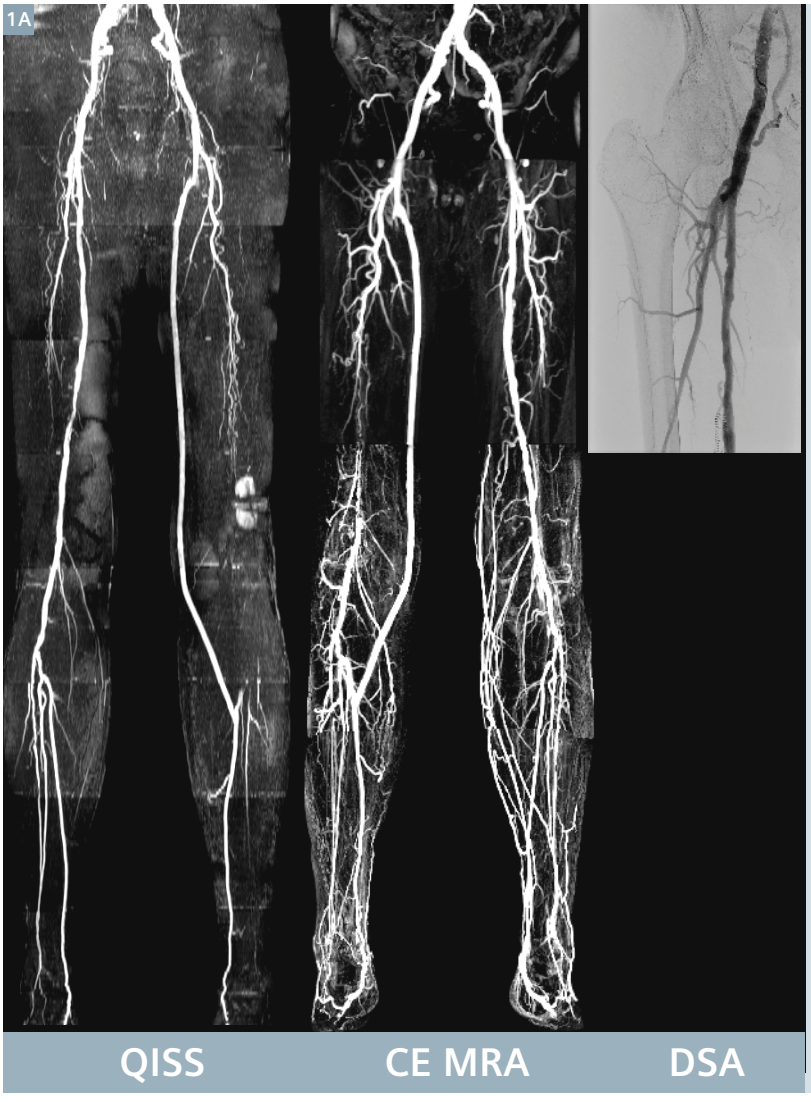

## Case 1

A 67-year-old male with a history of diabetes mellitus, hypercholesterolemia, and hypertension presented with worsening symptoms of peripheral arterial disease. Five years ago he underwent arterial bypass surgery from the left common femoral artery to the posterior tibial artery with good results. He developed progressively worsening intermittent claudication in the right leg over the last year. His ankle brachial index was 0.62 in the right leg and 1.15 in the left leg. He initially underwent conservative management in a supervised exercise program with limited success. He was then referred for non-invasive imaging with contrast-enhanced MR angiography (CEMRA). His glomerular filtration rate at the time of the CEMRA was greater than 60 cc/min. He underwent a standard 2-injection hybrid CEMRA protocol of the pelvis and lower extremities, which consisted of time resolved TWIST of the calves followed by a timed stepping table, 4-station acquisition of the pelvis and lower extremities on a 3T MAGNETOM Skyra scanner. 0.2 mmol/kg of Gadopentetate dimeglumine was injected intravenously using a divided injection protocol. CEMRA demonstrated a patent left femoral-distal bypass graft and a focal stenosis in the right superficial femoral artery. There was significant venous contamination of the calf vessels bilaterally, more severe on the right, which precluded accurate assessment of the runoff vessels. A QISS non-contrast MRA exam, performed at the same imaging session just before the contrast injection, also showed a patent left femoral-distal bypass graft and a focal stenosis in the right superficial femoral artery. The runoff vessels were much better delineated by QISS and performed as well as TWIST and better than CEMRA in this region, with three-vessel runoff on the right and single-vessel runoff on the left via the left posterior tibial artery.

* QISS is pending 510(k) clearance and is not commercially available in the US.

1B

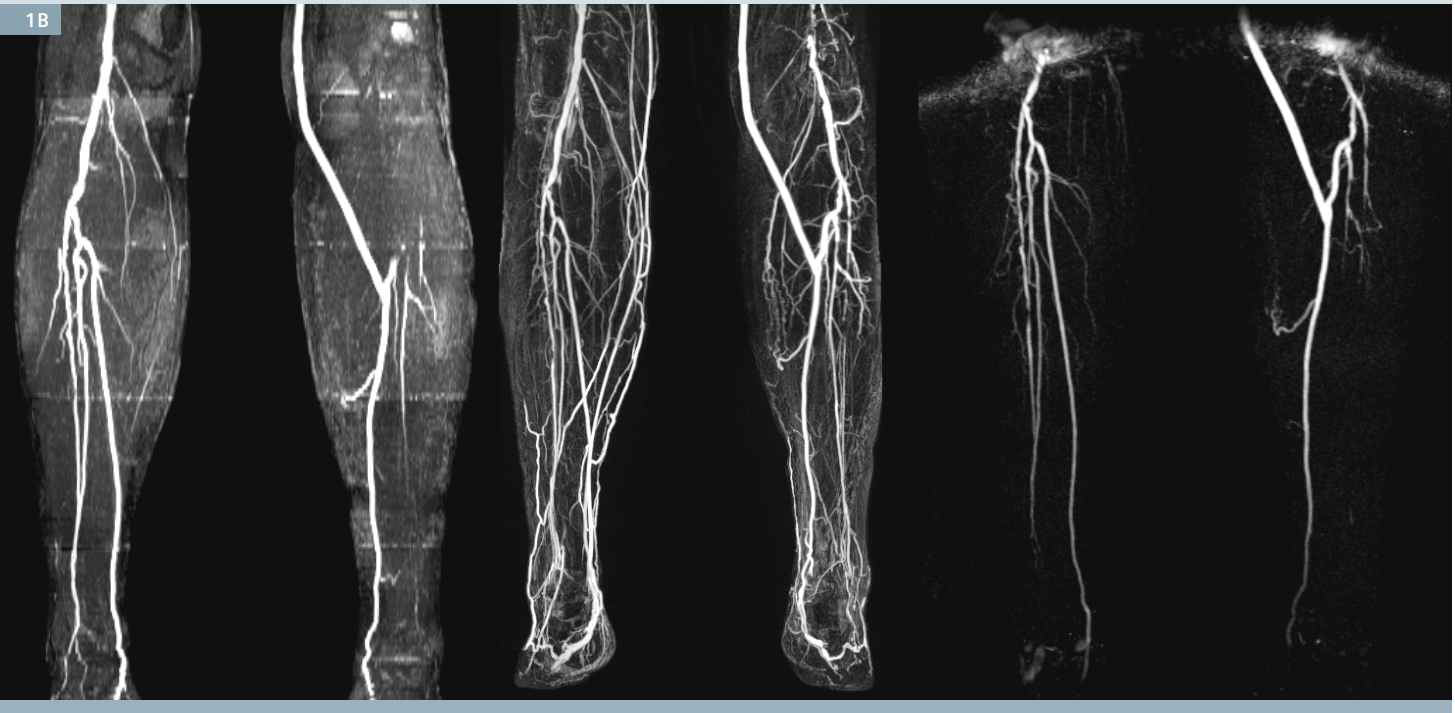

## Case 2

A 79-year-old male with hypertension, prostate cancer, and ischemic cardiomyopathy status post coronary artery bypass surgery, presented with worsening bilateral intermittent calf claudication. He was unable to walk one block without pain. He initially underwent non-invasive vascular testing; however ankle brachial indices were found to be invalid due to extensive calcification in the runoff vessels. He then underwent CT angiography, which showed extensive calcification of his peripheral vasculature, notably of the calves, which limited assessment of stenosis severity of the infrapopliteal vessels.

The patient was referred for contrast-enhanced MRA, which confirmed CT findings with diffuse mild disease in the inflow and outflow segments and demonstrated bilateral moderate to severe tibial artery disease. Assessment of the left tibial vessels was limited by venous contamination, precluding evaluation of the distal anterior tibial and posterior tibial arteries. QISS MRA was performed for further assessment of the tibial vasculature, confirming patency of the bilateral posterior tibial and peroneal arteries, with occlusion of the anterior tibial arteries. There was perfect agreement between QISS MRA and CEMRA in the right calf, and QISS MRA was diagnostic in the left calf, demonstrating similar findings compared to CT angiography without the limitation of artifact from diffuse vascular calcificaitons. In particular, the left plantar arteries are patient on QISS MRA while the dorsalis pedis is seen to be occluded. Of note, the symmetric loss of signal noted in the pelvis and proximal thighs on QISS MRA is typical for 'striping' artifacts from intermittent ectopy resulting in misgating. The symmetry of this appearance reassures the reader that this represents artifact rather than real disease. If poor gating limits evaluation of a particular station, the station can be reacquired in just 45 seconds without the need to re-shim.

2

## Case 3

An 86-year-old male with a history of cancer, hypertension and diabetes presented with left leg claudication. The patient had a history of renal dysfunction with eGFR < 30 ml/min/1.73 m², so contrast-enhanced MRA was not an option. The referring physician therefore ordered a non-contrast MRA. The QISS images showed a long left-sided superficial femoral artery occlusion with single-vessel runoff to the foot via the posterior tibial artery. On-table angiography in the operating room, using minimal amounts of contrast, confirmed the vascular findings and a bypass graft was placed. Therefore, this patient with severe renal dysfunction was diagnosed and treated without the need for a gadolinium-based contrast agent and minimal iodinated contrast.


## Discussion

In this report, we described three cases that illustrate the potential utility of non-contrast MR angiography using QISS in the clinical setting. QISS MRA is a simple to use technique that provides excellent image quality with high diagnostic yield in relatively short acquisition times. Besides, QISS MRA can be an alternative to CEMRA, thereby resulting in significant cost savings by avoiding costs associated with gadolinium contrast administration and point of care eGFR testing. QISS protocol can be run in about half the time of a standard CEMRA runoff protocol leading to improved patient throughput. Since QISS is largely automated and image processing occurs inline, technologists can be attending to other tasks while scanning is taking place, leading to greater staff efficiency.

Traditionally, non-contrast MR angiography of the lower extremities relied on an ECG-gated 2D time of flight approach. However, this approach has the disadvantage of very long acquisition times and variable image quality, particularly in regions of disease and vessel tortuosity [5]. Newer approaches have focused on subtractive methods, using either fast spin echo [6] or balanced steady state free precession readouts [7]. These techniques depend on the variation in blood signal between systole and diastole. Both arteries and veins appear bright in diastole, whereas only veins are visible in systole. Therefore, a subtracted dataset can produce a pure arterial image. Unfortunately, this imaging technique can be unreliable and its complexity, e.g. the requirement to subtract two image sets and necessary patient specific adjustments reduces clinical utility and makes it challenging to use for technologists who do not have extensive experience with it.

The QISS technique acquires stacks of axial slices to cover the region of interest, which in the case of the peripheral vasculature is from pelvis to feet. Each image stack is acquired near the magnet isocenter in order to

avoid artifacts from off-resonance effects. Each stack automatically undergoes inline maximum intensity projection (MIP) processing. Auto compose assembles these together at the end of the acquisition to produce a MIP of the entire peripheral vasculature. A key advantage of QISS is the simplicity of the acquisition technique and protocol set up, reducing dependence on experienced MR technologists. ECG leads are applied at the beginning of the test and the patient is placed supine, feet first with a peripheral vascular coil as with the usual runoff protocol. Since it is an axial acquisition, there is no time spent with setting up slices orientations and there is no risk to excluding regions of the vascular anatomy, as can occur with oblique coronal acquisitions tailored to the vascular anatomy to optimize the imaging time. The acquisition time is typically 8-10 minutes depending on heart rate. The images are acquired without operator intervention enabling the technologist to perform other tasks while scanning is taking place, and improving work efficiency. Moreover, since most of the image processing occurs inline, there is no need for advanced image analysis using other software algorithms or specialized post-processing staff.

Initial experience at 3T revealed two sporadic image quality issues in pelvic and abdominal stations: (1) Undesirable venous signal and (2) insufficient arterial conspicuity. These are possibly related to $B_1$-field inhomogeneity issues typically seen at higher field strengths. Subsequent patients were scanned using a modified version of QISS in which the venous contamination problem was addressed using an optimized FOCI adiabatic RF pulse for the Tracking Saturation pulse; arterial conspicuity was improved by scanning every other heartbeat for the top 3 stations covering pelvic and abdominal regions.

QISS MR angiography has been extensively validated in the medical literature, both at 1.5T and 3T. The initial paper by Hodnett et al. [8], which evaluated 53 patients at 1.5T in a two-center trial using both contrast-enhanced MRA and digital subtraction angiography as reference standards, found high sensitivities and specificities for QISS when compared to both CEMRA and DSA. In fact, QISS performed slightly better that CEMRA when compared to DSA in a patient subgroup and, also in this study, QISS performed well irrespective of renal function. In a second study of 25 patients with diabetes mellitus, QISS compared well to both CEMRA and DSA for detection of significant disease [4]. In another study comparing QISS to a non-contrast, ECG-gated 3D single shot fast spin echo pulse sequence in 20 patients, QISS demonstrated superior specificity and image quality, and was more robust in the abdominal and pelvic regions [9]. QISS MRA has also been extensively studied at 3T and results are similar to 1.5T showing high diagnostic accuracy and excellent image quality [10]. Recent technical advances promise to overcome limitations of $B_1$ field inhomogeneity and high power deposition, thereby further improving the performance at 3T.

Each of our cases demonstrates some of the advantages of QISS MRA.

Case 1 is of a diabetic patient who had previously undergone a left leg bypass graft. Stepping table contrast-enhanced MR angiography using a four-station approach on a 3T MAGNETOM Skyra resulted in venous contamination in the calf vessels due to suboptimal timing of contrast agent injection, precluding accurate evaluation. Early venous enhancement in this case was likely due to fast transit down the left leg due to the bypass graft and soft tissue inflammation in the right leg. Venous contamination is known to occur in up to 20% of cases using a single injection, stepping table CEMRA protocol. Several attempts to solve this problem for CEMRA include using a 2-injection protocol, where the calves are imaged first, or else attaching blood pressure cuffs on the thighs to slow venous return. Both approaches lengthen and complicate the protocol. Another solution is to use QISS as an alternative or adjunct to CEMRA. In our case, the QISS images clearly show the left sided bypass graft and the calf vessels without any overlap of adjacent veins.

In case 2, non-invasive vascular testing was non-diagnostic due to heavily calcified vessels, which also impaired diagnosis by CT angiography. Most of the disease was confined to the infra-popliteal segments. QISS was comparable to CEMRA for depiction of the runoff vessels and both were superior to CTA.

In case 3, a patient with diabetes presented with left leg claudication but had renal dysfunction with an eGFR of 50 ml/min. The referring physician did not want to use either a MR or CT contrast agent, so that QISS MR angiography provided a helpful diagnostic solution. The QISS images showed a long left-sided superficial femoral artery occlusion with single vessel runoff to the foot, which was sufficient information for the vascular surgeon to plan arterial bypass.

In conclusion, QISS MR angiography is a robust, simple and reliable non-contrast technique that can be used at 1.5T and 3T. QISS MRA has been extensively evaluated in several studies, including diabetic patients in whom renal dysfunction and vascular calcifications are particularly common and infra-popliteal disease is usually more severe. QISS MRA should become the non-contrast MRA technique of choice in patients with renal dysfunction. It may be particularly suitable for diabetic patients or those already on dialysis where vascular calcification is particularly prevalent. Although QISS MRA is robust with an imaging protocol that can be run without patient-specific modifications, patients with frequent ectopy or irregular arrhythmias demonstrate symmetric mis-gating artifacts (Fig. 2) which can reduce image quality of QISS MRA. QISS MRA can also be employed as an alternative to CEMRA resulting in potential cost savings by avoiding the costs of the contrast agent and associated infusion paraphernalia, as well as by improving patient throughput.

References

1. Hiatt WR, Hoag S, Hamman RF. Effect of diagnostic criteria on the prevalence of peripheral arterial disease. The San Luis Valley Diabetes Study. Circulation 1995;91:1472-9.
2. Sadowski EA, Bennett LK, Chan MR, et al. Nephrogenic systemic fibrosis: risk factors and incidence estimation. Radiology 2007;243:148-57.
3. Edelman RR, Sheehan JJ, Dunkle E, Schindler N, Carr J, Koktzoglou I. Quiescent-interval single-shot unenhanced magnetic resonance angiography of peripheral vascular disease: Technical considerations and clinical feasibility. Magnetic resonance in medicine : official journal of the Society of Magnetic Resonance in Medicine / Society of Magnetic Resonance in Medicine 2010;63:951-8.
4. Hodnett PA, Ward EV, Davarpanah AH, et al. Peripheral arterial disease in a symptomatic diabetic population: prospective comparison of rapid unenhanced MR angiography (MRA) with contrast-enhanced MRA. AJR American journal of roentgenology 2011;197:1466-73.
5. Offerman EJ, Hodnett PA, Edelman RR, Koktzoglou I. Nonenhanced methods for lower-extremity MRA: a phantom study examining the effects of stenosis and pathologic flow waveforms at 1.5T. Journal of magnetic resonance imaging : JMRI 2011;33:401-8.
6. Lanzman RS, Blondin D, Schmitt P, et al. Non-enhanced 3D MR angiography of the lower extremity using ECG-gated TSE imaging with non-selective refocusing pulses--initial experience. RoFo : Fortschritte auf dem Gebiete der Rontgenstrahlen und der Nuklear-medizin 2010;182:861-7.
7. Lanzman RS, Schmitt P, Kropil P, Blondin D. [Nonenhanced MR angiography techniques]. RoFo : Fortschritte auf dem Gebiete der Rontgenstrahlen und der Nuklearmedizin 2011;183:913-24.
8. Hodnett PA, Koktzoglou I, Davarpanah AH, et al. Evaluation of peripheral arterial disease with nonenhanced quiescent-interval single-shot MR angiography. Radiology 2011;260:282-93.
9. Ward EV, Galizia MS, Usman A, Popescu AR, Dunkle E, Edelman RR. Comparison of quiescent inflow single-shot and native space for nonenhanced peripheral MR angiography. Journal of magnetic resonance imaging : JMRI 2013;38:1531-8.
10. Knobloch G, Gielen M, Lauff MT, et al. ECG-gated quiescent-interval single-shot MR angiography of the lower extremities: initial experience at 3 T. Clinical radiology 2014;69:485-91.



## Contact

Maria L. Carr, RT.R (CT)(MR)
Project Research Manager
Department of Radiology
Northwestern University
Feinberg School of Medicine
737 N. Michigan Ave., Suite 1600
Chicago, IL 60611
USA
Phone: +1 312-926-5292
m-carr@northwestern.edu


# Imaging Diabetics with MR

James Carr (Northwestern Memorial Hospital, Chicago, IL, USA)

One of the challenges when it comes to imaging diabetics is the fact that it's a multi-system disorder.

See what just has been introduced on the software side to help physicians diagnose complications associated with diabetes, making contrast agent unnecessary and benefitting diabetic patients.


Check out the interview at:

**https://www.youtube.com/watch?v=LptMIhAsqu4**

# MUST Project: A Quantitative MRI Evaluation of Structural and Functional Changes in Myocardial and Skeletal Muscles Induced by Ultra-Endurance Running

M. Viallon[1]; L. Gergele[1]; G.P. Millet[2]; C. Le Goff[3]; K. Moulin[1]; C. de Bourguignon[1]; P. Andonian[1]; R.B. van Heeswijk[4]; H. Feliciano[4]; J. Kuijer[5]; M. Stuber[4]; O. Beuf[1]; P. Croisille[1]

[1] CHU de Saint Etienne, CREATIS, UMR CNRS 5220 INSERM U1040 INSA-Lyon, Université de Lyon, France
[2] ISSUL, Institute of Sport Sciences, Université of Lausanne, Switzerland
[3] Department of Chimie clinique, University of Liège, Belgium
[4] Center for BioMedical Imaging (CIBM), University and University Hospital of Lausanne, Switzerland
[5] Department of Physics and Medical Technology VU University Medical Center Amsterdam, Netherlands

## Ultra-endurance trail: An outstanding model to challenge qMRI in the study of the adaptive responses to extreme load and stress conditions

A post-industrial, technology-based society is leading, on the one hand, to an increasingly sedentary lifestyle, and on the other, to a growing interest in endurance sports. An example of this is participation in ever longer trail or ultra-marathon running races. However, whilst moderate exercise is clearly an important therapy for cardiovascular health [1], the effects of more extreme physical exercise are still unclear. An ultra-endurance trail is any running/walking event longer than the 42.195 km (26.2 miles) marathon distance, on footpaths or trails with various positive/negative slopes, elevations and conditions (mountain, desert, etc.). Some ultra-marathons require several days for completion, adding the stress of sleep deprivation to the exercise-induced physical difficulty. Ultra-trailers participating in such an extreme mountain ultra-marathon (MUM) can reach significant levels of inflammation and fatigue [2] that raise a very understandable interest within the scientific community [3]. Indeed, an ultra-marathon represents a unique and outstanding reversible model to study acute consequences of extreme load and stress on human organs. Moreover, with each subject being his or her own control, this model offers a window to screen the inter-individual susceptibility to injuries and limits of the adaptive responses. Therefore, given the fascination

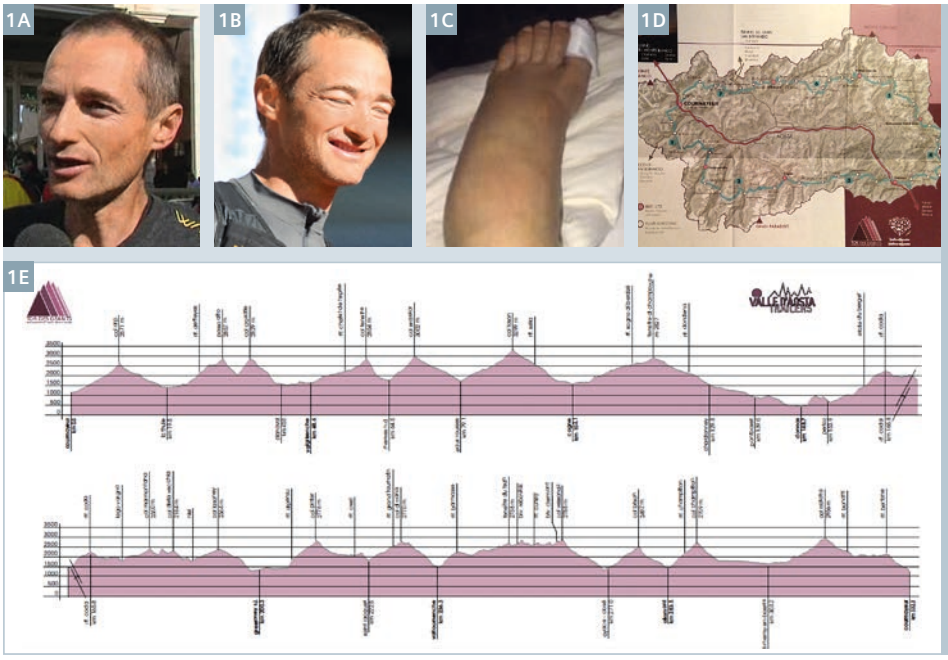


**1** **(1A)** Ultra-trailer (Antoine Duillon 2e TDG 2014) before the race and **(1B)** after the race: Water retention can be clearly seen on the face that looks swollen and much bumpier with difficulties for the subject to keep his eyes wide open. **(1C)** Swollen feet two days after arrival. **(1D)** Map of the 'Tor des géants' ultra-trail (330 km, 24,000 m positive elevation) http://www.tordesgeants.it/fr.

inspired by the athletes' performance and the fact that the ability to run long distances has played an important role in human evolution, there has been a very strong motivation to explore the underpinning physiological changes induced by extreme MUM using Magnetic Resonance Imaging (MRI) especially at the skeletal and cardiac muscles level.

MRI is renowned for its unique capacity to examine soft tissues, to perform longitudinal studies, and to show inflammation. It recently reached new maturity to quantify the tissues' injuries, offering new quantitative indices (T1, T2 and diffusion mapping) that allow the non-invasive determination of the pathophysiological changes within the tissue, and therefore the following and characterization of adaptations and alterations in the muscle both immediately after exercise and throughout the recovery process. MUM-induced microstructural and functional modifications in skeletal muscle and myocardium, as well as inflammatory mechanisms in these muscles, have indeed never been explored using novel advanced quantitative MRI (qMRI) techniques. Such MRI findings will allow us to better understand the time-course of degeneration and regeneration of myocardial and skeletal muscle tissues caused by several days of extreme physical load as well as the differences between the two types of muscles. Ultra-trail hence represents a 'real-life' and longitudinal model for assessing quantitative non-invasive and local (organ-specific) imaging biomarkers on a wide range of tissue changes – from acute intense to subtle subclinical changes – and for correlating them with advanced blood biomarkers.

## An on-site research lab at the foot of Mont-Blanc in Courmayeur, Italy

The whole project of performing an international study on a cohort of ultra-trailers before, immediately after, and three days after, the race, required the logistical achievement of installing a 30 m long, 45 tons truck containing a whole-body MRI scanner within the beautiful city of Courmayeur, in Italy's Aosta Valley. A biochemistry laboratory for on-site immediate conditioning of all biomedical samples at all time-points was also needed. Thanks to the mutual interests of Siemens Healthcare, Swiss engineers and the medical team of the Aosta public hospital, it was possible to have our favorite 1.5T cardiac MR system (MAGNETOM Avanto) within an Alliance medical truck for 3 weeks in the center of Courmayeur, less than 100 m from the finishing line of the world's most extreme mountain ultra-marathon: The 'Tor des Géants'.

Our team of scientists would also like to pay tribute to the incredible welcome given to our project by the organizers and medical team in


2 Ultra-trailer from 'Tor des Géants' 2014 edition and 1.5T MAGNETOM Avanto in Courmayeur.

charge of the event's safety and research management.

## 330 km, 24,000 m positive elevation, ~100-150 hours running, 4-10 hours sleeping, 3 x 90 min MR scans, 50 athletes

The 'Tor des Géants' is an extreme MUM, famous for being the longest distance for such events (330 km), and boasting the highest positive elevation (24,000 m). All participating ultra-trailers also point to the unmatched atmosphere of this event within an extraordinary landscape at the feet of the highest mountains in the Alps.

Fifty ultra-trailers volunteered for a non-invasive and longitudinal quantitative MRI exploration performed prior to, during, and after the 'Tor des Géants'.

Cardiac and skeletal muscle, as well as brain examinations, were conducted in three 90-minute MR sessions and three-step examinations. The study protocol has been approved by the Aosta Valley Ethics Committee. At the cardiac level, the 30 min imaging protocol included standard Cine-bSSFP[1] imaging,
but also MR-tagging to investigate changes of both global and regional function changes after the event and after recovery. Magnitude short- and long- axis CSPAMM images [4, 5] were processed using InTag post-processing toolbox (Creatis, Lyon, France) implemented in OsiriX software (Geneva, Switzerland) to perform quantitative myocardial strain analysis. Motion estimation is based on the Sine Wave Modeling approach [6]. Cine bSSFP images will also be processed by feature tracking analysis and regional and global peak circumferential ($E_{cc}$), longitudinal ($E_{ll}$) strains as well as peak rotation and torsion will be derived using both techniques. Quantitative T1 mapping [7], T2 mapping [8, 9] and diffusion (multiple b values and multiple directions for both DTI and IVIM modeling) MRI sequences were furthermore acquired to evaluate the sensitivity of these new quantitative indexes in addition to potential biomarkers to explore changes occurring in myocardium.

[1] The product is still under development and not commercially available yet. Its future availability cannot be ensured.

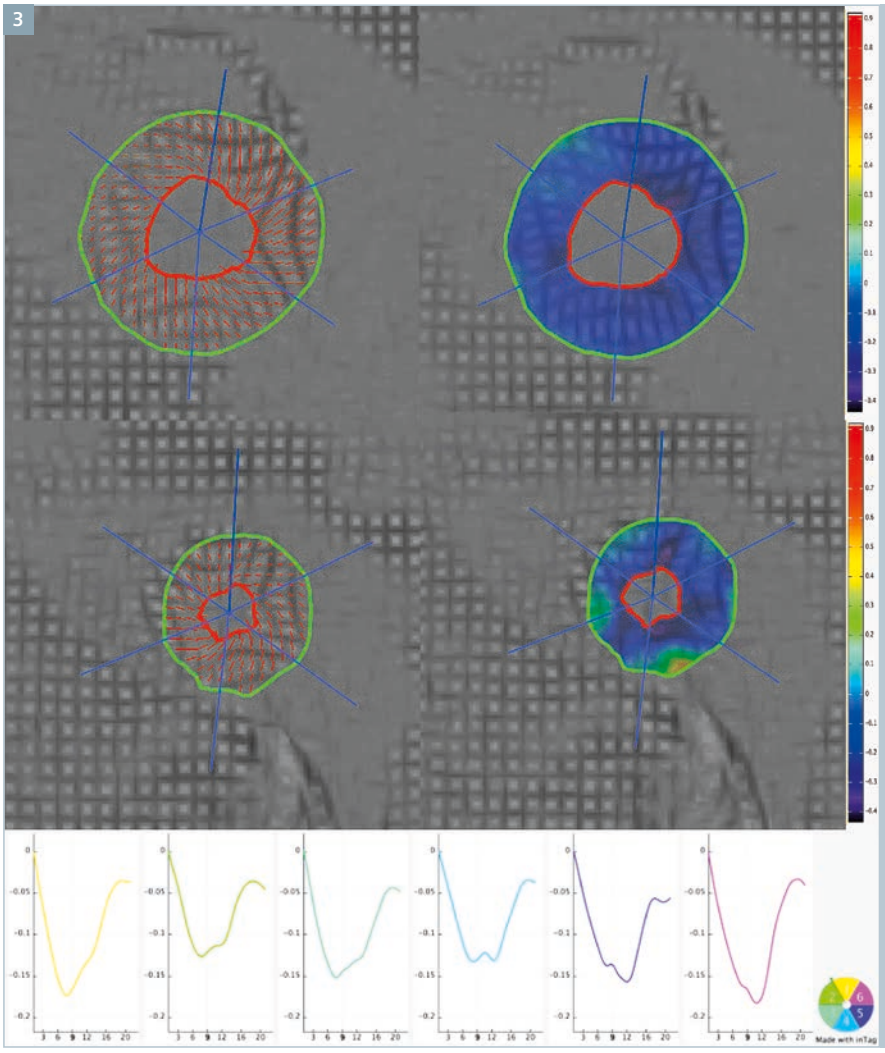

3 Myocardial mid short-axis tagged image (CSPAMM) with superimposed displacement maps (left) and end-systolic peak circumferential strain (right) at basal (top) and apical levels (bottom) illustrating the basal clockwise rotation and counter-clockwise rotation of the apex. At the bottom, typical curves of the circumferential strain over time in AHA segments (inTag, OsiriX, Creatis, Lyon: www.creatis.insa-lyon.fr/InTag).

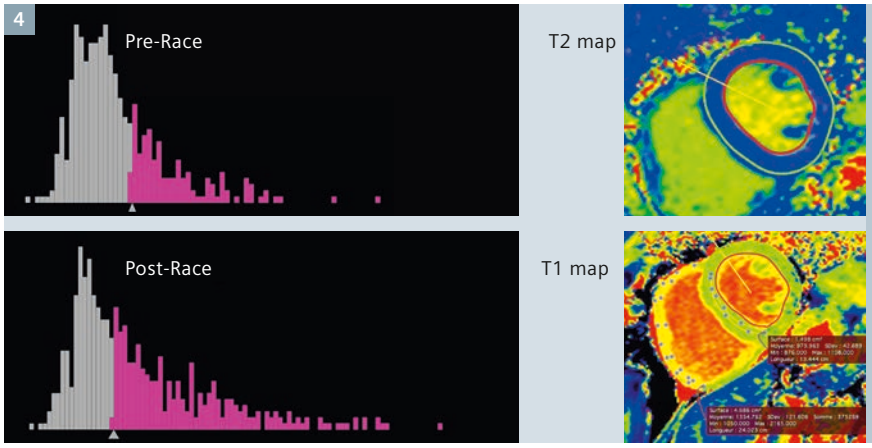


4 T1 and T2 maps as well as corresponding histograms before and after the race (intensities above the fixed threshold of 55 ms are displayed in pink) using CMRSegtools (CREATIS, Lyon, France, www.creatis.insa-lyon.fr/CMRSegTools). Mean T1 values in left and right myocardium are displayed in OsiriX (http://www.osirix-viewer.com).

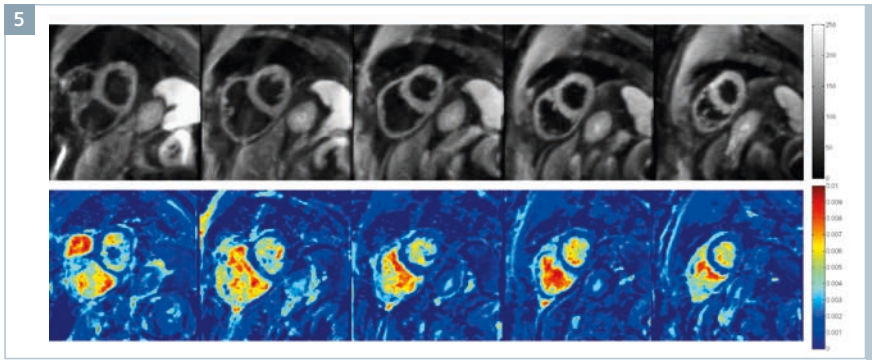


5 Diffusion-weighted images (b=200, upper row) and corresponding ADC maps (lower row) obtained using a monopolar prepared ECG gated SE-EPI sequence.

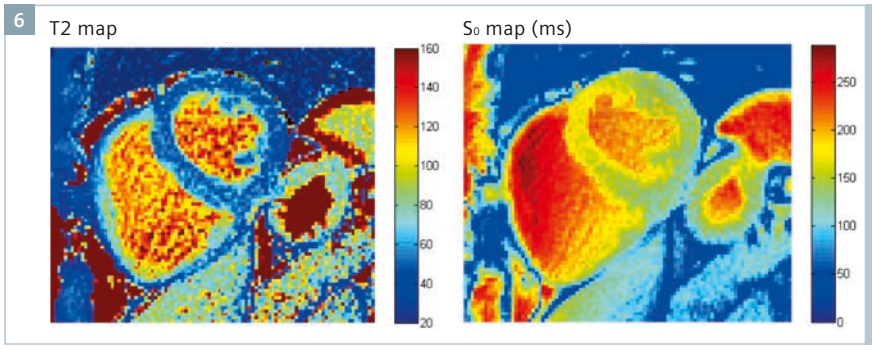


6 High resolution T2 maps and corresponding $S_0$ map obtained in athletes prior to the race using a three-echoes T2-prepared radial bSSFP sequence.

*Reprinted with permission from R.B. Van Heesjwick, JACC cardiovascular Imaging 2015 [9].*

The second step was a 30 min skeletal muscle examination, including a full quadriceps multi-echo isotropic 3D Dixon sequence (two-point Dixon, in and out of phase images, fat (F) and water (W) calculated images), a 3D multi-echoes (eight echoes), multi-flip-angle Dixon sequence for T2*, T1, fat fraction (FF), fat (F) and water (W) image calculation [10]. A STEAM diffusion sequence was also realized to screen any mean diffusion (MD), apparent diffusion coefficient (ADC), fraction of anisotropy (FA) as well as IVIM parameters (D, D* and f) exercise induced physiological variations. A multi-echoes T2 spin-echo sequence was also acquired for advanced T2 compartimental analysis.

Finally, a 15 min head examination concluded the series of tests, including a diffusion scan, and T2-weighted imaging using a standard 3 mm T2 TSE as well as a T2 multi-echo sequence.

## Preliminary results and discussion

The redistribution of water into the muscle, in particular, has never been scrutinized using advanced quantitative MRI techniques such as T1, T2 and diffusion mapping, but also fat (F) and water (W) fraction mapping, immediately following extreme MUM and a few days of recovery. Our goal was to investigate the sensitivity and specificity of these quantitative MR derived parameters to follow-up the kinetics of the potential inflammatory phenomena caused by the ultra-trail and their links to the physiological processes involved in this controlled and reversible model of myocardial tissue stress. This study should provide new insights into the physiological mechanisms involved during ultra-endurance, and also during the recovery, at the cardiac and peripheral muscle level.

Leg muscle damage is frequently reported by the trailers after eccentric loading conditions such as in extreme MUM. Under these circumstances, muscles that provide most

of the control and regulation of limbs' movement during downhill running (e.g. vastus medialis), appear strongly hyperintense on T2-weighted images after exercise, while others, such as semitendinosus muscles appear to be preserved. Patterns of inflammatory damages were identified as hyperintense hazy lesions in the thigh muscles as shown in figure 7. In our data, such patterns were mainly observed in vastii (intermedius, lateralis, and/or medialis) muscles but were not associated with any identified symptoms when present, without noticeable bruising at the time of imaging. Post-processing and segmentation of all individual muscle groups will allow precise evaluation of specific swelling. Our data showed more frequent inflammation patterns at the level of the vastus intermedius, a priori regardless of the effects of fatigue, performance or pain.

Several MRI and ultrasound studies have shown the existence of functional and biochemical alterations in the myocardium after prolonged intense exercise. Published echocardiography studies demonstrated systolic and diastolic transient left ventricle (LV) dysfunction with abnormal strains, and changes in LV torsion kinetics with decreased and delayed peak torsion as well as depressed peak untwisting [11]. Le Gerche et al. described cardiac remodeling of the right ventricle (RV) that could be associated with long-standing endurance training, with cumulative exposure to endurance competition further enhancing cardiac remodeling [12]. Late gadolinium enhanced techniques have also highlighted small areas of myocardial fibrosis [12]. Structural, functional and electrical changes of the athlete's heart, probably linked to the disproportionate hemodynamic stress on the RV during endurance activity, appears to lead to exercise-induced heart phenotype, which in turn requires specific reading during diagnosis in order not to dramatize findings that would be the evident sign of abnormalities in 'normal' subjects. Moreover, some arrhythmias appeared to be more prevalent amongst our endurance athletes.

7

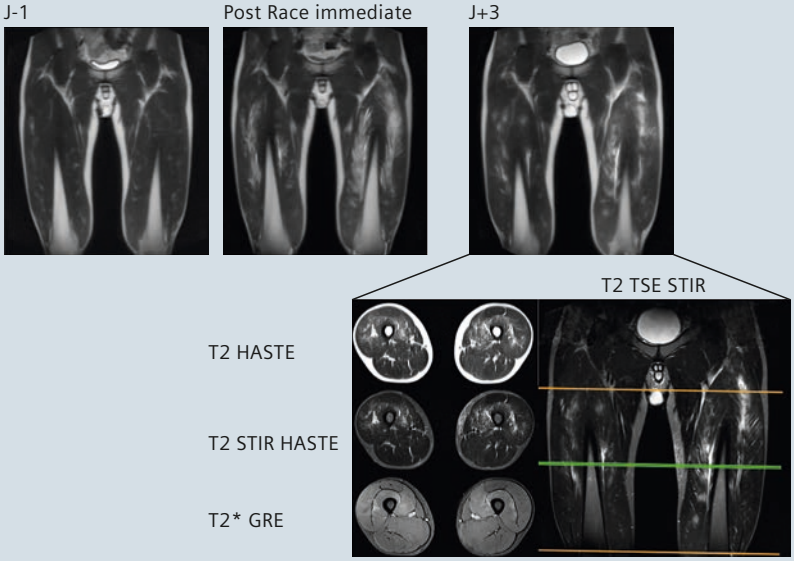


7 T2-weighted coronal images of the upper leg obtained prior the race, immediately after and 3 days after arrival. High-resolution STIR and axial images displayed hazy hyperintense lesions within the thigh muscles.

8

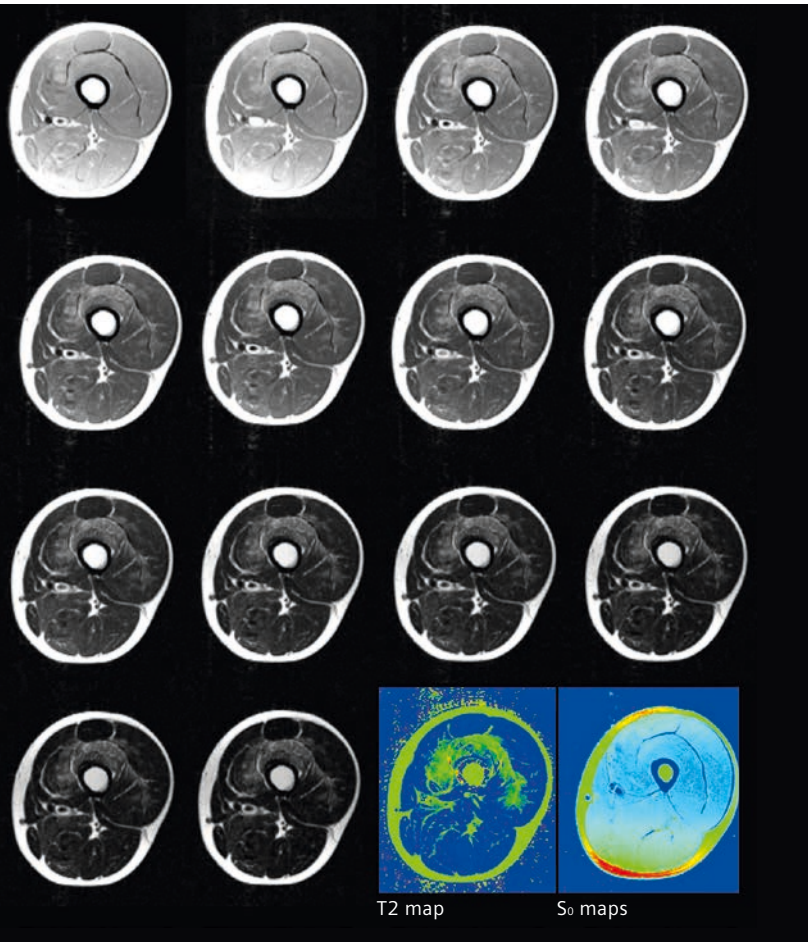


8 Series of 13 axial T2-weighted images obtained in the thigh muscles using a multi-echo spin-echo sequence and its corresponding calculated T2 and $S_0$ maps.

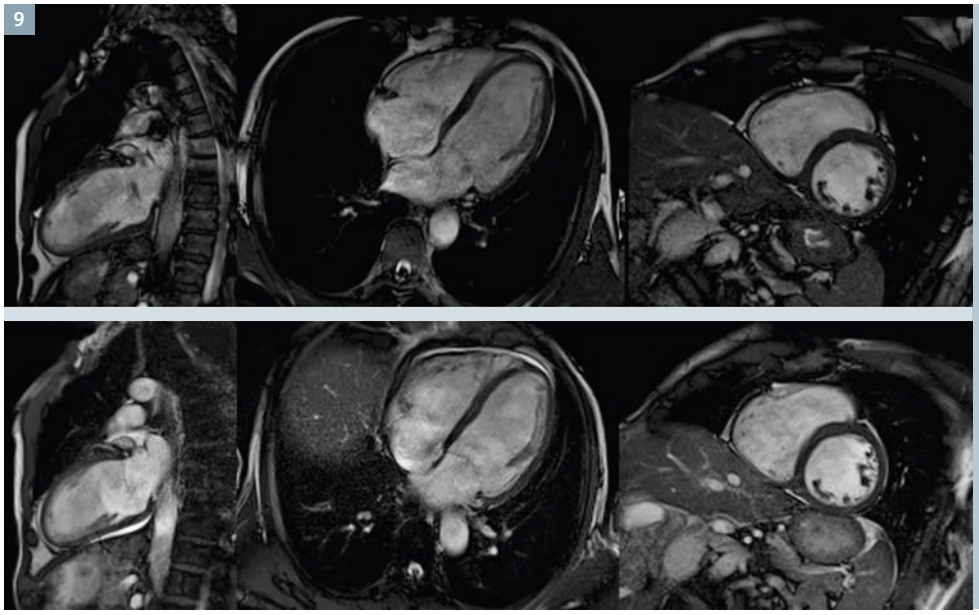

9 b-SSFP morphologic image pre- and post-race immediately showing clearly a pericardial effusion and exercise-induced athletes' heart phenotype with LV cardiac remodeling.

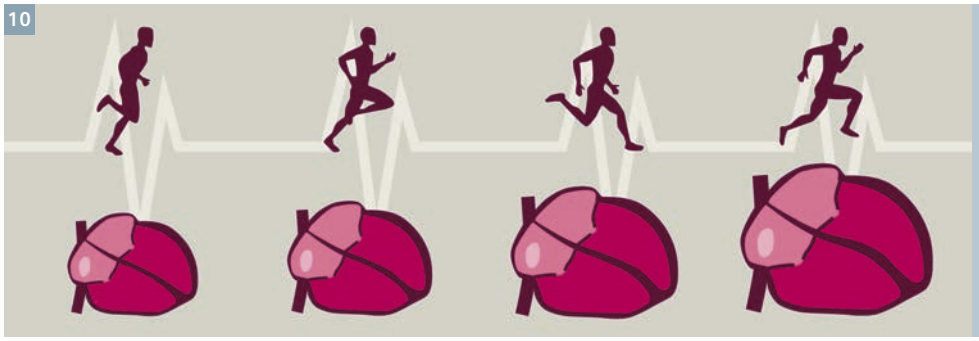

10 Exercise-induced ARVC. *Adapted with permission from the doctoral thesis of A. La Gerche. Herzschr Elektrophys 2012.*

Additional knowledge will be acquired from the extensive collection of blood biomarkers that have been obtained before, half-way, at the end of the race, and after three days of recovery. Indeed, while it has been shown that muscular and myocardial biomarkers are increased in MUM [2], little is known about their kinetics related to the distance, even if over 200 km the biomarkers increased more in the second half than in the first one [13]. Together with biomarkers of the inflammation and oxidative stress, the response of emerging biomarkers of cardiac stress and remodeling (Galectin-3, ST2, GDF15) will help to better understand myocardial damage that is likely to occur with such major stress for the body.

## Conclusion

This study aimed to characterize a new model of human tissue stress with clinical and biological inflam-matory responses close to severe conditions such as those met in intensive care units. From an imaging perspective, it is a unique opportunity for MRI researchers to validate MR-derived organ specific quantitative biomarkers with an accelerated kinetics where each subject is its own control. It will also provide new insights into the physiological mechanisms involved during ultra-endurance exercise, and its impact on the human body.

The preliminary results confirm previous work conducted in flat ultra-marathons, underlying potential risks from intense endurance activities that can lead to sports injuries. Peripheral muscles and articulations are probably on the frontline of damage, with noble organs such as the brain and myocardium which appear to suffer in a minor extend from the intense and/or extreme activities. There is definitely a social cache to excess performance in trail. Moreover, the world of sport places an ever-increasing demand on the athletic community without addressing the appropriateness of such burdens on either professional athletes or recreational athletes who run longer and harder races than ever before.

This article does not aim at negating the obvious fact that physical activity can reduce cardiovascular risk and mortality, and that it is essential for well-being in our sedentary and permanently connected cybernetic society. The optimal dose of physical activity and its benefits in terms of cardiovascular or all-cause mortality is still an open debate, and a recent study has shown in a cohort of 55,137 adults followed over 15 years, that running 5-10 min/day and at slow speed <6 miles/h is associated with marked reduced mortality, without any further benefit from increased distance, frequency,

amount or speed [14]. The upper limit of the dose-response of vigorous-intensity activities is unclear and needs to be individually clarified. Various studies have suggested that excessive endurance sports may induce adverse cardiovascular effects such as arrhythmias and myocardial damage [15, 16]. From a broader perspective, MRI can definitely help in the early recognition of exercise-induced tissue damage, and this study, testing innovating quantitative imaging methods in conditions close of those met with fragile patients – hence difficult to include in clinical trials – will accelerate the transfer and the validation of the newly developed organ-protection therapies.

We therefore also hope that it will provide our athletes with the benefits of the organ-protection therapies that are at the development or evaluation stages, so that they can pursue athletic glory in greater safety.

## Acknowledgements

This work was performed within the framework of the LABEX PRIMES (ANR-11-LABX-0063) of Université de Lyon, within the program "Investissements d'Avenir" (ANR-11-IDEX-0007) operated by the French National Research Agency (ANR). The authors thanks all ultra-trailers that volunteered for the MUST project, the VDA trailers and Courmayeur city representatives for their technical assistance. The authors also thank Siemens Healthcare and Guerbet, Carestream, Supersonic Imagine, and Sysmex for their support. The authors are especially grateful to Bavo von Riet (Siemens Healthcare) for his efficient help in setting up the whole project, Nicolas Hermann for his kindness, availability and expertise, Bernard Borloz and Jan Philipp Gelzer (Siemens Switzerland) and, last but not least, Serge Ripart (Siemens France).

### References

1 Shiroma EJ, Sesso HD, Lee IM (2012) Physical activity and weight gain prevention in older men. Int J Obes (Lond) 36, 1165-1169.
2 Saugy J, Place N, Millet GY, Degache F, Schena F, Millet GP (2013) Alterations of Neuromuscular Function after the World's Most Challenging Mountain Ultra-Marathon. PLoS One 8, e65596.
3 Millet GP, Millet GY (2012) Ultramarathon is an outstanding model for the study of adaptive responses to extreme load and stress. BMC Med 10, 77.
4 Fischer SE, McKinnon GC, Maier SE, Boesiger P, MagnReson Med 1993 30(2): 191-200.
5 Kuijer JP, Jansen E, Marcus JT, van Rossum AC, Heethaar RM (2001) Improved harmonic phase myocardial strain maps. Magn Reson Med 46, 993-999.
6 Arts T, Prinzen F, Delhaas T, Milles J, Rossi A, Clarysse P (2010) Mapping Displacement and Deformation of the Heart With Local Sine-Wave Modeling. IEEE Trans Med Imaging
7 Messroghli DR, Radjenovic A, Kozerke S, Higgins DM, Sivananthan MU, Ridgway JP (2004) Modified Look-Locker inversion recovery (MOLLI) for high-resolution T1 mapping of the heart. Magn Reson Med 52, 141-146.
8 Giri S, Chung YC, Merchant A, Mihai G, Rajagopalan S, Raman SV, Simonetti OP (2009) T2 quantification for improved detection of myocardial edema. J Cardiovasc Magn Reson 11, 56.
9 van Heeswijk RB, Piccini D, Feliciano H, Hullin R, Schwitter J, Stuber M (2014) Self-navigated isotropic three-dimensional cardiac T mapping. Magn Reson Med
10 Leporq B, Ratiney H, Pilleul F, Beuf O (2013) Liver fat volume fraction quantification with fat and water T1 and T 2* estimation and accounting for NMR multiple components in patients with chronic liver disease at 1.5 and 3.0 T. Eur Radiol 23, 2175-2186.
11 Nottin S, Doucende G, Schuster I, Tanguy S, Dauzat M, Obert P (2009) Alteration in left ventricular strains and torsional mechanics after ultralong duration exercise in athletes. Circ Cardiovasc Imaging 2, 323-330.
12 La Gerche A, Burns AT, Mooney DJ, Inder WJ, Taylor AJ, Bogaert J, Macisaac AI, Heidbuchel H, Prior DL (2012) Exercise-induced right ventricular dysfunction and structural remodelling in endurance athletes. Eur Heart J 33, 998-1006.
13 Kim HK, Sohn DW, Lee SE, Choi SY, Park JS, Kim YJ, Oh BH, Park YB, Choi YS (2007) Assessment of left ventricular rotation and torsion with two-dimensional speckle tracking echocardiography. J Am Soc Echocardiogr 20, 45-53.
14 Lee DC, Pate RR, Lavie CJ, Sui X, Church TS, Blair SN (2014) Leisure-time running reduces all-cause and cardiovascular mortality risk. J Am Coll Cardiol 64, 472-481.
15 Andersen K, Farahmand B, Ahlbom A, Held C, Ljunghall S, Michaelsson K, Sundstrom J (2013) Risk of arrhythmias in 52 755 long-distance cross-country skiers: a cohort study. Eur Heart J 34, 3624-3631.
16 Neilan TG, Januzzi JL, Lee-Lewandrowski E, Ton-Nu TT, Yoerger DM, Jassal DS, Lewandrowski KB, Siegel AJ, Marshall JE, Douglas PS, Lawlor D, Picard MH, Wood MJ (2006) Myocardial injury and ventricular dysfunction related to training levels among nonelite participants in the Boston marathon. Circulation 114, 2325-2333.


## Contact

Magalie Viallon, Ph.D.
CREATIS, UMR CNRS 5220 - INSERM U1044
Service de Radiologie Hôpital Nord,
Université J.Monnet Saint-Etienne
Pôle de Recherche et d'Enseignement Supérieur
(PRES) Université de Lyon (France)
Phone: +33 4 77 82 84 36
magalie.viallon-croisille@creatis.insa-lyon.fr
http://www.creatis.insa-lyon.fr

The entire editorial staff at Bristol Heart Institute, University of Bristol and at Siemens Healthcare extends their appreciation to all the radiologists, technologists, physicists, experts and scholars who donate their time and energy – without payment – in order to share their expertise with the readers of MAGNETOM Flash.

MAGNETOM Flash – Imprint



Publisher:
**Siemens AG**
Medical Solutions
Business Unit Magnetic Resonance,
Karl-Schall-Straße 6, D-91052 Erlangen,
Germany

**Guest Editor:**
Dr. Chiara Bucciarelli-Ducci, MD, PhD, FESC, FRCP
Consultant Senior Lecturer in Cardiology / Non-Invasive Imaging at the Bristol Heart Institute, University of Bristol, UK. Imaging lead of the Bristol National Institute of Health Research (NIHR) Biomedical Research Unit (BRU) Co-Director of the Clinical Research and Imaging Centre (CRIC Bristol)

**Editor-in-chief:** Antje Hellwich (antje.hellwich@siemens.com)

**Editorial Board:** Wellesley Were; Ralph Strecker; Sven Zühlsdorff, Ph.D.; Gary R. McNeal, MS (BME); Peter Kreisler, Ph.D.

**Production:** Norbert Moser, Siemens AG, Medical Solutions

**Layout:** Agentur Baumgärtner, Friedrichstraße 4, D-90762 Fürth, Germany

**Printer:** G. Peschke Druckerei GmbH, Taxetstrasse 4, D-85599 Parsdorf b. Munich, Germany



We welcome your questions and comments about the editorial content of MAGNETOM Flash. Please contact us at magnetomworld.med@siemens.com.

Manuscripts as well as suggestions, proposals and information are always welcome; they are carefully examined and submitted to the editorial board for attention. MAGNETOM Flash is not responsible for loss, damage, or any other injury to unsolicited manuscripts or other materials. We reserve the right to edit for clarity, accuracy, and space. Include your name, address, and phone number and send to the editors, address above.

MAGNETOM Flash is also available on the internet:

**www.siemens.com/magnetom-world**

SIEMENS

# MAGNETOM Flash

The Magazine of MRI

Issue Number 1/2015 | SCMR/EuroCMR Edition

Not for distribution in the US

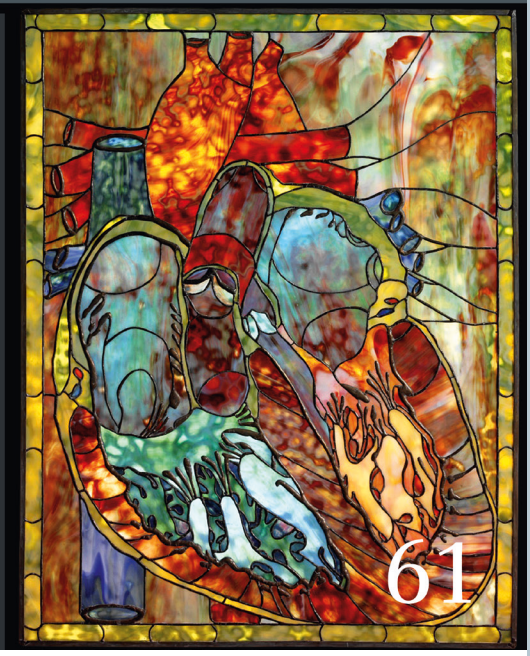




**Please enter your business address**

Institution

Department

Function

Title

Name

Street

Postal Code

City

State

Country

MR system used

**Please include me in your mailing list for the following Siemens Healthcare customer magazine(s):**

☐ Medical Solutions

☐ MAGNETOM Flash

☐ SOMATOM Sessions

☐ AXIOM Innovations

**Stay up to date with the latest information**

**Register for:**

E-mail

☐ Yes, I consent to the above information being used for future contact regarding product updates and other important news from Siemens.

☐ unsubscribe from info service

Please print clearly!

# MAGNETOM Flash


Siemens AG
Healthcare
Magnetic Resonance
Antje Hellwich – Marketing
P.O. Box 32 60
D-91050 Erlangen
Germany

→ Visit www.siemens.com/magnetom-world for case reports, clinical methods, application tips, talks and much more clinical information.

## SUBSCRIBE NOW!

– and get your free copy of future MAGNETOM Flash! Interesting information from the world of magnetic resonance – gratis to your desk. Send us this postcard, or subscribe online at www.siemens.com/MAGNETOM-World

On account of certain regional limitations of sales rights and service availability, we cannot guarantee that all products included in this brochure are available through the Siemens sales organization worldwide. Availability and packaging may vary by country and is subject to change without prior notice. Some/All of the features and products described herein may not be available in the United States.

The information in this document contains general technical descriptions of specifications and options as well as standard and optional features which do not always have to be present in individual cases, and which may not be commercially available in all countries. Due to regulatory reasons their future availability cannot be guaranteed. Please contact your local Siemens organization for further details.

Siemens reserves the right to modify the design, packaging, specifications, and options described herein without prior notice. Please contact your local Siemens sales representative for the most current information.

Note: Any technical data contained in this document may vary within defined tolerances. Original images always lose a certain amount of detail when reproduced.

*MAGNETOM 7T is still under development and not commercially available yet. Its future availability cannot be ensured. This research system is not cleared, approved or licensed in any jurisdiction for patient examinations. This research system is not labelled according to applicable medical device law and therefore may only be used for volunteer or patient examinations in the context of clinical studies according to applicable law.

Not for distribution in the US


**Global Business Unit**

Siemens AG
Medical Solutions
Magnetic Resonance
Henkestraße 127
DE-91052 Erlangen
Germany
Phone: +49 9131 84-0
www.siemens.com/healthcare

**Local Contact Information**

**Asia/Pacific:**
Siemens Medical Solutions
Asia Pacific Headquarters
The Siemens Center
60 MacPherson Road
Singapore 348615
Phone: +65 6490 6000

**Canada:**
Siemens Canada Limited
Healthcare
1550 Appleby Lane
Burlington, ON L7L 6X7, Canada
Phone +1 905 315-6868

**Europe/Africa/Middle East:**
Siemens AG, Healthcare
Henkestraße 127
91052 Erlangen, Germany
Phone: +49 9131 84-0

**Latin America:**
Siemens S.A., Medical Solutions
Avenida de Pte. Julio A. Roca No 516, Piso
C1067 ABN Buenos Aires, Argentina
Phone: +54 11 4340-8400

**USA:**
Siemens Medical Solutions USA, Inc.
51 Valley Stream Parkway
Malvern, PA 19355-1406, USA
Phone: +1 888 826-9702

**Global Siemens Headquarters**

Siemens AG
Wittelsbacherplatz 2
80333 Muenchen
Germany

**Global Siemens Healthcare Headquarters**

Siemens AG
Healthcare
Henkestraße 127
91052 Erlangen
Germany
Phone: +49 9131 84-0
www.siemens.com/healthcare


Order No. A91MR-1000-112C-7600 | Printed in Germany | CC MR 2692 02151. | 

**www.siemens.com/magnetom-world**